AFWAL-TR-81-3179

DEVELOPMENT OF AN AEROACOUSTIC METHODOLOGY TO EVALUATE HEATSHIELD MATERIAL PERFORMANCE

A. L. LAGANELLI

SCIENCE APPLICATIONS, INC.
994 OLD EAGLE SCHOOL ROAD
WAYNE, PENNSYLVANIA 19087

FEBRUARY 1982

FINAL REPORT FOR PERIOD FEBRUARY 1981 TO JANUARY 1982

FLIGHT DYNAMICS LABORATORY
AIR FORCE WRIGHT AERONAUTICAL LABORATORIES
WRIGHT PATTERSON AIR FORCE BASE
DAYTON, OHIO 45433

NOTICE

When Government drawings, specifications, or other data are used for any purpose other than in connection with a definitely related Government procurment operation, the United States Government thereby incurs no responsibility nor any obligation whatsoever; and the fact that the government may have formulated, furnished, or in any way supplied the said drawings, specifications, or other data, is not to be regarded by implication or otherwise as in any manner licensing the holder or any other person or corporation, or conveying any rights or permission to manufacture use, or sell any patented invention that may in any way be related thereto.

This report has been reviewed by the Office of Public Affairs (ASD/PA) and is releasable to the National Technical Information Service (NTIS). At NTIS, it will be available to the general public, including foreign nations.

This technical report has been reviewed and is approved for publication.

Leonard L Shaw

LEONARD L. SHAW, Project Engineer
Acoustics and Sonic Fatigue Group

Glenn G. Ormbrek

GLENN G. ORMBREK, Project Engineer
Non-Metals Engineering Branch

FOR THE COMMANDER

RALPH L. KUSTER, JR, Colonel, USAF
Chief, Structures and Dynamics Division
Flight Dynamics Laboratory

DAVEY L. SMITH, Chief
Structural Integrity Branch

Albert Olevitch

ALBERT OLEVITCH, Chief
Non-Metals Engineering Branch
Systems Support Division

Richard T. Goddard

RICHARD T. GODDARD, Colonel, USAF
Chief, Systems Support Division
Materials Laboratory

"If your address has changed, if you wish to be removed from our mailing list, or if the addressee is no longer employed by your organization please notify AFWAL/FIBED, W-PAFB, OH 45433 to help us maintain a current mailing list".

Copies of this report should not be returned unless return is required by security considerations, contractual obligations, or notice on a specific document.

UNCLASSIFIED

SECURITY CLASSIFICATION OF THIS PAGE (When Data Entered)

REPORT DOCUMENTATION PAGE	READ INSTRUCTIONS BEFORE COMPLETING FORM
1. REPORT NUMBER: AFWAL-TR-81-3179	2. GOVT ACCESSION NO.: AD-A115666
	3. RECIPIENT'S CATALOG NUMBER:
4. TITLE (and Subtitle): DEVELOPMENT OF AN AEROACOUSTIC METHODOLOGY TO EVALUATE HEATSHIELD MATERIAL PERFORMANCE	5. TYPE OF REPORT & PERIOD COVERED: FINAL REPORT: Feb. 1981 to Jan. 1982
	6. PERFORMING ORG. REPORT NUMBER: SAI-057-82R-013
7. AUTHOR(s): Anthony L. Laganelli	8. CONTRACT OR GRANT NUMBER(s): F33615-81-C-3209
9. PERFORMING ORGANIZATION NAME AND ADDRESS: Science Applications, Inc. 994 Old Eagle School Road, Suite 1018 Wayne, Pennsylvania 19087	10. PROGRAM ELEMENT, PROJECT, TASK AREA & WORK UNIT NUMBERS: 24010158/61101F
11. CONTROLLING OFFICE NAME AND ADDRESS: Flight Dynamics Laboratory (AFWAL/FIBED) Air Force Wright Aeronautical Laboratories Wright Patterson Air Force Base, Ohio 45433	12. REPORT DATE: February 1982
	13. NUMBER OF PAGES: 129
14. MONITORING AGENCY NAME & ADDRESS(if different from Controlling Office)	15. SECURITY CLASS. (of this report): UNCLASSIFIED
	15a. DECLASSIFICATION/DOWNGRADING SCHEDULE: N/A

16. DISTRIBUTION STATEMENT (of this Report)

Approved for public release; Distribution unlimited.

17. DISTRIBUTION STATEMENT (of the abstract entered in Block 20, if different from Report)

18. SUPPLEMENTARY NOTES

19. KEY WORDS (Continue on reverse side if necessary and identify by block number)

Aeroacoustics	Rough Walls
Fluctuating Pressure	Ported Holes
Power Spectral Density	Backface Gages
Cross-Power Spectral Density	Tape Wrapped Carbon Phenolic

20. ABSTRACT (Continue on reverse side if necessary and identify by block number)

An experimental program was conducted in the AFWAL Mach 6 and AEDC Shock Tube facilities in which acoustic fluctuating pressure data were acquired on flat plate TWCP specimens featuring smooth and rough surfaces. The TWCP specimens were instrumented with five Gulton microphones. The microphones placed in the model consisted of flush, ported, and backface (blind hole) locations. Several ℓ/d ported orifices were examined as well as depths from the boundary layer surface for the backface gages.

(over)

DD FORM 1 JAN 73 1473 EDITION OF 1 NOV 65 IS OBSOLETE

UNCLASSIFIED

SECURITY CLASSIFICATION OF THIS PAGE (When Data Entered)

The AEDC tests were structured to examine optimum ported orifices prior to the AFWAL Mach 6 tests. The TWCP specimens were exposed to turbulent boundary layer conditions at tunnel stagnation pressures of 700, 1400, and 2100 psi with a total temperature of 1100°R, respectively.

It was concluded that the AFWAL Mach 6 open jet facility has a high freestream noise content. The extended Reynolds number range ($>10^7$) indicated the importance of Reynolds number on acoustic algorithms for power magnitude and power spectral density. A correlation was developed for the ported hole sensors that can be related to the flush mounted sensors. Characterizing the backface (blind hole) gages with surface mounted sensors will require further data interpretation due to vibration. In general, rough walls augmented the acoustic energy levels as expected. A biased rough pattern (20° angled to flow) indicated that acoustic measurements could be used as a diagnostic technique to determine the surface characteristics of TWCP ablation patterns.

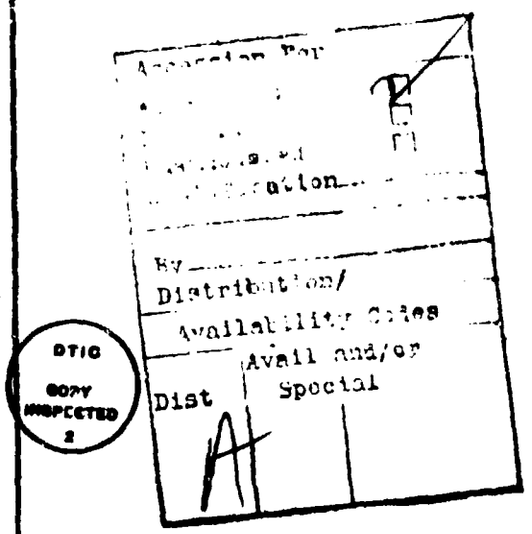

FOREWORD

The objective of the proposed program, which was supported by the AFWAL laboratory director funds, was to develop an insitu measuring technique to rank candidate ablation materials. In particular, the study was directed at evaluation of the candidate heatshield materials relative to ablation/erosion/roll torque performance. Noting the limited time and use of standard measuring techniques (acoustic microphones) the program was deemed ambitious with a high risk factor. However, the high potential as a ground test diagnostic technique and possible flight vehicle application lent the program within the scope of laboratory director funds. The potential of the orogram and the opportunity to characterize ablation materials was recognized by three branches within AFWAL, namely FIMB, FIBE and the MLBE branch of the Materials Laboratory. Also to be noted is the contributed value ($50K) accorded by Arnold Engineering Development Center (AEDC) who showed an equal interest in the project. AEDC provided a shock tube and personnel to study the ported hole gage response prior to the AFWAL Mach 6 tests.

The results of the program have demonstrated the feasibility of using acoustic sensors to characterize material ablation patterns. Moreover, the data acquired for ported holes on smooth and rough surfaces has advanced the state-of-the-art acoustic measuring techniques. It was also demonstrated that more attention should be given to data processing to determine the optimum functional acoustical format to present data. As a consequence of the high freestream noise content of the AFWAL Mach 6 open jet facility together with its high freestream Reynolds number capability, it is recommended that the data be further evaluated after freestream and boundary

layer measurements are made in the facility.

The author wishes to acknowledge the various personnel who contributed toward the effort. The list is very long and not wanting to slight anyone, only major groups will be sited. Appreciation is first extended to D. Smith (FIBE), M. Buck (FIMG) and W. Kessler (MLSE) who supported the project through the laboratory director, L. Shaw (FIBE) who was the contractor monitor and B. Strike (AEDC) who was instrumental in obtaining the funds to support the shock tube tests. Appreciation is also extended to all the AFWAL and AEDC personnel who provided the various services of data acquisition, data processing, instrumentation, model and wind tunnel support. Special thanks are extended to D. Rogers (GE) and A. Fiore (AFWAL/FIMG) whose efforts are strongly reflected in this investigation.

TABLE OF CONTENTS

		Page
SECTION 1.0	INTRODUCTION	1
	1.1 OBJECTIVES	2
SECTION 2.0	BACKGROUND	3
	2.1 PREVIOUS WORK	4
SECTION 3.0	BENCHTEST (PORTED HOLE DESIGN)-AEDC SHOCK TUBE TESTS	7
SECTION 4.0	AFWAL MACH 6 TESTS (SMOOTH/ROUGH WALLS) . .	13
	4.1 AFWAL M = 6 FACILITY	13
	4.2 MODEL DESCRIPTION	13
	4.3 INSTRUMENTATION, SIGNAL CONDITIONING AND DATA RECORDING	14
SECTION 5.0	DISCUSSION OF RESULTS	17
SECTION 6.0	ASSESSMENT	28
	REFERENCES	70
	APPENDIX A - SHOCK TUBE DATA	72
	APPENDIX B - SMOOTH WALL DATA	81
	APPENDIX B - ROUGH WALL DATA	100

LIST OF ILLUSTRATIONS

No.	Title	Page
1	Root-Mean-Square Pressure Fluctuation vs. Mach Number for Attached Turbulent Flow	38
2	Comparison of Present Normalized Spectral Measurements with Other Spectral Data and Theory	39
3	Wall Pressure Spectra. No Pressure Gradient. Outer Variable Scaling	40
4	AEDC Boundary Layer Acoustic Measurements at Mach 4	41
5	Measured Acoustic Spectra (Uncorrected for Roll-Off Due to Port Damping)	42
6	AEDC Shock Tube	43
7	AEDC Shock Tube and Test Equipment	44
8	Ported Hole Models with Acoustic Gages	45
9	Smooth Wall Ported Hole Model with Single Circumference Gage Locations	46
10	Smooth Wall Ported Hole Model with Multi-Circumference Gage Locations	47
11	Rough Wall Ported Hole Model	48
12	Response of PCB Flush Mounted Sensor	49
13	Response of Flush Mounted Gulton Microphone	50
14	Typical Response for Ported Gulton Microphone with Step Function	51
15a	Flush-Mounted Transducers - Response to Pressure Step Imposed by Shock Moving Past Surface Mounted Transducers	52
15b	Effect of Ported Hole Length to Diameter Ratio	53
16	Dynamic Response of Ported Gages Tested in AEDC Shock Tube	54
17	M = 6 Wind Tunnel Nozzle, Jet, and Collector Configuration	55
18	TWCP Specimen Mounting Plate	56
19	AFWAL Mach 6 Facility with Test Plate and TWCP Specimens	57
20	Typical Gage Location/Model Geometric Characteristics	58
21	Signal Conditioning & Data Recording	59
22	Smooth Wall Power Spectral Density for Flush Mounted Gages	60
23	Transmissibility Characteristics for a Smooth Wall Ported Hole Gage	61

LIST OF ILLUSTRATIONS (Cont'd.)

No.	Title	Page
24	Comparison of Transmissibility with Tunnel Pressure for Smooth Wall Ported Hole	62
25	Backface (Blind Hole) Gage Response for Smooth Wall Conditions	63
26	Rough Wall Power Spectral Density Distribution with Flush Mounted Sensors	64
27	Comparison of Smooth and Uniform Rough Wall Flush Mounted Sensors	65
28	Comparison of Smooth and Uniform Roughness Ported Gages	66
29	Cut-off Frequency Characteristics for Ported Cages Air Rough Surfaces	67
30	Backface (Blind Gage) Acoustic Response for Uniform Rough Wall Conditions	68
31	Backface (Blind Gage) Acoustic Response for Uniform Rough Wall Conditions	69

LIST OF TABLES

No.	Title	Page
1	Summary of Shock Tube Shots	30
2	Specimen Hole Size/Location Identification AFWAL M = 6 Test on TWCP	31
3	AFWAL M = 6 Test Matrix Acoustic/Material Response Test Program	32
4	AFWAL M = 6 Test Matrix Acoustic/Material Response Test Program	33
5	Acoustic Material Response Test Program AFWAL M = 6 Test Facility Data Reduction Requirements - Subsets . .	36
6	Effects of Roughness Direction - X-PSD Magnitude . .	37

LIST OF SYMBOLS

Bu	blowing parameter, $(C_{p_{inj}}/C_{p_{air}})(2\lambda/C_f)$
C_f	skin friction coefficient
C_p	specific heat
d	ported hole diameter
f	frequency
F_c	compressibility transformation function on skin friction
F_{k_s}	compressibility transformation function for roughness Reynolds number
F_x	compressibility transformation function for local Reynolds number
F_θ	compressibility transformation function for momentum thickness Reynolds number
h	enthalpy
k_s	equivalent sand grain roughness height
ℓ	ported (orifice) hole length
m	Sutherland viscosity exponent, $(\mu \sim T^m)$
M	Mach number
p	boundary layer static pressure
$\tilde{p}$	root-mean-square (rms) acoustic pressure
q	dynamic pressure
r	adiabatic recovery factor
Re_{k_s}	Reynolds number based on roughness height, $(\rho_e u_e k_s/\mu_e)$
Re_x	Reynolds number based on local streamwise length, $(\rho_e u_e x/\mu_e)$
Re_θ	Reynolds number based on momentum thickness, $(\rho_e u_e \theta/\mu_e)$
t	time
T	temperature

x	streamwise length
u	velocity component parallel to surface
u_τ	friction velocity, $(\sqrt{\tau_w/\rho_w})$
v	volume

GREEK SYMBOLS

γ	specific heat ratio (C_p/C_v)
δ	boundary layer thickness
δ^*	boundary layer displacement thickness
θ	boundary layer momentum thickness
λ	blowing parameter $(\rho v)_w/(\rho u)_e$
μ	molecular viscosity
ν	kinematic viscosity, (μ/ρ)
ξ^*	general parameter, defined by Equation (15b)
ρ	density
$\bar{\tau}$	time
τ	shear stress
ϕ	power spectral density
ω	frequency - radians/seconds
$\bar{\omega}$	parameter, defined by Equation (11)

SUBSCRIPTS

1,2	upstream, downstream of normal shock
aw	adiabatic wall conditions
c	compressible flow
e,∞	boundary layer edge conditions (∞ for flat plates)
i	incompressible flow
o/o	without roughness and blowing
w	wall conditions

SUPERSCRIPTS

o	total boundary layer conditions
*	Eckert reference state

1.0 INTRODUCTION

Several new candidate reentry vehicle heatshield materials have become available in the last decade. Their development has been motivated by the need for improved ablation performance which is required for the advanced missions/vehicles. As a result, the development of new fibers/resins and manufacturing techniques was initiated. However, one must still resort to conventional test techniques to evaluate these materials; namely, by arc tunnel, rocket exhaust, and flight tests. In the former two, insitu measurements consist of indepth thermocouple response and post test examination to determine the material performance characteristics. Capabilities to evaluate reentry performance have not been fully developed inasmuch as ground test facilities do not simulate all facets of the reentry environment. In flight test applications, the candidate material is exposed to nigher energy conditions; however, insitu measurements are limited and sometimes subjective in that the resulting environment is not well characterized yet these data must be used to judge the heatshield performance characteristics under full scale conditions.

More recently, a number of ground test experiments have been developed that consider a two step approach to examine specific material characteristics; for example, roll torque. The first step is to ablate the candidate material in an arc type facility and the second test, in a cold flow facility. The latter is used to determine forces (lateral/axial) that contribute to roll torque as a result of the ablation conditioning of the surface. An alternate test approach has provided useful roll torque information whereby a candidate material is mounted on a special sting/air-bearing system that allows the model to spin freely in a direction resulting from the ablation roughening process. Although roll torque data are obtained

in this manner, the rotating system does not allow for ablation performance data to be obtained. In all of the above testing, surface topography via photography and indepth post test examination have contributed significantly to the material evaluation process.

A different approach is proposed that combines many of the above concepts while providing a technique for insitu measurements to characterize and rank candidate heatshield materials. This technique consists of using acoustic technology that measures the fluctuating pressure environment (boundary layer) on the candidate material. This technique has been successfully used to characterize structural/component integrity of BRV's and aircraft. The technique was recently developed in an AFFDL sponsored program (AFFDL-TR-77-59)[1] where the pressure fluctuations were correlated to local boundary layer conditions for smooth wall surfaces. Moreover, it has been shown[2,3] that rough walls yield significant variations in pressure magnitude and power spectra thereby allowing for an opportunity to characterize rough (ablated) surfaces. The effect of roll torque can be acquired by the cross-spectral functions in spatial resolution.

1.1 OBJECTIVES

The objective of the program is to provide a technique to examine surface characteristics on tape wrapped carbon phenolic (TWCP) heatshield candidates. The technique employs the use of acoustic sensors that have been successfully used in other experimental programs to characterize boundary layer behavior with surface conditions. The experimental program consists of shock tube tests for gage/ported hole calibration and wind tunnel tests.

2.0 BACKGROUND

The methodology to be developed in this investigation will be to examine TWCP materials featuring fiber/resin/filler systems which are subjected to damage/ablation/roughness using ported and backface acoustic gages. An instrument was recently developed[4] that used a boundary layer acoustic monitor (BLAM) to determine transition onset for R/Vs. Wind tunnel tests with BLAM gages at Philco Ford and NSWC indicated the possibility of flight application. Subsequent flight tests (STM-12/STM-13) have shown that transition movement was detectable with this gage. Smooth wall TWCP specimens will be used in the proposed program to develop the backface gage response (i.e., the material transmission properties). Both bench test (shock tube) and cold flow wind tunnel tests will be used to calibrate the backface gage with the flow environment and wall shear levels. The backface gage will be compared to ported flush mounted sensors to ensure the validity of the calibration. The reason for the ported gage is to ensure the integrity of the measurements on a roughened surface, i.e., for local dynamic similarity, the hole size should be on the order of the rms roughness height, which in turn is usually less than the sensor diameter when flush mounted. A schematic of the proposed system is shown below.

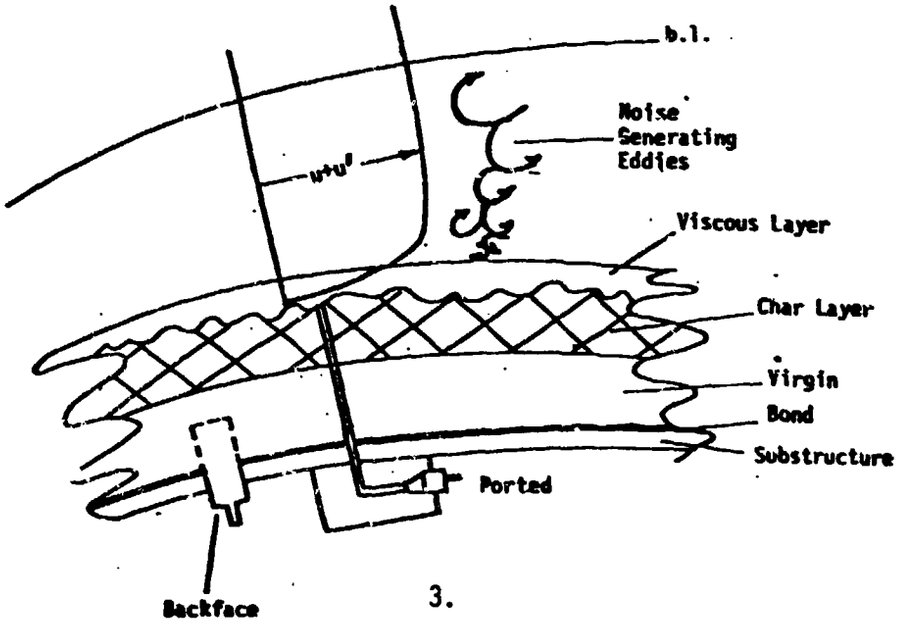

Since the fluctuating pressure field is directly related to wall shear[5], which in turn is a scaling parameter for ground/flight simulation, the power magnitude offers an attractive means to characterize candidate heatshield materials. In particular, wall shear can be directly related to ablation/roughness and subsequent roll torque behavior. An example of the latter can be found in the recent reentry heatshield performance evaluation by Martellucci, et al.[6].

2.1 PREVIOUS WORK

Figure 1 shows the predicted power magnitude (rms) compared to data and other theories. These data were obtained on a variety of model shapes and wind tunnel walls. The significant contribution of the algorithms developed in Reference 1 was the inclusion of viscous effects and compressibility on shear levels. This is noted when considering the power spectral density (smooth walls) which is functionally represented as

$$\Phi(\omega) = \Phi(\omega)\,[\tilde{p},\ (\delta^*\omega)/U_e]$$

where the displacement thickness (δ^*) and velocity (U_e) are typical characteristic length and edge velocity of the boundary layer. Figure 2 shows the normalized power spectra as a function of Strouhal number. The prediction method of Reference 1 is shown compared to data with the compressibility parameter (ϵ_T) as a parameter. It is noted that the prediction technique reduces to the classic incompressible work of Bull[7].

The above relations have been developed for smooth walls. As surface conditions change, such as ablation/roughness, the turbulent boundary shear characteristics are augmented as is the noise level. Measurements on rough surfaces have shown that

$$C_{f)rough} > C_{f)smooth}$$

and

$$\tilde{p}_{rough} >> \tilde{p})_{smooth}$$

thereby allowing for a qualitative measurement of surface characteristics. Figure 3 shows the power spectra of data from smooth and rough surfaces taken from the incompressible experiments of Burton[2]. A comparison to Figure 2 shows the power spectra distribution of Burton is in agreement with that of the classic works of Bull[7] for smooth walls. The effect of roughness on power spectra is seen in the slope for Strouhal numbers > 1. In this situation the increase in wall shear resulting from surface roughness augments the noise level and subsequently the power spectra. Variations in power spectra together with power magnitude from smooth to rough ablated surfaces will be used to characterize material behavior.

Figures 4 and 5 show acoustic measurements of flush and ported gages obtained in the AEDC von Karman Tunnel A facility at Mach 4. This unpublished work, recently uncovered, features several type acoustic sensors installed on a sharp/cone cylinder. Gage installation included flush, ported (straight and 90°), and a backface crystal. No details of port length or backface depth were provided. Figure 4 shows the model, tunnel conditions, gage installation and gage type. Figure 5 displays the acoustic spectra at several tunnel conditions. The data are uncorrected for roll-off due to port damping as was the case in the previous figures. Turbulent boundary layer conditions prevailed on the model for stagnation pressures greater than 30 ~ 35 psia. Insert Figure 5-a shows that the backface gage response is in

concert with the flush mounted sensor. This is also depicted in Figure 5-e which shows the SPL as a function of Frequency. Figures 5-b and 5-d show the acoustic spectra for various flush/ported sensors at several tunnel conditions. One notes that the ported sensors display a lower level than the flush mounted sensors with the straight port yielding a higher value than the 90° ported arrangement. Figure 5-c shows the spectra at laminar boundary layer conditions (15 psia) which can be interpreted as a measure of tunnel noise content.

Ported gages (Kulite) used in previous investigations[8] have indicated that the time response characteristics are identical to flush mounted sensors. Moreover, the Helmholtz "bottle" resonance frequencies, if the port is designed properly, will not be a problem[9] at supersonic/hypersonic conditions. It should be noted that ported designs have, in general, not been successful on TWCP reentry applications. This is a consequence of the charring/outgassing of the phenolic in the cavity as well as local conditions at the surface surrounding the cavity opening. Hence, the use of super-position of experiments, i.e., high enthalpy flow to create RV surface conditions and subsequent cold flow testing to characterize the material/environment appears as an attractive technique to assess material response. The combination of experiments together with backface acoustic sensor development can lead to insitu measurements during an actual ablation process.

3.0 BENCHTEST (PORTED HOLE DESIGN) - AEDC SHOCK TUBE TESTS

A series of shock tube tests were conducted at the Arnold Engineering Development Center (AEDC) to determine gage response characteristics relative to transform functions, rise time and Helmholtz frequency effects on ported hole (orifices) designs. Both smooth and rough surfaces were examined where the latter featured a 20 grit (0.037 inch average height) sand grain type surface. Figure 6 shows a schematic of the shock tube apparatus while Figures 7 and 8 show photographs of the apparatus and test equipment as well as the actual test models with acoustic gages. Figures 9 through 11 show schematic drawings of the models and the hole combinations that were tested. Six Gulton type MVA-2400 microphones were used in the test series. The gages were placed in the various hole combinations with one gage always flush mounted for reference. An AEDC PCB type 112A21 quartz transducer was also flush mounted to provide the test standard.

Shock tube vacuum pressure and model hole cavity volume (void between the orifice and gage diaphragm) were varied. Tests were made with a clear gage diaphragm, silicone grease coated diaphragm (as well as filling cavity) and RTV rubber coated diaphragms (which provided an exact known cavity volume). Shock tube characteristics are obtained from standard isentropic and normal shock relations. The following schematic depicts the shock tube parameters

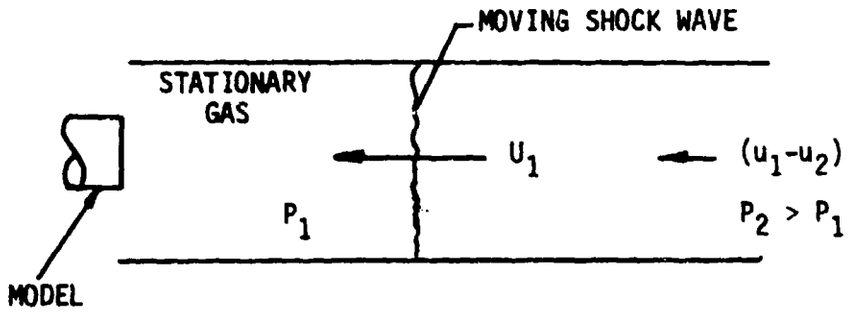

For a normal shock wave (stationary) with an observer traveling with the shock

$$M_2 = M_1 \sqrt{T_1/T_2}\ (\rho_1/\rho_2) \quad .$$

On the other hand, a moving shock requires a coordinate change (prime terms) such that

$$M_2' = \frac{C_1}{C_2} M_1 - M_2 \quad \text{for } C = \sqrt{\gamma g RT} \quad .$$

Then the Mach number traveling over the test model can be expressed as

$$\frac{M_2'}{M_1} = \sqrt{\frac{T_1}{T_2}} - \frac{M_2}{M_1} = (1 - \rho_1/\rho_2)\sqrt{T_1/T_2} \quad .$$

If one considers an average upstream Mach number M_1 of 3 together with the isentropic relations, the test Mach number becomes $M_2' = 1.36$. The ratio of total to static pressure is given by

$$\frac{P_{o2}'}{P_2} = \left[1 + \frac{\gamma-1}{2}(M_2')^2\right]^{\gamma/(\gamma-1)} = 3.0 \quad .$$

In order to have the static pressure (vacuum pressure in shock tube test section) in the range of the AFWAL M = 6 tests, the above is written as

$$\frac{P_{o2}'}{P_1} = \frac{P_{o2}'}{P_2} \cdot \frac{P_2}{P_1} \simeq 30 \quad .$$

Hence, values of vacuum pressure of 0.015 psia to 0.05 psia were tested. Finally, the response time for the ported sensors to reach maximum output is given by

$$t = \frac{128\,\mu\ell}{\pi d^4 P_f}\left[\frac{V_o}{2} + V_c\right] \ell n \frac{(P + P_f)(P_i - P_f)}{(P - P_f)(P_i + P_f)}$$

The data were recorded on a 14 channel magnetic tape. Select gages were examined on oscilloscopes during the test sequence to determine gage response to rise time. The data were processed on a Spectral Dynamic 360 Digital Signal Processor. The digitized data was subsequently placed on a transit tape that provides blocks (1024 points) of data for specific analysis time, trace patterns and transform functions for various test conditions. Table 1 shows a summary of the test shots (113 test conditions).

Figures 12 through 14 represent typical processed data. Figure 12 shows the flush mounted PCB gage with a step function drawn through the gage output response. This sensor was compared to the Gulton flush mounted sensor (Figure 13) where good agreement is noted. Figure 14 represents a typical ported gage response. Input/output transform functions are noted in terms of a scale factor in psi (or dB). Essentially, the difference (Δ) can be applied to a ported signal over the frequency range to correct the gage response to that of a flush mounted sensor. Further discussion concerning gage corrections will be given in later sections.

Figure 15 represents typical results of the AEDC shock tube results. Essentially, the shock wave imparted a pressure step of approximately 0.43 psi to the transducer over a recorded signal output of nominally 833 microseconds.

Figure 15a shows the flush mounted Gulton and PCB gage response were excellent comparison as noted. Figure 15b compares the ported hole gage response to the flush mounted sensors. Appendix A presents several runs from the AEDC shock tube tests. It should be noted that several test runs featured a blind hole gage that rendered little or no gage response depending cavity volume characteristics. These data were considered questionable due to the short time exposure and further analysis was deferred to the AFWAL M = 6 test for blind hole gage response.

One interesting aspect of the AEDC shock tube results is shown in Figure 16. Here, an estimate of the ported hole characteristics based on real time transducer output demonstrates the consistency of the calibrated results. A correlation is shown for the dynamic pressure as a function of the shock pressure and time of response. The dynamic pressure is expressed as that value for the time ($\bar{\tau}$) to reach 63.2% of the shock pressure (P_f). This is schematically shown below:

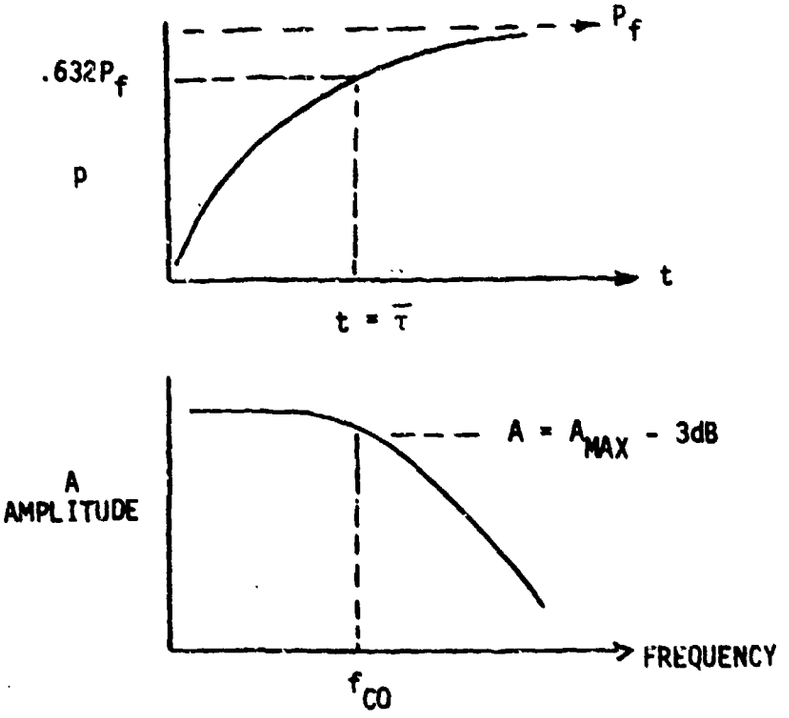

The cut-off frequency f_{co} ($= 1/2\pi\bar{\tau}$) also occurs at the 63.2% cut-off time ($\bar{\tau}$). The signal amplitude at the cut-off frequency is the maximum amplitude (A_{max}) less 3dB. If the correlation developed by the AEDC is corroborated by the AFWAL M = 6 tests, one can use the results to predict the dynamic response of any ported hole knowing the pressure field (P_f). This assumes a cut-off frequency of -3dB and a 6dB decay per octave correction. This result strongly suggests that the above phenomena can be simulated by a single pole filter resistance/capacitance circuit response. This circuit is schematically shown as

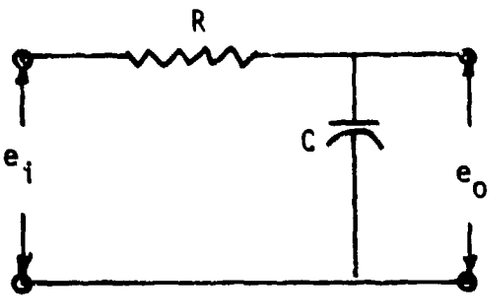

where

$$X_C = \frac{1}{\omega C}$$

$$Z = R - j/\omega C$$

$$e_o = \frac{X_C \angle -90^o}{Z} = \frac{-j}{\omega C Z} \quad .$$

At the cut-off frequency, f_{co}

$$X_C = R$$

$$Z = \sqrt{2}\, R \angle -45^o \quad .$$

The following table illustrates the power drop-off (dB) per octave at multiplicative values of cut-off frequency.

f_{co}	R	X_C	Z	θ	e_o/e_i	dB
0.5	1	-2	2.236	-63.4^o	$.894\angle -26.6^o$	- 0.97
0.8	1	-1.25	1.60	-51.3	$.781\angle -38.7^o$	- 2.14
1.0	1	-1	1.414	-45^o	$.707\angle -45^o$	- 3
1.5	1	-2/3	1.702	-33.7	$.5546\angle -56.3^o$	- 5.12
2.0	1	-1/2	1.118	-26.6^o	$.447\angle -63.4^o$	- 7
3.0	1	-1/3	1.054	-18.4^o	$.316\angle -71.6^o$	-10
6.0	1	-1/6	1.014	-9.5^o	$.154\angle -80.5^o$	-15.7
10.0	1	-1/10	1.005	-5.7	$.0995\angle -84.3^o$	-20.0

Although the above is not quite a 6dB drop per octave, it would appear possible to construct the power spectral density for flush and ported designs based on the AEDC correlation. This is schematically illustrated as follows:

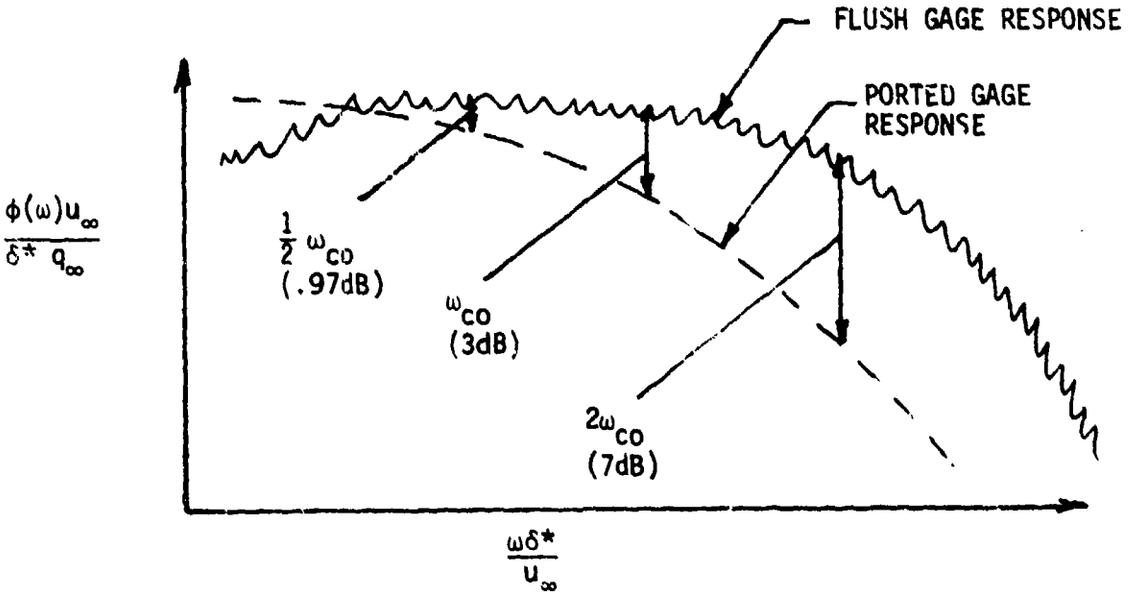

One can calculate the cut-off frequency based on port design and measure the difference between a ported and flush gage response. The AFWAL M = 6 test shculd provide an opportunity to determine if the shock tube results of AEDC can be generalized to the steady flow behavior of the AFWAL facility as well as variations in higher pressure levels.

4.0 AFWAL MACH 6 TESTS (SMOOTH/ROUGH WALLS)

4.1 AFWAL M = 6 FACILITY

The AFWAL Mach 6 high Reynolds number wind tunnel operates at a Mach number of approximately six over a unit Reynolds number range of 10^7 to 3 x 10^7 per foot. The Reynolds number is varied by changing the stagnation pressure from 700 through 2100 psia while maintaining a constant stagnation temperature of 900^{o}R. Lower values of stagnation temperature (900^{o}R) are possible. The facility's maximum running time is approximately 100 seconds (high unit Reynolds number condition). Figure 17 shows a schematic of the facility. Flow field angularity has been shown to be negligible during several calibration tests. Further details or the Mach 6 facility can be obtained in Reference 10.

4.2 MODEL DESCRIPTION

The model used in the M = 6 tests consists of a flat plate geometry approximately 15 inches by 14 inches with a 3 inch by 8.5 inch trailing section. The TWCP specimens were mounted on the trailing plate and flush aligned with the leading section. Figure 18 shows the trailing section of the mounting plate while Figure 19 shows the model and specimens in the AFWAL Mach 6 facility. The TWCP specimens consisted of two smooth and two roughened models. One smooth model consisted of ported holes while the other contained blind holes at various depths. In both cases a flush mounted sensor was installed for reference. The rough model consisted of a machined square pattern that

was 0.040 inch x 0.040 inch x 0.020 inches high. One of the rough models was cut 20^{0} biased to the flow direction with the same pattern. In both cases, ported holes were located in the specimens. For the blind hole rough wall tests, the smooth specimen (SM-2) previously tested was machined to the above roughness pattern giving three actual specimens. In order to accommodate a range of l/d orifices, the specimens (smooth/rough) were drilled to a larger diameter and the tests were repeated. Figure 20 shows a typical TWCP specimen and the acoustic gage locations while Table 2 identifies specimen hole size and location. The specimens are 3 inches by 3 inches and approximately 0.040 inches thick The gages were located to investigate longitudinal, lateral and cross-flow spectra of the boundary layer when subject to smooth and rough surfaces.

4.3 INSTRUMENTATION, SIGNAL CONDITIONING AND DATA RECORDING

The accompanying block diagram (Figure 21) shows the signal conditioning and data recording system. Eleven foot lengths of high temperature miniature coaxial cable coupled the signals from the ten Gulton quarter-inch microphones out of the wind tunnel to in-line unity-gain Kistler Model 558 impedance converters which preserved the best possible signal-to-noise ratio while driving the long coaxial cables to the control room. Intech auto-gain amplifiers were used to provide the gain necessary to attain signal levels close to the tape recorder full-scale values in order to fully utilize the available dynamic range. The auto-gain feature of the Intech amplifiers was not used because of the short test time and the large transient signal levels encountered during model injection into the flow. Fixed gains, based on anticipated signal levels, were used and the commutated, pulse amplitude modulated Intech gain indicator outputs were recorded on one track of the

magnetic tape. A portable oscilloscope was used to observe the tape recorder input signal levels.

All data were recorded using a Honeywell Model 100, 14 track tape recorder with all microphones in a given test specimen recorded by the same head in order to minimize time displacement errors. Time code information was also recorded on one track and voice commentary was put on an edge track in order to assure proper data identification. Quick-look analysis capability was provided by a Spectral Dynamics Model SD312 third-octave analyzer and by Vu-Data monitor oscilloscopes.

Tables 3 and 4 show the complete AFWAL Mach 6 test matrix. The former represents the smooth wall tests while the latter the rough wall tests. A comment section has been added to indicate test peculiarities and model gemoetric changes. One should also note the comments concerning location of the flush mounted gages during the rough wall tests. Here, the location of the gage relative to the roughness height was examined to determine optimum effectiveness. The tables were structured in terms of AFWAL test # (and date) together with acoustic recording number. Model identification, facility pressure levels and hole size changes are also recorded. Acoustic gage identification has also been recorded to ensure proper gain factors during data processing.

A two channel analyzer was used at WPAFB to examine the smooth wall results. A transmissibility function was identified to characterize ported and backface gages relative to the flush mounted sensors. However, the backface gage response will require further analysis and interpretation. The transmissibility function is defined as

$$\sqrt{PSD/PSD_{ref}}$$

where PSD_{ref} is the power spectral density of a reference gage; in this case the flush mounted sensor. On the basis of the brief analysis provided by the two channel analyzer, a data subset of Tables 3 and 4 was made for further analysis. Table 5 contains the data subset as well as analysis required for the AFWAL Mach 6 tests. Twelve test conditions have been selected. This includes four (4) smooth wall and eight (8) rough wall tests. The latter are contained on two tapes. The table shows the acoustic record number, data, tape number and tunnel pressure condition for proper identification. Also shown are the specimens (model) and gage or recorder number. There are five gages on each specimen and two specimens were tested at each tunnel condition. In addition to the above, acoustic plotting requirements have been identified, together with appropriate gages, as well as a comment column.

Three acoustic parameters were sited for plotting purposes. These included the power spectral density (PSD) as a function of frequency (not 1/3 octave band), transmissibility and X-PSD also as a function of frequency. The reference PSD, identified on Table 5, is the flush mounted sensor on one/or both specimens. Although several X-PSD have been identified, only the magnitude was obtained as opposed to the real and imaginary components. This was a consequence of examining the relative magnitude difference between smooth, rough (square uniform pattern) and rough-biased pattern. Co and Quad functions were not generated for this report. Appendix B contains selected processed data from the subset of Table 5.

5.0 DISCUSSION OF RESULTS

Relative to the objectives of the program,i.e., to characterize TWCP material as potential roll torque contributors, the study clearly indicates that the acoustic methodology can be used to determine cross flow behavior due to roughness. The above was demonstrated using flush and ported sensors in a cold flow (T_∞^0 = 1100^{0}R) facility. However, use of backface (blind gages) to characterize boundary layer behavior requires further analysis of the processed data.

The AFWAL Mach 6 facility operates in a free stream Reynolds number range of 1 to 3 x 10^7. The specimens were located 18.5 inches from the test model leading edge giving a local Reynolds number value of 1.5 to 4.5 x 10^7. This high Reynolds number characteristic is an order of magnitude greater than that experienced in previous wind tunnel acoustic tests (for example, AEDC von Karman Tunnels A and B, NSWC Mach 8 and NASA Ames Mach 4, 8, and 10 facilities). Moreover, the open jet and collector AFWAL Mach 6 type facility is known to have significant free stream noise characteristics. Figure 22 demonstrates this behavior. Smooth wall PSD distributions are shown for flush mounted acoustic gages at two facility operating pressures. In both cases, the signal is generally linear out to 20 KHz as opposed to the roll-off characteristics that are associated with acoustic gages for frequencies $\geq$ 10KHz. In order to assess the contribution of free stream noise to boundary layer noise, the algorithms developed in Reference 1 were used to predict both power magnitude (rms pressure) and PSD. The following tunnel conditions were used:

$M_\infty = 5.88$, $U_\infty = 3400$ ft/sec, $T^0_\infty = 1100^0R$

p^0_∞ (lb_f/in^2)	P_∞ (lb_f/in^2)	q_∞ (lb_f/ft^2)	δ^* (ft)
700	.502	12.145	0.0155
1400	1.00	24.29	0.01325
2100	1.502	36.435	0.01217

The power magnitude is expressed as

$$\tilde{p}/q_\infty = 0.006\ \varepsilon_T \tag{1}$$

where the compressibility factor, ε_T, based on adiabatic wall conditions becomes

$$\varepsilon_{T_{aw}} = (1 + 0.13\ M_\infty^2)^{-0.64} \quad . \tag{2}$$

In the above, the rms pressure is defined as

$$(\tilde{p})^2 = \int_0^\infty \phi(f)df = \int_0^f \phi(f)df + \int_f^\infty \phi(f)df \tag{3}$$

The PSD is given as

$$\frac{\phi(\omega)u_\infty}{q_\infty^2\ \delta^*} = \frac{(.006)^2\ \varepsilon_T\ \frac{2}{\pi}}{1 + \frac{1}{\varepsilon_T^4}\left(\frac{\omega\delta^*}{u_\infty}\right)^2} \tag{4}$$

and as $\omega \to 0$, Eq. (4) becomes

$$\phi(\omega \to 0) \simeq \frac{q_\infty^2\ \delta^*}{u_\infty}\ \left(\frac{2}{\pi}\right)\ \varepsilon_T\ (.006)^2 \quad . \tag{5}$$

Measured values of the power magnitude were approximately 1/5 of the calculated values. This could imply that free stream noise is the dominating mode or that the energy level was not sufficiently integrated into the frequency spectrum $\geq$ 20 KHz. This would indicate that the second integral term on the RHS of Eq. (3) is a significant contribution to the power magnitude. Normally, this portion of the spectrum can be neglected due to the roll-off of the PSD distribution at frequencies $\geq$ 20 KHz. To ensure that this interpretation is correct, one can measure the PSD at low frequencies ($\leq$ 500 Hz) and compare the results to calculated values using Eq. (5). If indeed the free stream noise content is the dominating source, then the ratio of PSD measured to calculated should be $\simeq$ 1/25 as suggested by the definition of power magnitude (Eq. (3)). Using the Mach 6 facility parameters together with Eq. (5), the ratio of measured to calculated PSD for $f \rightarrow 0$ was determined to be $\simeq$ 1/5 thereby indicating that the signal is measuring boundary layer noise as well as free stream noise.

A further check was made on the PSD distribution by calculating the level at 20 KHz. Equation (4) was used together with the facility parameters and it was determined that the mean of the measured value was approximately twice the calculated value. Again, the above gives evidence that the measured noise source is boundary layer as well as free stream. It is concluded that the high Reynolds number capability of the AFWAL Mach 6 facility together with the open jet characteristics can lead to a combined high energy content yielding uniform PSD levels out to and beyond 20 KHz.

Figure 23 shows the transmissibility within the frequency spectrum for a smooth wall ported sensor. The ported gage response is normalized by the flush mounted sensor (PSD_{ref}). If one considers the correlation developed in the AEDC shock tube tests, the cut-off frequency for the ported hole is f_{co} = 2.65 KHz. Moreover, the cut-off frequency should occur at 3 dB from the reference level (in this case the flush sensor). Since the ordinate represents the square root of the PSD ratio, then the definition of the sound pressure level would yield

$$3dB = 20 \log_{10} p/p_{ref}$$

and p/p_{ref} = 0.707. An inspection of Figure 23 indicates that the AEDC correlation works for the smooth wall ported hole tested at Mach 6. One should also note the cylic behavior of the ported sensor for f > 5 KHz indicating a possible resonance (Helmholtz) condition.

Figure 24 shows the transmissibility function at two levels of tunnel pressure. In both cases, the ported hole was normalized by the flush mounted sensor for the smooth wall conditions. The higher tunnel pressure condition is normally the same as that of the lower pressure. The cut-off frequency for the ported design was calculated to be 6.3 KHz. For this test case, the measured results are higher than the calculated value. However, the signal appears to be dropping off toward the calculated value at the point where possible resonant conditions may prevail.

Figure 25 shows a typical response for the backface (blind hole) gage response. The transmissibility function is displayed over the frequency spectrum where the backfaced gages were normalized by the flush mounted sensor. Both PSD (shown in Appendix B) and the transmissibility function show a very erratic behavior. One trend is noted that relates to the depth of the gage relative to the specimen surface; namely, that the pressure decreases with depth of the sensor. It is also interesting to note that gages close to surface respond much like the flush mounted sensors. Moreover, the signal reduction with depth suggests the possibility of developing a correlation to the flush mounted sensors. However, the erratic nature of signal should be studied together with material characteristics before attempting any correlation.

Figures 26 and 27 display the PSD distributions for uniform rough wall flush mounted sensors at the three tunnel test pressures. In Figure 26, the PSD level is seen to increase with tunnel stagnation pressure as noted for the smooth wall case (Figure 22). However, a significant up-swing in the signal occurs for frequencies $\geq$5 KHz. This characteristic is opposite to that of the smooth wall results where roll-offs are expected. This phenomenia cannot be fully explained. It is evident that energy is boundary layer related. One possible explanation is the occurrence of shocks emanating from the roughness pattern in the boundary layer. These shockletts can contribute low scale eddies in the higher frequency range thereby causing the increase in PSD distribution. Figure 27 compares the rough and smooth wall PSD distributions at the

upper and lower tunnel pressures. In both cases the rough wall yields higher PSD's and subsequent power magnitude. The normalized power magnitude of rough to smooth rms pressure in of the order of 1-1/2. The increase in power magnitude and PSD with roughness is in agreement with the incompressible work of References 2 and 3.

Figures 28 and 29 show the uniform rough wall effects with ported holes. In Figure 28 two ported hole locations are compared to a comparable position for a smooth wall condition. The PSD's are shown in terms of the transmissibility function. A variation exists for two identical holes at two locations on the specimen (i.e., position 4 and 10). This result was typical of many of the tests. An examination of the Mach wave generated from the leading edge of the test model indicated its potential effect along the left leading edge of the specimen (position 4) which could result in higher PSD values. When comparing to the smooth wall result, one notes the absence of the cyclic nature above 5 kHz for the rough models. Moreover, the ported gage response for rough surfaces (for many test cases) did not appear to be as erratic as the smooth surface. Figure 29 shows a test condition where the gage response is not as clear as the previous case. Two ported holes are shown with the same ℓ/d ratio of the ported hole. If one considers the AEDC correlation, a cut-off frequency of 750 Hz occurs which is shown to be lower than the 1/32" diameter hole and higher than the 1/64" diameter hole. In general, the AEDC correlation for cut-off frequency did not appear to work for the rough wall cases. The measured p/p_{ref} were normally greater than prediction.

Figures 30 and 31 show the backface (blind hole) gage response for uniform rough wall conditions. The data are compared to comparable smooth wall conditions. For the shallow depth locations ($\leq$ 1/8 inch) the rough wall transmissibility function shows lower pressure levels than the smooth wall case. On the other hand, the deeper locations ($\geq$ 3/16 inches) tend to have the same characteristics for both smooth and rough walls. As in the smooth wall test cases, data interpretation is very difficult and will require further examination.

As noted previously, the power magnitude of the X-PSD were examined to determine the effect of biased roughness (i.e., when the uniform 0.04 inch x 0.04 inch x 0.020 inch high pattern was skewed 20^{o} to the flow direction - Figure 20). Co and Quad cross-correlation functions were not obtained due to timing constraints of the program. If the power magnitude of the X-PSD showed a significant effect, further data processing would be warranted. Table 6 has been constructed to indicate the X-PSD power magnitudes. Smooth, uniform and biased rough wall conditions are shown. The X-PSD locations are identified on Table 5 and subsequent hole locations in Figure 20. It is clearly seen that the X-PSD power magnitude for the biased rough surface shows a higher level than the corresponding smooth or uniform rough cases at all tunnel pressure conditions. The one exception is location 9-7 for test run number 20. However, reduced data show gage 9 to be questionable. The fact that the X-PSD power magnitudes for the smooth and uniform rough cases are approximately the same indicates that acoustic sensors can be used to characterize ablated TWCP specimens for potential roll torque contributors.

The effects of roughness on the power magnitude can be evaluated by considering the wall shear in a boundary layer with a rough surface.

If one considers the classic Prandtl-Schlichting skin friction law (with/without roughness), there results

$$C_{f_i} = [2.87 + 1.58 \log \frac{x}{k_s}]^{-2.5} \tag{6}$$

and

$$C_{f_{i,o/b}} = [2 \log_{10} Re_{x_i} - 0.65]^{-2.3} \tag{7}$$

where the subscripts i and o/b represent incompressible and non-roughness/non-blowing, respectively. It should be noted that Seidman[11] examined several incompressible skin friction laws and found all to be bracketed by the above on the high side and by Droblenkov[12] on the low side. Equations (6) and (7) will be transformed into the compressible plane using a technique by Laganelli et al.[13] based on the Eckert reference enthalpy. This technique was developed from the work of Spalding et al[14]. The transformation equations with blowing, but not roughness, are given as:

$$\frac{C_{f_i}}{C_{f_c}} = F_c^* = \frac{\rho_e}{\rho^*} \left[\frac{2}{B_u} \left(\sqrt{1 + B_u} - 1\right)\right]^{-2} \tag{8}$$

$$\frac{Re_{\theta_i}}{Re_{\theta_c}} = F_\theta^* = \mu_e/\mu^* \, (1 + B_u)^{-\bar{\omega}} \tag{9}$$

$$\frac{Re_{x_i}}{Re_{x_c}} = \frac{F_\theta^*}{F_c^*} = F_x^* = \frac{\mu_e}{\mu^*} (1 + B_u)^{-\bar{\omega}} \frac{\rho^*}{\rho_e} \left[\frac{2}{B_u} \left(\sqrt{1 + B_u} - 1\right)\right]^2 \tag{10}$$

where

$$B_u = (C_{p_{inj}}/C_{p_{air}}) \frac{(\rho v)_w}{(\rho u)_e} \frac{1}{c_f/2} \tag{11a}$$

and

$$\bar{\omega} = (h_w/h_e)^{-1/8} + \frac{1}{8} M_e \tag{11b}$$

Subscripts θ and x indicate values based on momentum thickness and streamwise length respectively, while the asterisk (*) refers to properties based on the Eckert reference enthalpy (with surface blowing)

$$\frac{h^*}{h_e} = \frac{1}{2} + \left(1 + \frac{h_w}{h_e}\right) + .22r\left(\frac{\gamma-1}{2}\right) M_e^2 \quad . \tag{12}$$

To account for the effects of roughness on skin friction in the absence of blowing, Fenter[15] employed a transformation function technique using the van Driest transformation. Several parameters were required depending on the range of the roughness Reynolds number. Winter and Gaudit[16] considered a transformation function for roughness that assumes F_c and F_θ remain invarient with roughness. Further they assumed that wall conditions influence the flow through the roughness function in the form

$$f = f\left(\frac{k_s u_\tau}{\nu_w}\right)$$

and therefore that the required equivalent value of Rek_s should give the same value of $k_s u_\tau/\nu_w$ as for incompressible flow. Hence, we define

$$F_{k_s} = \frac{Rek_{s,i}}{Rek_{s,c}} = \left(\frac{\rho_e}{\rho_w}\right)^{1/2} \left(\frac{\nu_e}{\nu_w}\right) \left(\frac{1}{F_c^*}\right)^{1/2} \quad . \tag{13}$$

In the above, F_c^* has been adopted to account for blowing effects, i.e., if Equation (7) allowed for $B_u \to 0$, then $F_c^* = F_c = \rho_e/\rho^*$ which is the non-blowing transformation function.

When Equations (7) through (10) and (13) are substituted into Equations (6) and (7), the skin friction normalized by the non-blowing/non-roughness value ($C_{f_{o,o}}$) becomes:

$$\frac{C_f}{C_{f_{o/o}}} = \frac{\left[\frac{2}{B_u}\left(\sqrt{1+B_u}-1\right)\right]^2 \left[0.8686\ (\ell n \mathcal{J} + \ell n Re_x) - 0.65\right]^{2.3}}{\left[2.87 + 0.6862\left(-\ell n \xi^* + \ell n \frac{Re_x}{Re_{k_s}}\right)\right]^{2.5}} \tag{14}$$

where

$$\mathcal{J} = F_x = \left(\frac{h^*}{h_e}\right)^{-(m+1)} \tag{15a}$$

and

$$\xi^* = \left(\frac{F_x^*}{F_{k_s}^*}\right)^{-1} = \left(\frac{h^*}{h_e}\right)^{(m+1/2)} \left(1 + r\,\frac{\gamma-1}{2} M_e^2\right)^{-(m+1/2)} \left(\frac{h_w}{h_{aw}}\right)^{-(m+1/2)} \cdot \frac{(1+B_u)^{\omega}}{\left[\frac{2}{B_u}\left(\sqrt{1+B_u}-1\right)\right]} \tag{15b}$$

It should be noted that the transformation functions appearing with asterisks (*) represent blowing conditions. If one allows $B_u \to 0$, all transformation functions reduce to the basic non-blowing values found in classical literature. Moreover, the viscous properties μ^* and ρ^* are related to h^* through the Sutherland viscous relation $\mu^* \sim (T^*)^m$ and the equation of state $\rho^* \sim \frac{1}{T^*}$. The Sutherland equation can be used to determine the viscous exponent (m). For the present investigation a value of m = 4/5 was used. The above technique was recently developed by Laganelli and Sontowski[17].

If one considers the AFWAL Mach 6 facility conditions for air adiabatic wall with no mass transfer (Bu = 0), Equation (14) becomes:

$$\frac{C_f}{C_{f_{o/o}}} \simeq \frac{3. \times 10^2}{\left[4.6 - 0.69\ \ell n\ k_s\right]^{2.3}} \tag{16}$$

The actual roughness pattern used in the experiments consisted of a 0.040 inch x 0.040 inch x 0.020 inch high matrix. The above equations are based on a sandgrain rough surface. An equivalent sandgrain roughness height can be obtained by considering the projected area of the actual roughness height and spacing to the stream flow, i.e., the exposed surface area of the roughness element. Dirling[18] developed a technique to obtain an equivalent sandgrain roughness which can be expressed as

$$k_s/k_{actual} = 0.0164\ \lambda^{3.78} \tag{17}$$

for $\lambda = (Dk_{act})(A_p/A_s)^{-4/3}$. The parameter A_p/A_s is one for the tested roughness pattern while the spacing (D) to actual height ratio D/k_{act} is 2. The equivalent sandgrain roughness height ratio becomes $k_s/k_{act} = 0.225$ providing a value of k_s of 0.0045 inches.

The power magnitude (Figure 1) can then be written as

$$\left(\frac{\tilde{p}}{q_\infty}\right)_{rough} \simeq (0.006)\mathcal{F}_{T_{aw}}\ (C_f/C_{f_{o,o}}) \tag{18}$$

Using the equivalent sandgrain roughness (k_s = .0045 inches) Equation (16) becomes $C_f/C_{f_{o,o}} = 1.5$. Since $C_f/C_{f_{o,o}}$ is unity for smooth walls, the power magnitude should be augmented by 50% for the rough wall conditions. Measurements (Figure 27) have shown that $\tilde{p}_{rough}/\tilde{p}_{smooth}$ is on the order of 1.5 confirming the above calculation.

6.0 ASSESSMENT

The objective of the program was to characterize and rank material performance relative to ablation and possible roll torque contribution. In the process, the techniques developed could be used to provide insitu ablation test measurements as well as a possible technique for flight vehicle application. The program was deemed ambitious with high risk and high payoff. Although the data analyses will require further interpretation to assess the backface gage response, the program objectives are considered a success relative to using acoustic measuring techniques.

The smooth wall tests indicated that the AFWAL Mach 6 open jet facility has a high freestream noise content. Moreover, the high freestream Reynolds number capability of this facility indicates a significant Reynolds number effect on prediction of power magnitude and power spectral density. The ported hole response appeared to follow the AEDC prediction based on a cut-off frequency. Possible resonance conditions tended to occur for frequencies greater 6 kHz. The uniform PSD distribution over the spectrum suggested the analogy of an electrical RC curcuit to predict power characteristics. The backface gages tended to behave as the flush mounted sensors for depths $\leq$ 1/8 inch.

The rough wall tests presented several interesting phenomena. At all three test pressures, the flush mounted sensors in the rough surface displayed PSD's that tended to up-swing at frequencies greater than 10 kHz. This condition is opposite that expected where a roll-off occurs in the same frequency range. Since the smooth wall tests showed some roll-off, it is speculated that the increase in acoustic energy is a consequence of shocks emanating from the roughness patterns, a condition clearly observed from

Schlieren coverage of the tests. A technique is shown that predicts power magnitude for a rough surface. Measurements show that the power magnitude is greater for rough surface supporting the prediction method. The AEDC correlation did not appear to work for the ported gages on the rough surface. The ported sensors generally showed higher energy levels than those for a smooth wall, a condition that could be expected. No attempt was made to correlate the roughness effect. The backface gages in the rough wall specimens tended to show less energy than the smooth wall for depths $\leq$ 1/8 inch. For depths greater than 1/8 inch, both smooth and rough wall response appeared to be the same.

In the case of biased roughness (uniform pattern 20^{o} from flow direction), a definite direction characteristic was measured from the magnitude of the X-PSD's. These measurements clearly demonstrate that cross-spectra functions can be used to provide ablation pattern characteristics of candidate TWCP specimens. It should be noted that the power magnitude of the X-PSD's for both smooth and uniform rough walls were of the same order, a condition that was expected.

The backface gage measurements will require further interpretation. The constraint of mounting the gage in the TWCP specimen could have led to vibration problems as depicted in the processed data. Moreover, vibration of the gage cables also could have contributed to the problem. The technique used for gage mounting, i.e., direct drill/tap for the microphone head, actually simulated an accelerometer. Finally, the cavity volume for the backface gages appeared to be critical relative to signal response while it did not appear critical for the ported gages. In the latter case, orifice resonance would dominate.

TABLE 1. SUMMARY OF SHOCK TUBE SHOTS

SLEEVE	DATA SHOTS		TRIAL SHOTS	DATE
SMOOTH-1	25		5	3/10/81
SMOOTH-1 (with grease)	5		1	3/11/81
		30		
SMOOTH-2	5		1	3/11/81
SMOOTH-2	17		3	3/12/81
		52		
ROUGH-SG-1	-		3	3/12/81
SMOOTH-2	5		0	3/13/81
ROUGH-SG-1	3		0	3/13/81
		60		
	-		-	3/16/81
ROUGH-SG-1*	7		2	3/17/81
ROUGH-SG-1*(no cap on PCB)	15		8	3/17/81
		82		
SMOOTH-1* (no cap on PCB)	17		5	3/18/81
noise records SMOOTH-1* (no cap on PCB)	2		6	3/18/81
		101		
SMOOTH-2* (no cap on PCB)	12		2	3/19/81
TOTALS	113		30	

*RTV caps on transducer diaphragms
Gulton gages capped at all times
PCB gage capped for first seven runs

TABLE 2. SPECIMEN HOLE SIZE/LOCATION IDENTIFICATION

AFWAL M = 6 TEST ON TWCP

TEST SPECIMEN	HOLE LOCATION	HOLE SIZE(d) INCHES	HOLE DEPTH(L) INCHES	NEW HOLE DIA. (INCHES)	GAGE #	COMMENTS
SM-1* (Smooth)	1	1/16 P	1/8	.101 P	1015	Holes were opened to 0.101" Dia. for acoustic record #'s 43-47
	2	1/16 P	1/8	.101 P	1019	
	3	Flush	--	--	1010	
	4	1/16 P	1/4	.101 P	1025	
	5	1/16 P	1/4	.101 P	1044	
SM-2 (Smooth)	1	1/4 B	1/16		1007	
	2	1/4 B	1/8		1013	
	3	Flush	--		1017	
	4	1/4 B	3/16		1036	
	5	1/4 B	1/4		1024	
SM-2 (Rough)	1	1/4 B	1/16			Machined pattern of 0.04" x 0.04" x .02" (Square Pattern)
	2	1/4 B	1/8			
	3	Flush	--			
	4	1/4 B	3/16			
	5	1/4 B	1/4			
SG-1 (Rough)	1	1/64 P	1/4	1/32 P	1017	Machined square pattern .04" x .04" x .02" holes were opened
	2	1/32 P	1/4	1/16 P	1019	
	3	Flush	--	--	1047	
	4	1/64 P	1/8	1/32 P	1025	
	5	1/32 P	1/4	1/16 P	1043	
SG-2 (20^{o} Rough)	1	1/32 P	1/4		1007	Biased (20^{o}) machine pattern .04" x .04" x .02"
	2	1/16 P	1/4		1013	
	3	Flush	--		1010	
	4	1/32 P	1/8		1036	
	5	1/16 P	1/8		1024	

* SEE DWG DIAGRAM FOR HOLE LOCATIONS (Figure 20)

TABLE 3. AFWAL M = 6 TEST MATRIX

ACOUSTIC/MATERIAL RESPONSE TEST PROGRAM
AFWAL M = 6 FACILITY
T_∞° = 1100°R - SMOOTH WALL TESTS

TEST #	ACOUSTIC RECORD #	PRESSURE (PSIA)	SPECIMENS	COMMENTS*
12	39	700	SM-1/SM-2	• SM-1 has 1/16" holes (see specimen hole size/location I.D. table • Shocks from leading edge area
13	40	2100	SM-1/SM-2	
14	41	700	SM-1/SM-2	Repeat of #12 - higher OASPL experienced - believe due to T_w
15	42	2100	SM-1/SM-2	Repeat of #13
	Holes on SM-2 opened to 0.101" dia			
16	43	700	SM-1/SM-2	
17	44	2100	SM-2/SM-2	
18	45	700	SM-2/SM-2	Repeat of #16
19	46	1400	SM-2/SM-2	Model should show T_w effects due to prolonged flow exposure
20	47	2100	SM-1/SM-2	

* Above tests were conducted on 6/18/81. Several tests were conducted on 6/9 and 6/17/81 that are considered invalid due to noise/saturation electronic problems.

Inserts were mounted around specimens to ensure flow continuity from leading section

TABLE 4. AFWAL M = 6 TEST MATRIX

ACOUSTIC/MATERIAL RESPONSE TEST PROGRAM
AFWAL M = 6 FACILITY

T_∞° = 1100°R - ROUGH WALL TESTS* (8/4-6/81)

TEST #	ACOUSTIC RECORD #	PRESSURE (PSIA)	SPECIMEN (.04x.04x.02)	COMMENTS
1	11	700	SM-2/SG-1**	Flush gage on SG-2 has 0.030" ~ .040" RTV pad - see specimen hole/location I.D. table
2	12	1400		Aborted
3	13	1400		Excellent Schlieren
4	14	700		Aborted - pressure vent problem
5	15	700		
6	16	1400		Aborted - control valve problem
	8/5/81			
1	17	700	SM-2/SG-1	• SG-1 flush sensor at top of roughness • SM-2 flush sensor at bottom • Weak shocks @ leading edge • Improved Schlieren
2	18	1400	SM-2/SG-1	
3	19	2100	SM-2/SG-1	Increasing P_∞° shows excellent shocklets emanating from roughness
4	20	2000	SM-2/SG-1	Couldn't get enough pressure
5	21	2000	SM-2/SG-1	for 2100 psia

** SM-2 flush sensor located at bottom of roughness pattern
SG-1 flush sensor located at top of roughness pattern
(both RTV pads are smooth)

* The entire model - including TWCP specimens and inserts - was machined to 0.04" x 0.04" x 0.02" deep roughness pattern the specimens have been identified as SM-2 (with roughness pattern) and SG-1 and SG-2. SG-2 was machined with a 20° biased pattern to give a potential acoustic direction (@ roughness).

TABLE 4. AFWAL M = 6 TEST MATRIX

ACOUSTIC/MATERIAL RESPONSE TEST PROGRAM
AFWAL M = 6 FACILITY

T_∞° = 1100°R - ROUGH WALL TESTS(CONT'D)

TEST #	ACOUSTIC RECORD #	PRESSURE (PSIA)	SPECIMEN (.04x.04x.02)	COMMENTS
6	22	700	SM-2/SG-1	SM-2 flush gage 0.005" from bottom SG-1 flush gage 0.010" from bottom also backed out gage positions 1 & 4 on SG-1 one turn (cavity)
7	23	2100		
8	24	2100		Repeat of #23
9	25	700		Repeat of #22 - T_w effects possible due to flow exposure
	tape change (#2)			
10	1	2100	SM-2/SG-1	• Hole pattern dia. change (see hole-location I.D. tabel) on SG-2
			SM-2:	• Removed gages 2 (1013) and 5 (1024) gage 1 (1007) backed out 2 turns-flush (1010) positioned .005" from bottom
11	2	1400	SM-2/SG-1	• Excellent Schlieren and Test-gage response from Record #1 to #6
12	3	700		
13	4	2100		
14	5	1400		• Record #2 to #6 has gages located as described in #1 comment
15	6	700		

TABLE 4. AFWAL M = 6 TEST MATRIX

ACOUSTIC/MATERIAL RESPONSE TEST PROGRAM
AFWAL M = 6 FACILITY

T_∞° = 1100°R - ROUGH WALL TESTS(CONT'D)

TEST #	ACOUSTIC RECORD #	PRESSURE (PSIA)	SPECIMEN (.04x.04x.02) NORMAL/BIASED	COMMENTS
	8/6/81	TAPE #2		
1	17	2100	SG-1/SG-2	• Replaced SM-2 with SG-2 (biased roughness pattern) • SG-2 flush sensor (1047) has RTV pad cut to 0.04 x .04" pattern - top • SG-2 gage (1010)-Position 5 - switched to position 9 (1024) • Significant effect on shocklets (Schlieren) due to biased pattern • SG-2 flush sensor at bottom
2	18	1400	SG-1/SG-2	
3	19	700	"	
4	20	2100	"	Outstanding Schlieren
5	21	1400	"	
6	22	700	"	Above represent excellent set of data
	MODEL CHANGE			
7	23	2100	SG-1/SG-2	All gages backed out 1/4 ~ 1/2 turn on SG-2 (except flush sensor)
8	24	1400		
9	25	700	"	Above excellent data set

TABLE 5. ACOUSTIC MATERIAL RESPONSE TEST PROGRAM AFWAL M = 6
TEST FACILITY DATA REDUCTION REQUIREMENTS - SUBSETS

ACOUSTIC RECORD #	DATE	P_{∞}^{o} (PSIA)	TAPE #	MODEL	GAGES (RECORDER #)	PSD_{ref}	PSD*	$\sqrt{PSD/PSD_{ref}}^{*}$	X-PSD*	COMMENTS
SMOOTH-WALL										
39	6/18/81	700	1	SM-1	1,3,5,7,9	#5	ALL	ALL	(1-7)&(5-7)	SM-1 @ 1/16"D HOLES
				SM-2	2,4,6,8,10	#5	ALL	ALL	-	
40		2100	1	SM-1	↓	#5 & #6	ALL	ALL(BOTH)	(1-7)&(5-7)&(3-9)	
				SM-2	↓	#5	ALL	ALL	-	
43		700	1	SM-1	↓	#5	ALL	ALL	-	SM-1 @ 0.101"D HOLES
				SM-2	↓	#5	ALL	ALL	-	
44		2100	1	SM-1	↓	#5	ALL	ALL	-	
ROUGH-WALL										
17	8/5/81	700	1	SM-2	1,3,5,7,9	#5	ALL	ALL	-	• SG-1 @ 1/6" & 1/32"D HOLES
				SG-1	2,4,6,8,10	#5	ALL	ALL	-	• SM-2 FLUSH SENSOR AT BOTTOM
19		2100	1	SM-2	↓	#5	ALL	ALL	-	OF ROUGHNESS PATTERN
				SG-1	↓	#5(SM-2)	ALL	ALL	-	
2		1400	2	SG-1	↓	#5(SM-2)	ALL	ALL	-	• SG-1 @ 1/32" & 1/16"D HOLES
3		700	2	SG-1	↓	#5(SM-2)	ALL	ALL	(2-8)&(4-10)	
4		2100	2	SG-1	↓	#5(SM-2)&#6	ALL	ALL(BOTH)	(2-8)&(4-10)&(6-8)	
18	8/6/81	1400	2	SG-1	2,4,6,8,10	#9	ALL	ALL		• SG-1 HAS ROUGH RTV PAD
				SG-2	1,3,5,7,9	#9	ALL	ALL		• SG-2 BIASED PATTERN
19		700	2	SG-1	↓	#9	ALL	ALL		• SG-1 FLUSH SENSOR (REC.#6)
				SG-2	↓	#9	ALL	ALL	(1-7)&(6-7)	• SG-2 FLUSH SENSOR-.005"
20		2100	2	SG-1	↓	#9 & #6	ALL	ALL(BOTH)		FROM BOTTOM-LOCATED @ REC.#9
				SG-2	↓	#9 & #6	ALL	ALL(#9)	(1-7)&(9-7)&(3-5)	

*PLOTTING INSTRUCTIONS

- PSD vs. FREQUENCY — LOG-LOG @ 3 CYCLES (10^2, 10^3, 10^4, 10^5 FREQUENCY)
- TRANSMISSIBILITY $\sqrt{PSD/PSD_{ref}}$ vs. FREQUENCY — LOG-LOG @ 3 CYCLES (PICK RANGE FOR ORDINATE)
- X-PSD vs. FREQUENCY — @ 3 CYCLES ($10^2 \rightarrow 10^5$)

TABLE 6. EFFECTS OF ROUGHNESS DIRECTION - X-PSD MAGNITUDE

RUN #	p_∞^o	MODEL	MODEL SURFACE	X-PSD LOCATIONS	$\tilde{p}$ (psi)
40	2100	SM-1	SMOOTH	1-7	.0096
4	2100	SG-1	UNIFORM ROUGH	2-8	.0079
20	2100	SG-2	BIASED ROUGH	1-7	.024
40	2100	SM-1	SMOOTH	5-7	.0098
4	2100	SG-1	UNIFORM ROUGH	6-8	.012
20	2100	SG-2	BIASED ROUGH	5-7	.014
39	700	SM-1	SMOOTH	1-7	.0035
3	700	SG-1	UNIFORM ROUGH	2-8	.0029
19	700	SG-2	BIASED ROUGH	1-7	.0092
3	700	SG-1	UNIFORM ROUGH	2-8	.003
3	700	SG-1	UNIFORM ROUGH	4-10	.004
4	2100	SG-1	UNIFORM ROUGH	2-8	.008
4	2100	SG-1	UNIFORM ROUGH	4-10	.010
4	2100	SG-1	UNIFORM ROUGH	6-8	.012
20	2100	SG-2	BIASED ROUGH	1-7	.024
20	2100	SG-2	BIASED ROUGH	9-7	.014
20	2100	SG-2	BIASED ROUGH	3-5	.034

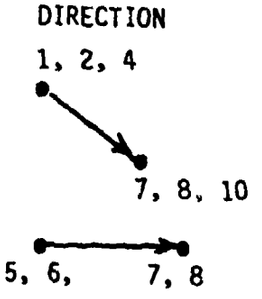

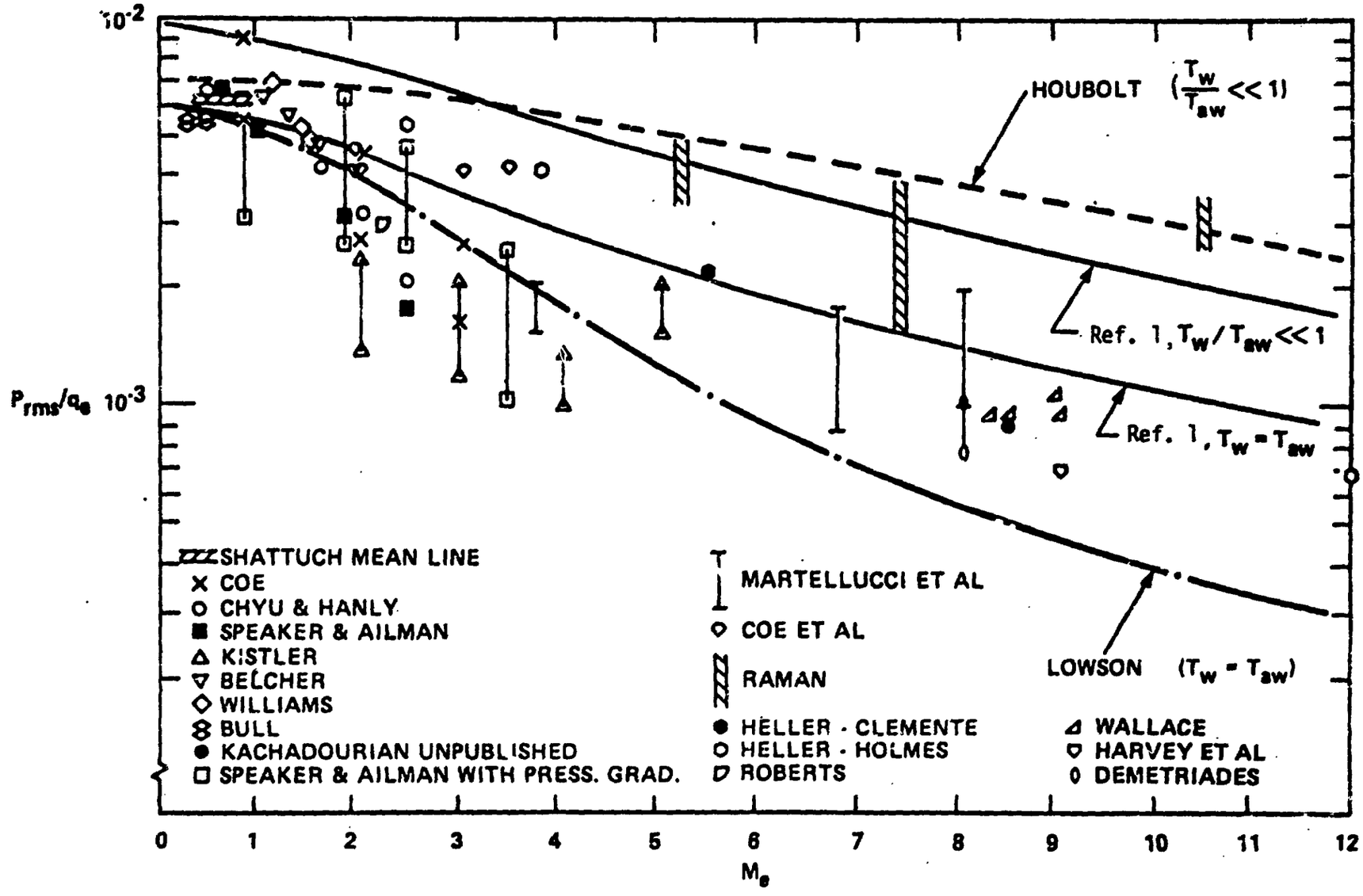

FIGURE 1. ROOT-MEAN-SQUARE PRESSURE FLUCTUATION VS. MACH NUMBER FOR ATTACHED TURBULENT FLOW

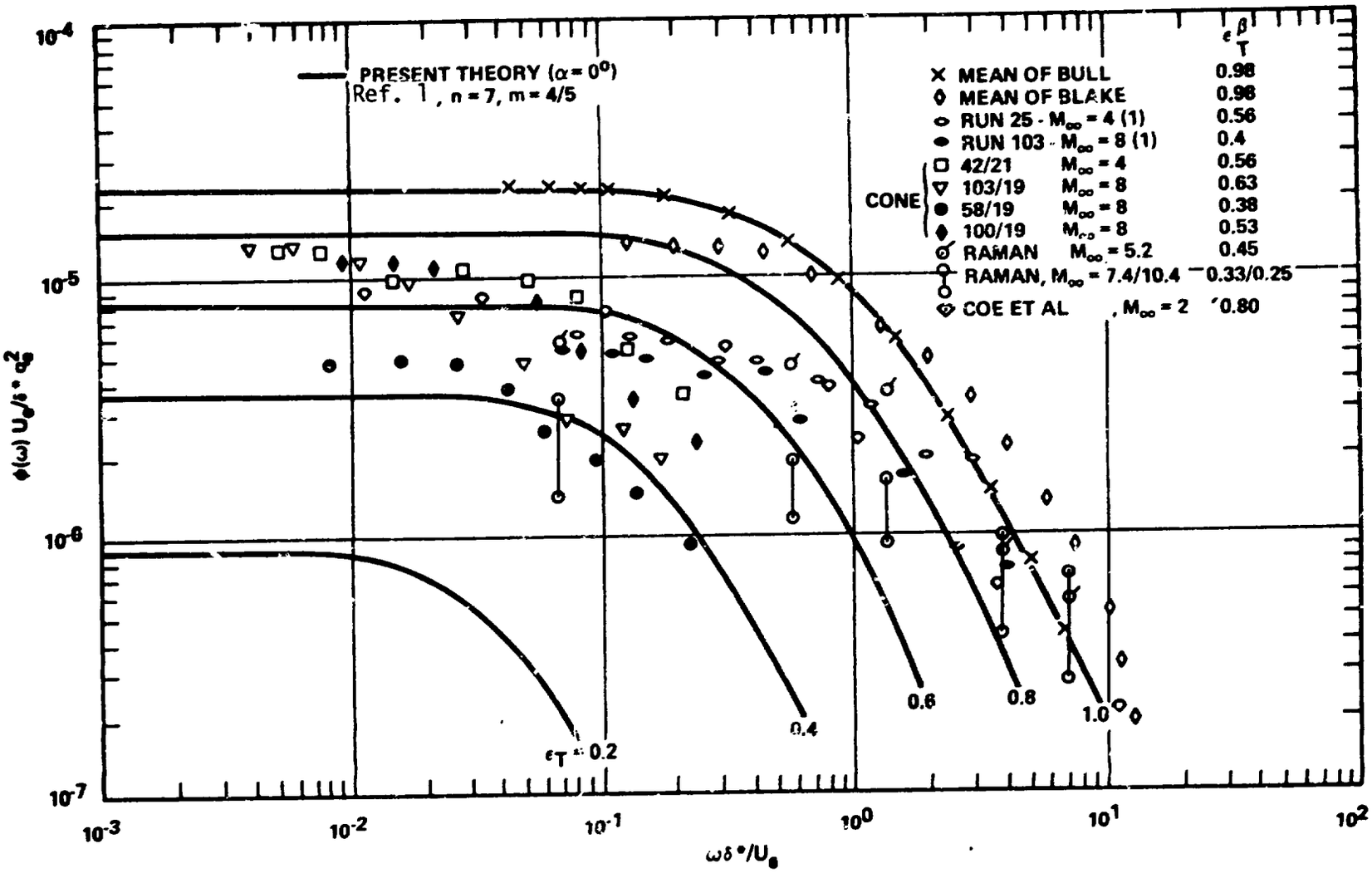

FIGURE 2. COMPARISON OF PRESENT NORMALIZED SPECTRAL MEASUREMENTS WITH OTHER SPECTRAL DATA AND THEORY

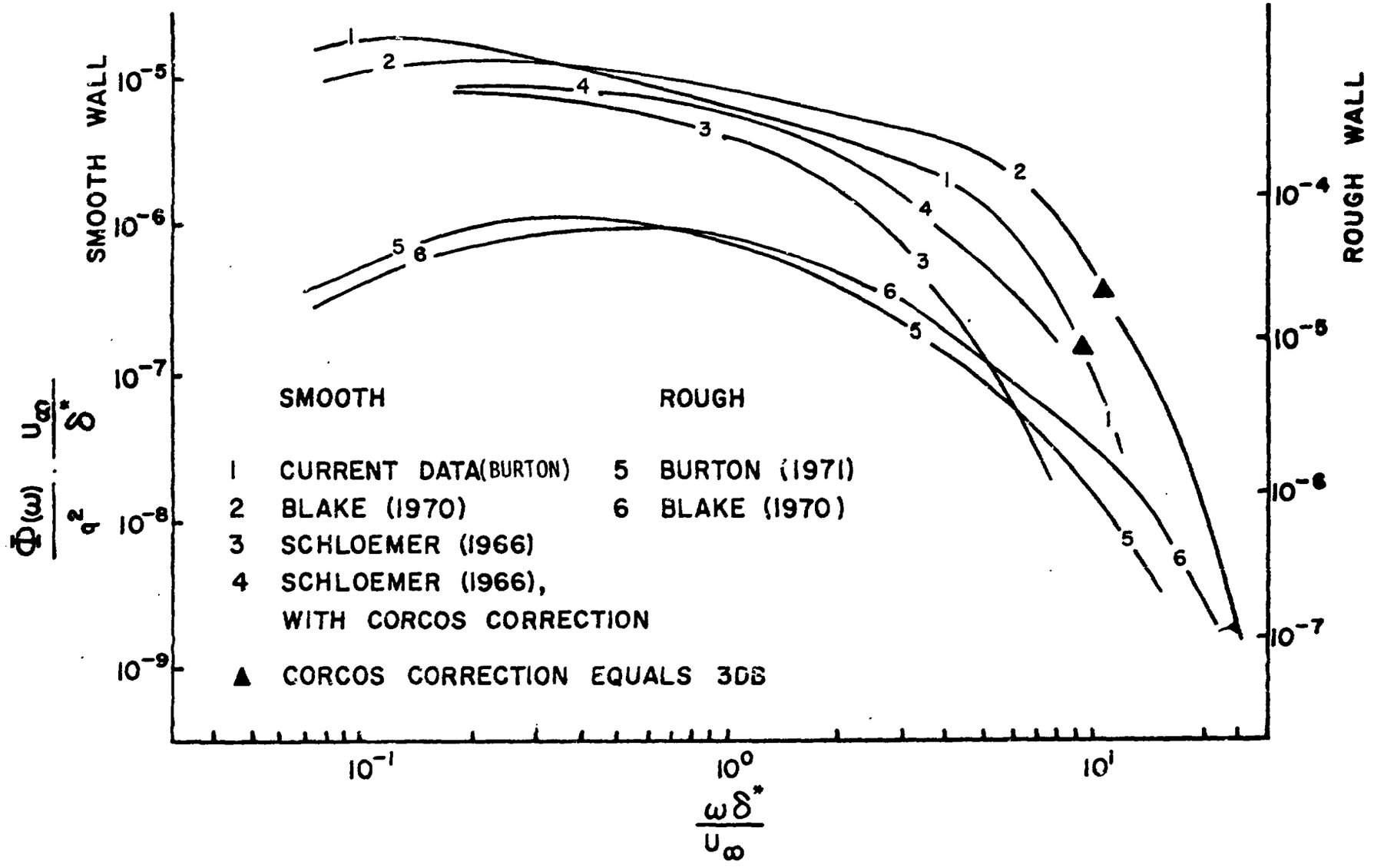

FIGURE 3. WALL PRESSURE SPECTRA. NO PRESSURE GRADIENT. OUTER VARIABLE SCALING.

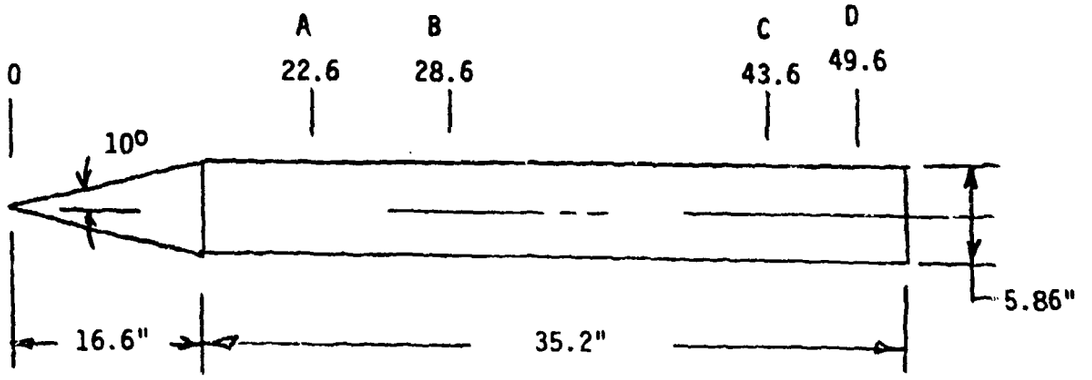

TEST MODEL

TEST - AEDC TUNNEL A @ $M_\infty = 4$

$15 \leq P_{0_\infty} \leq 73$ psia

$1.2 \quad Re_\infty/FT \leq 6 \times 10^5$

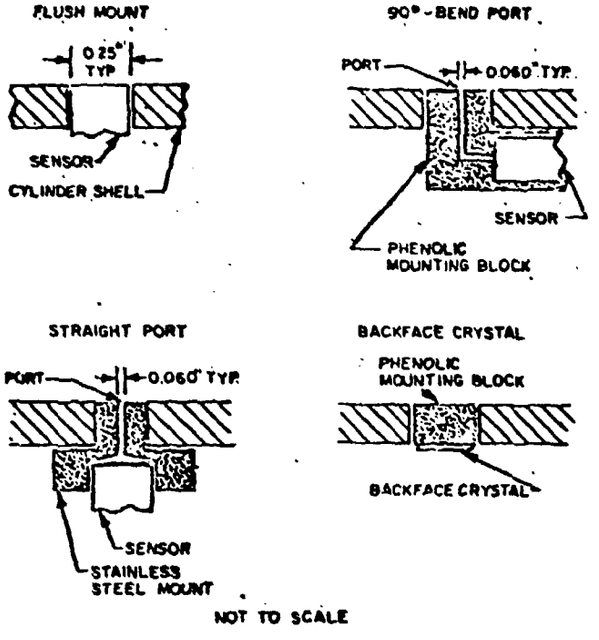

SENSOR TYPE

A - BACKFACE CRYSTAL*
A - BBN 1/4"D - FLUSH
B - CRL 1/2"D - STRAIGHT PORT
B - BBN 1/4"D - STRAIGHT PORT
C - BBN 1/4"D - STRAIGHT PORT
C - BBN 1/4"D - 90° PORT
D - CRL 1/2"D - STRAIGHT PORT
D - BBN 1/4"D - FLUSH

BBN - BOLT, BERANEK & NEWMAN
CRL - COLUMBIA RESEARCH LABS
(BOTH ARE PIEZOELECTRIC)

*LEAD-ZIRCONATE CRYSTAL

ACOUSTIC SENSOR INSTALLATION

FIGURE 4. AEDC BOUNDARY LAYER ACOUSTIC MEASUREMENTS AT MACH 4**

**Paper presented at AIAA 4th Aerodynamic Testing Conference, April 1969.

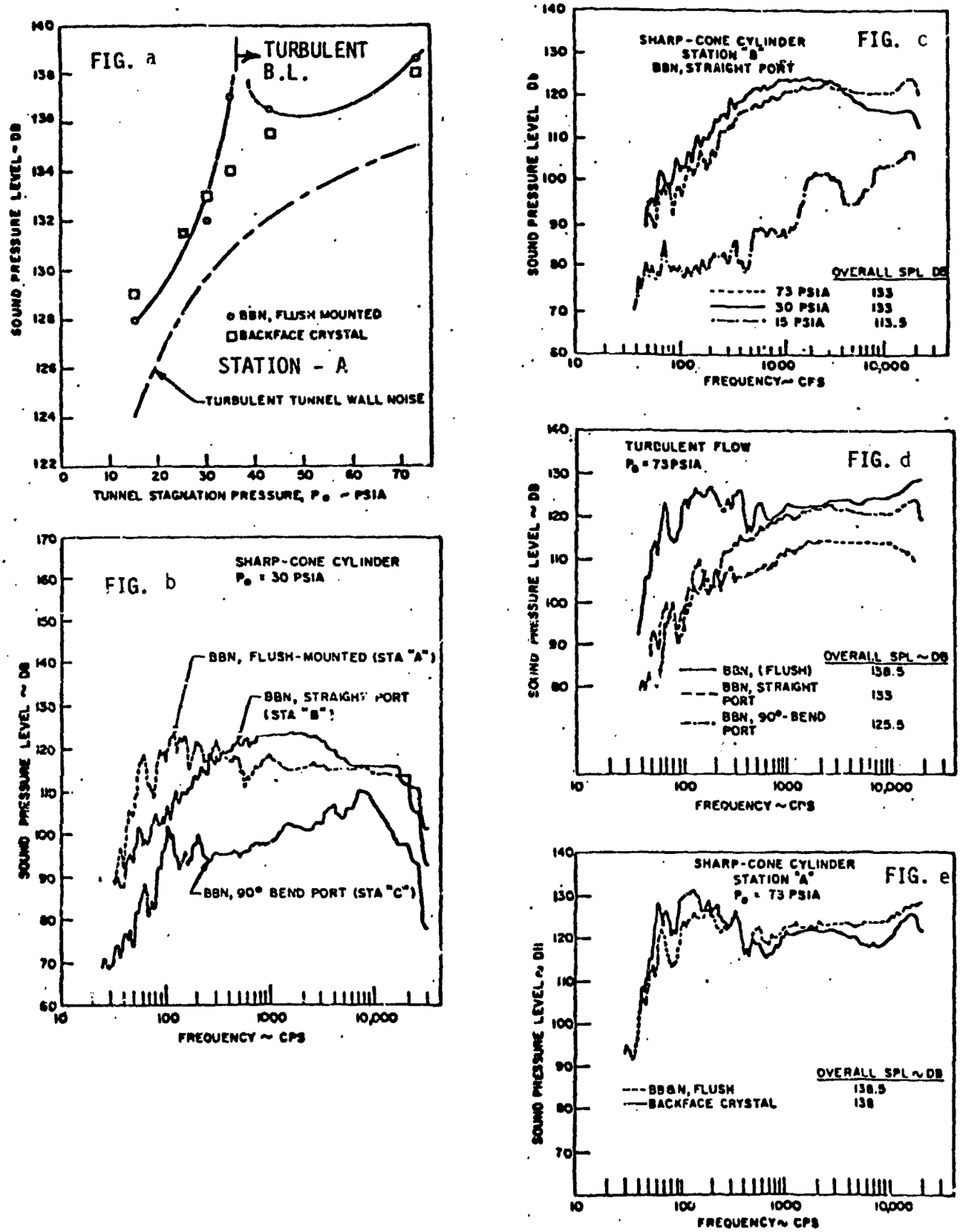

FIGURE 5. MEASURED ACOUSTIC SPECTRA (UNCORRECTED FOR ROLL-OFF DUE TO PORT DAMPING)

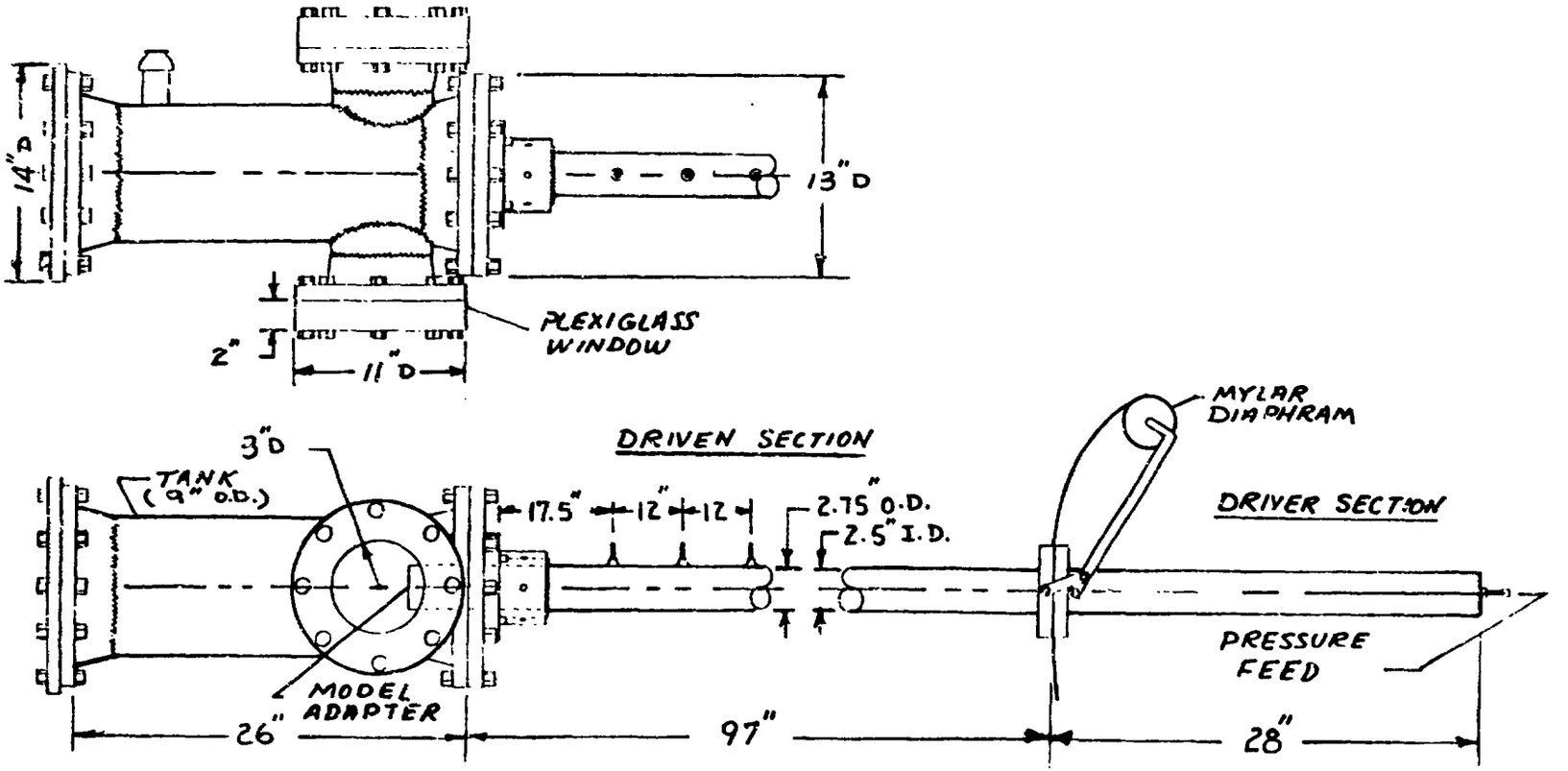

FIGURE 6. AEDC SHOCK TUBE

FIGURE 7. AEDC SHOCK TUBE AND TEST EQUIPMENT

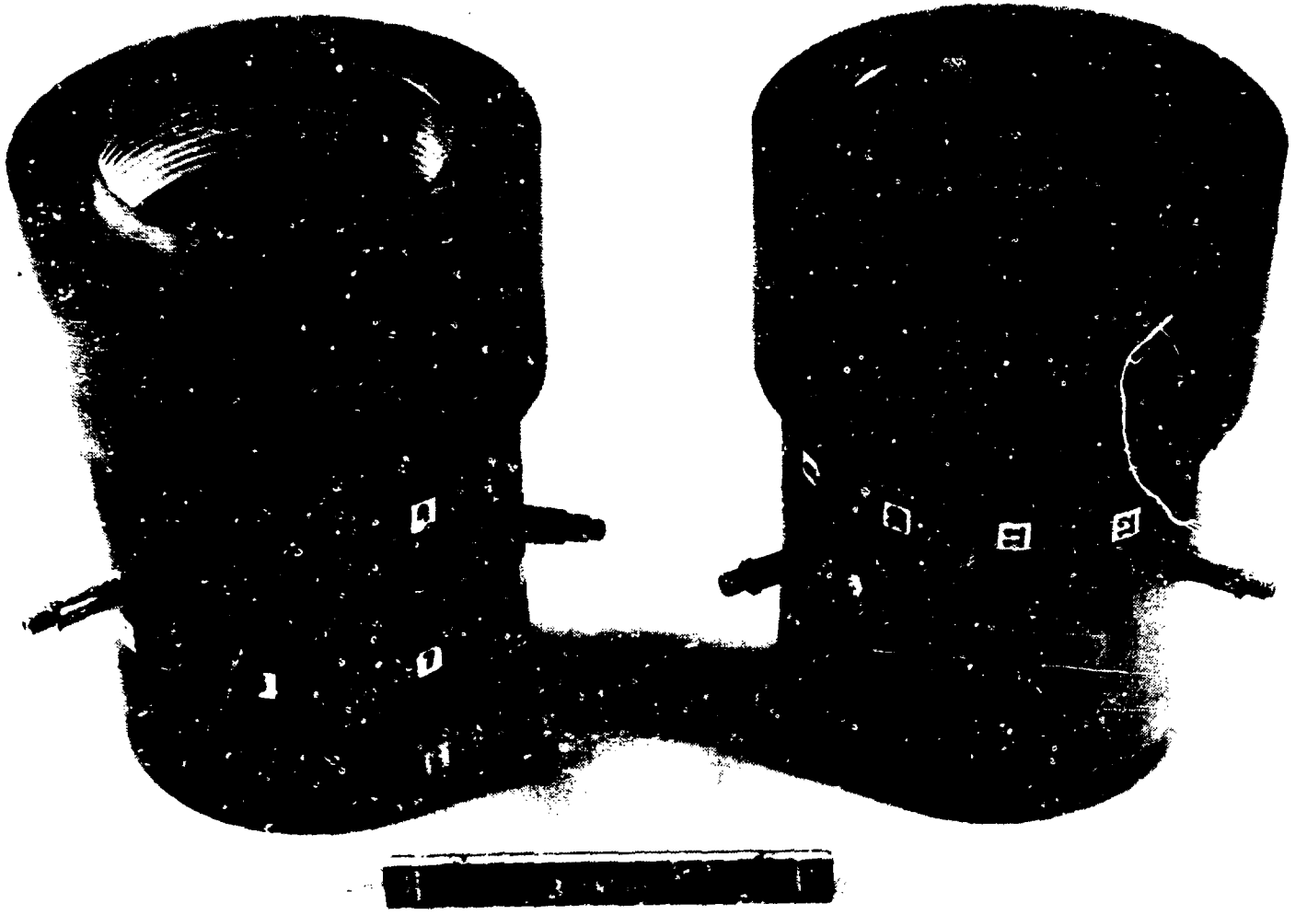

FIGURE 8. PORTED HOLE MODELS WITH ACOUSTIC GAGES

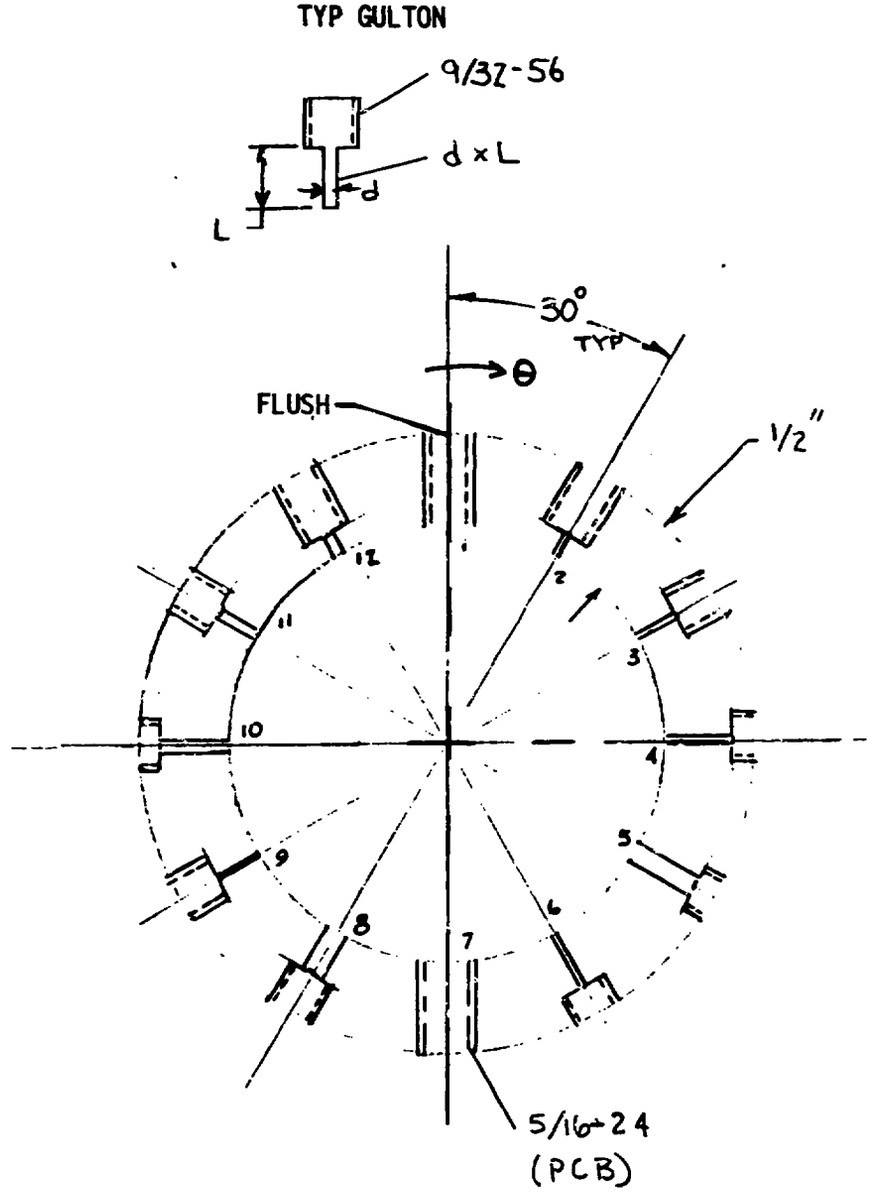

MODEL - SM-1 (FLUSH)

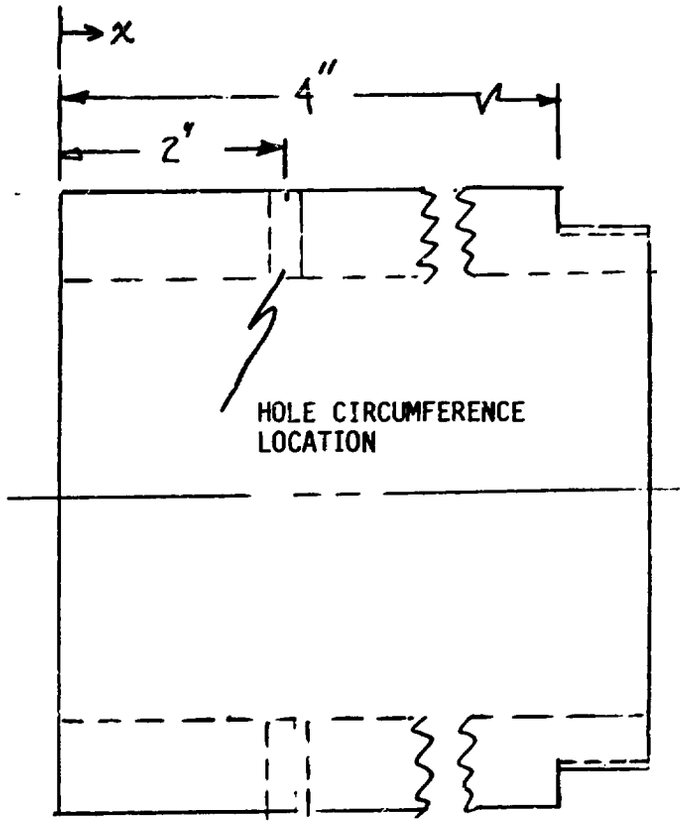

HOLE(θ)	L	d	HOLE(θ)	L	d
1(0)	THRU	9/32-56	7(180)	THRU	5/16-24
1(30)	1/8	1/32	8(210)	1/4	1/8
3(60)	1/4	1/32	9(240)	1/4	1/64
4(90)	3/8	1/32	9(240)	1/4	1/16
5(120)	3/8	1/8	10(270)	3/8	1/16
6(150)	3/8	1/64	11(300)	1/4	1/16
			12(330)	1/8	1/16

ALL HOLES @ X = 2"

FIGURE 9. SMOOTH WALL PORTED HOLE MODEL WITH SINGLE CIRCUMFERENCE GAGE LOCATIONS

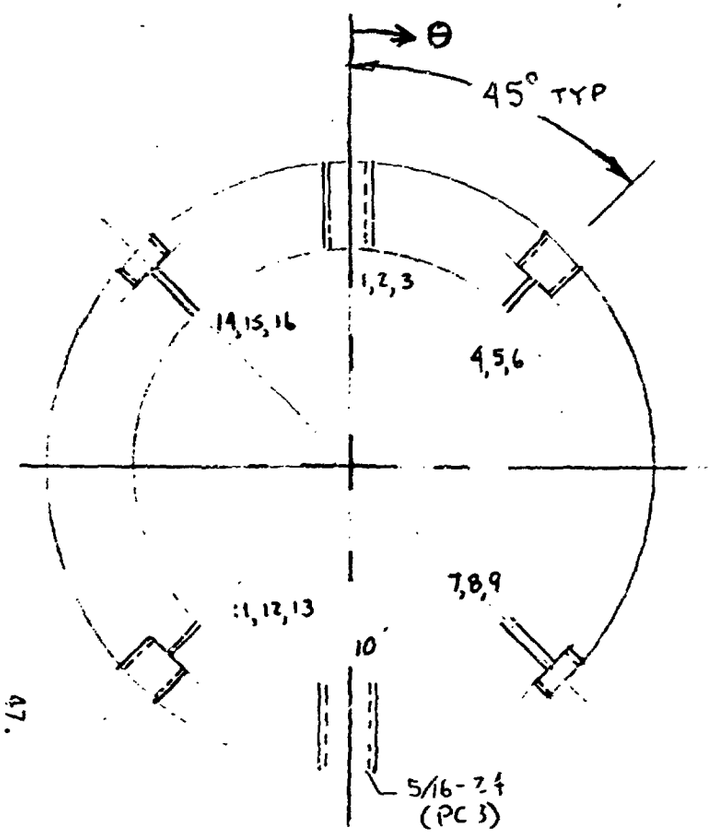

MODEL SM-2

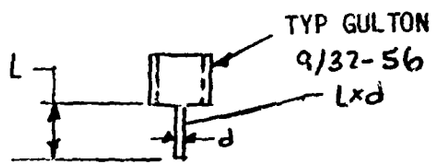

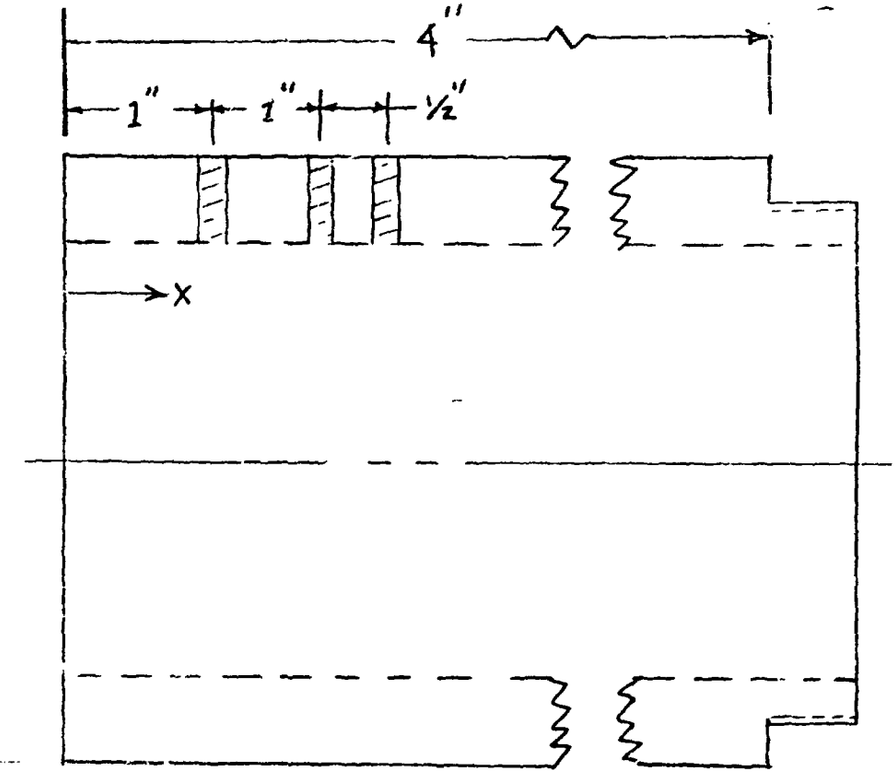

HOLE	θ	X	L	d	HOLE	θ	X	L	d
1	0	1	THRU	9/32-56	9	135	2-1/2	3/8	1/16
2	0	2	"	"	10	180	2	THRU	5/16-24
3	0	2-1/2	"	"	11	225	1	1/4	1/64
4	45	1	1/4	1/32	12	225	2	"	"
5	45	2	"	"	13	225	2-1/2	"	"
6	45	2-1/2	"	"	14	315	1	3/8	1/32
7	135	1	3/8	1/16	15	315	2	"	"
8	135	2	"	"	16	315	2-1/2	"	"

FIGURE 10. SMOOTH WALL PORTED HOLE MODEL WITH MULTI-CIRCUMFERENCE GAGE LOCATIONS

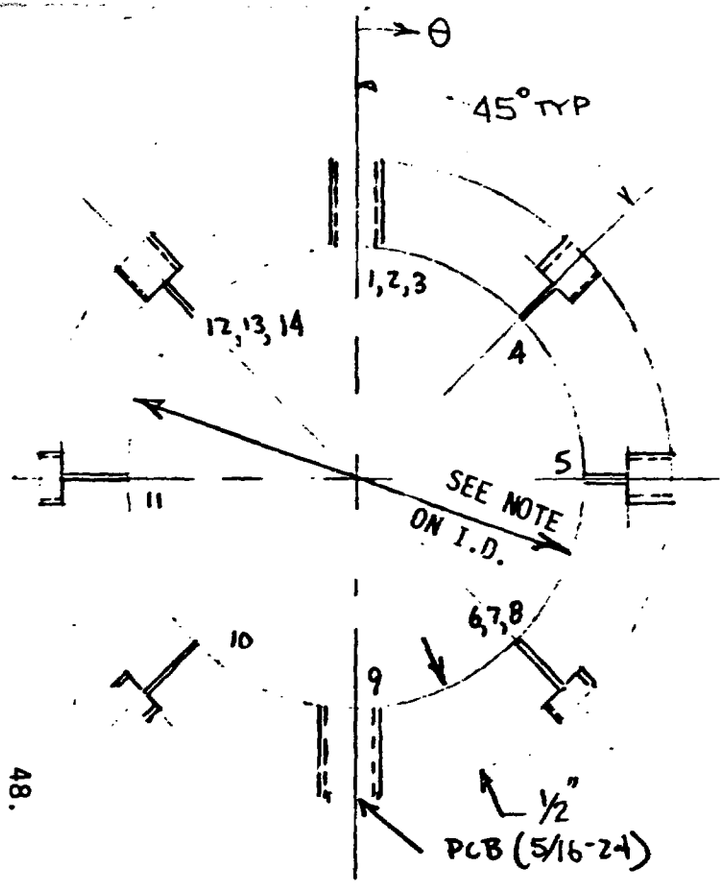

MODEL SG-1

NOTE: I.D. CUT TO ACCOMMODATE 20 GRIT ROUGHNESS PATTERN

FIGURE 11. ROUGH WALL PORTED HOLE MODEL

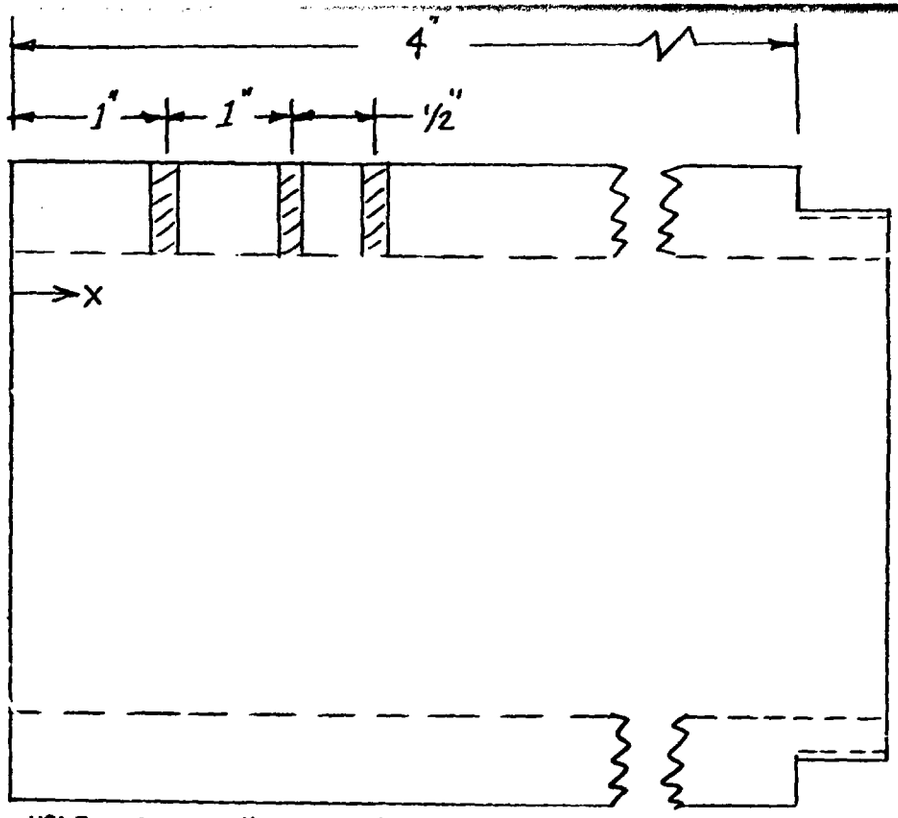

HOLE	θ	X	L	d
1	0	1	THRU	9/32-56
2	0	2	"	"
3	0	2-1/2	"	"
4	45	2	1/4	1/32
5	90	2	1/4	1/16
6	135	1	3/8	1/32
7	135	2	"	"
8	135	2-1/2	"	"
9	180	2	THRU	5/16-24
10	225	2	3/8	1/16
11	270	2	3/8	1/64
12	315	1	1/4	1/64
13	315	2	"	"
14	315	2-1/2	"	"

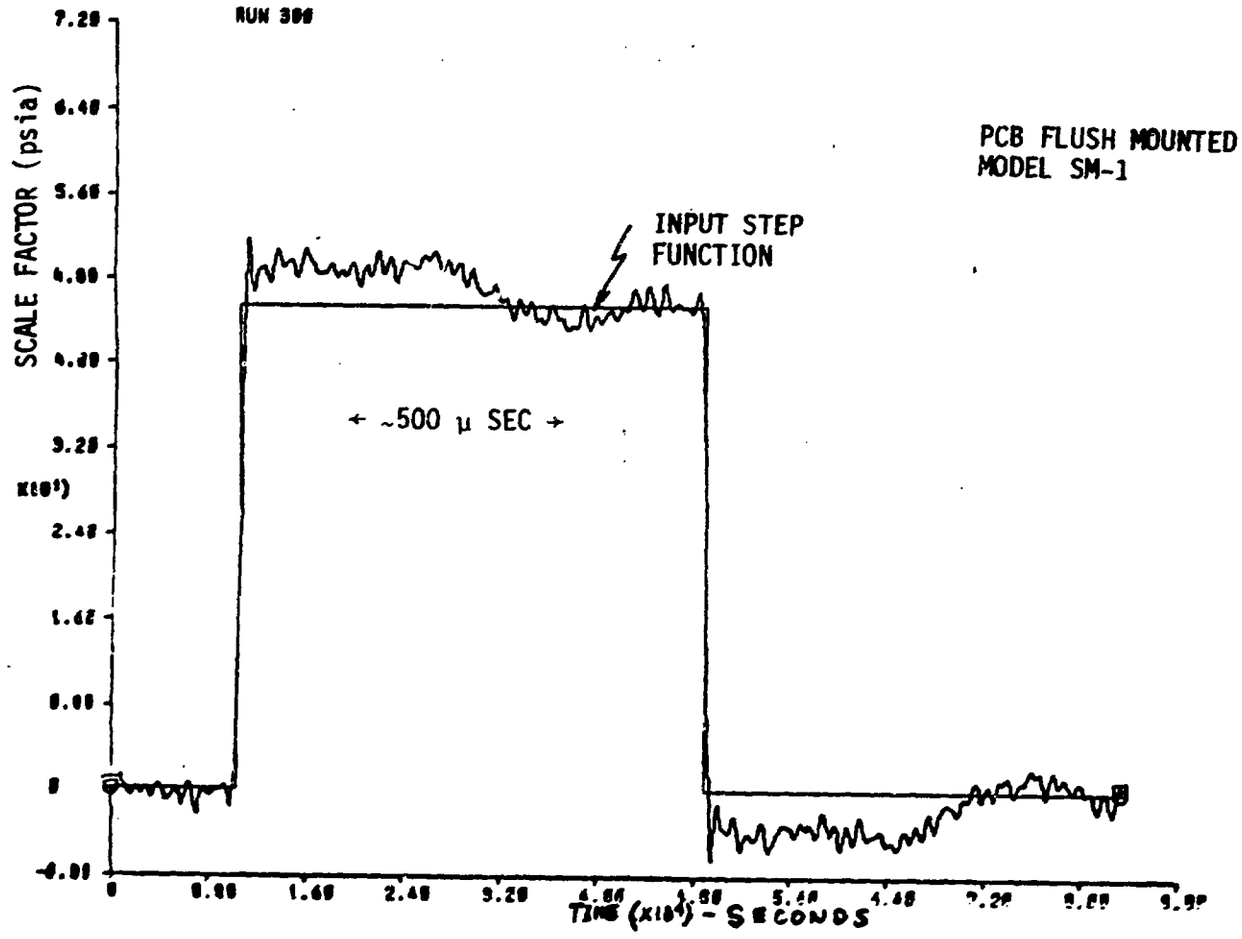

FIGURE 12. RESPONSE OF PCB FLUSH MOUNTED SENSOR

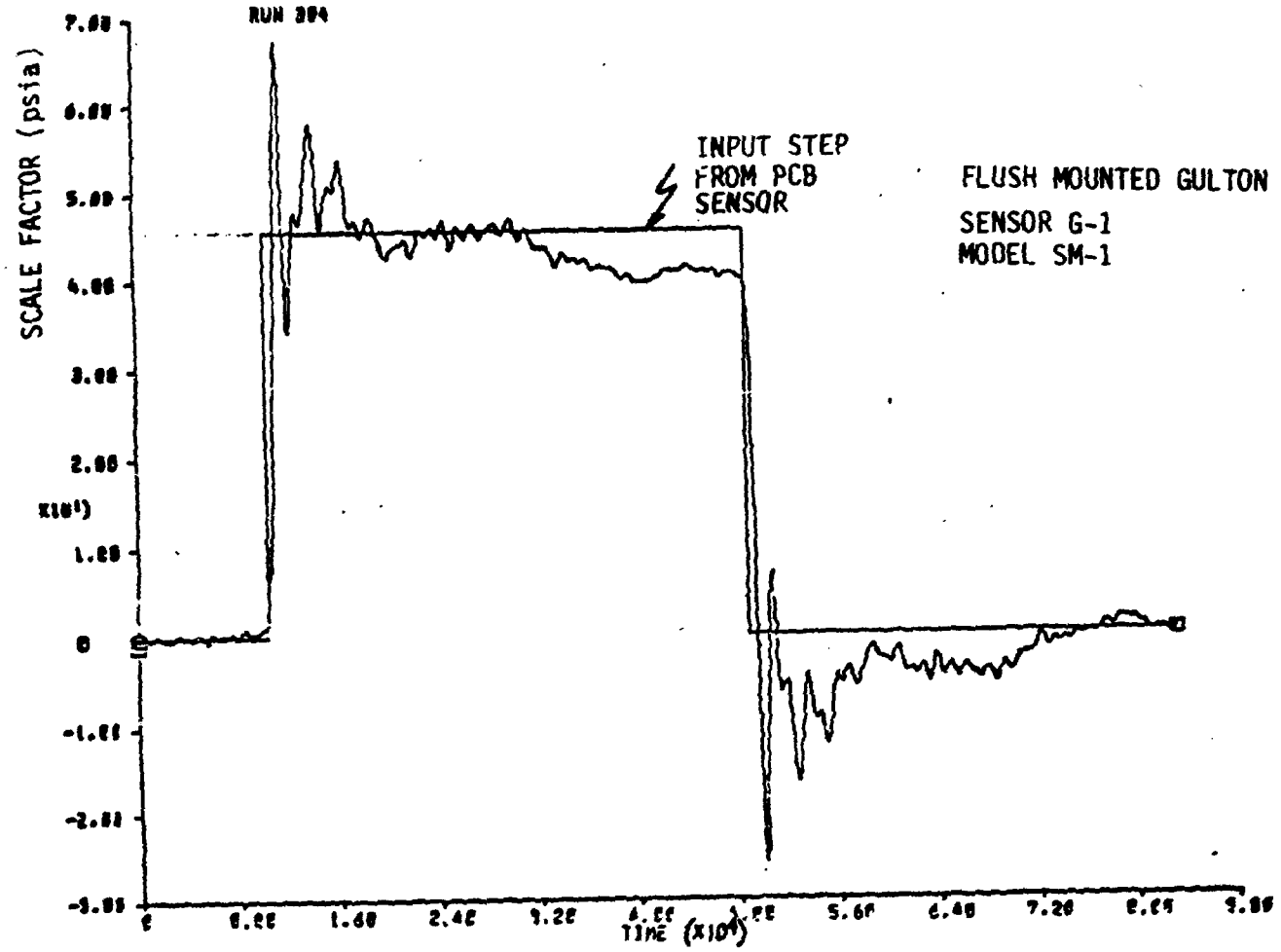

FIGURE 13. RESPONSE OF FLUSH MOUNTED GULTON MICROPHONE

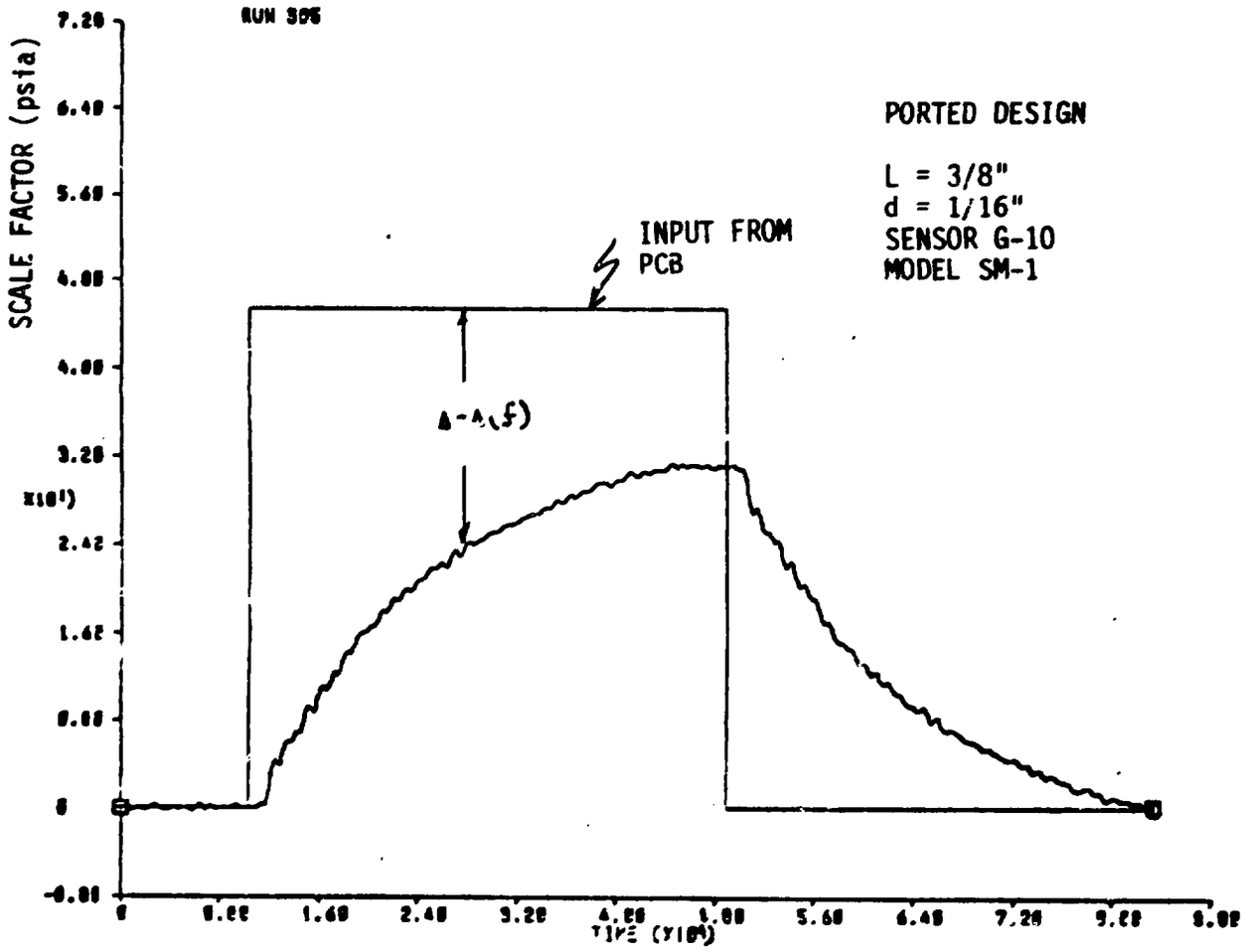

FIGURE 14. TYPICAL RESPONSE FOR PORTED GULTON MICROPHONE WITH STEP FUNCTION

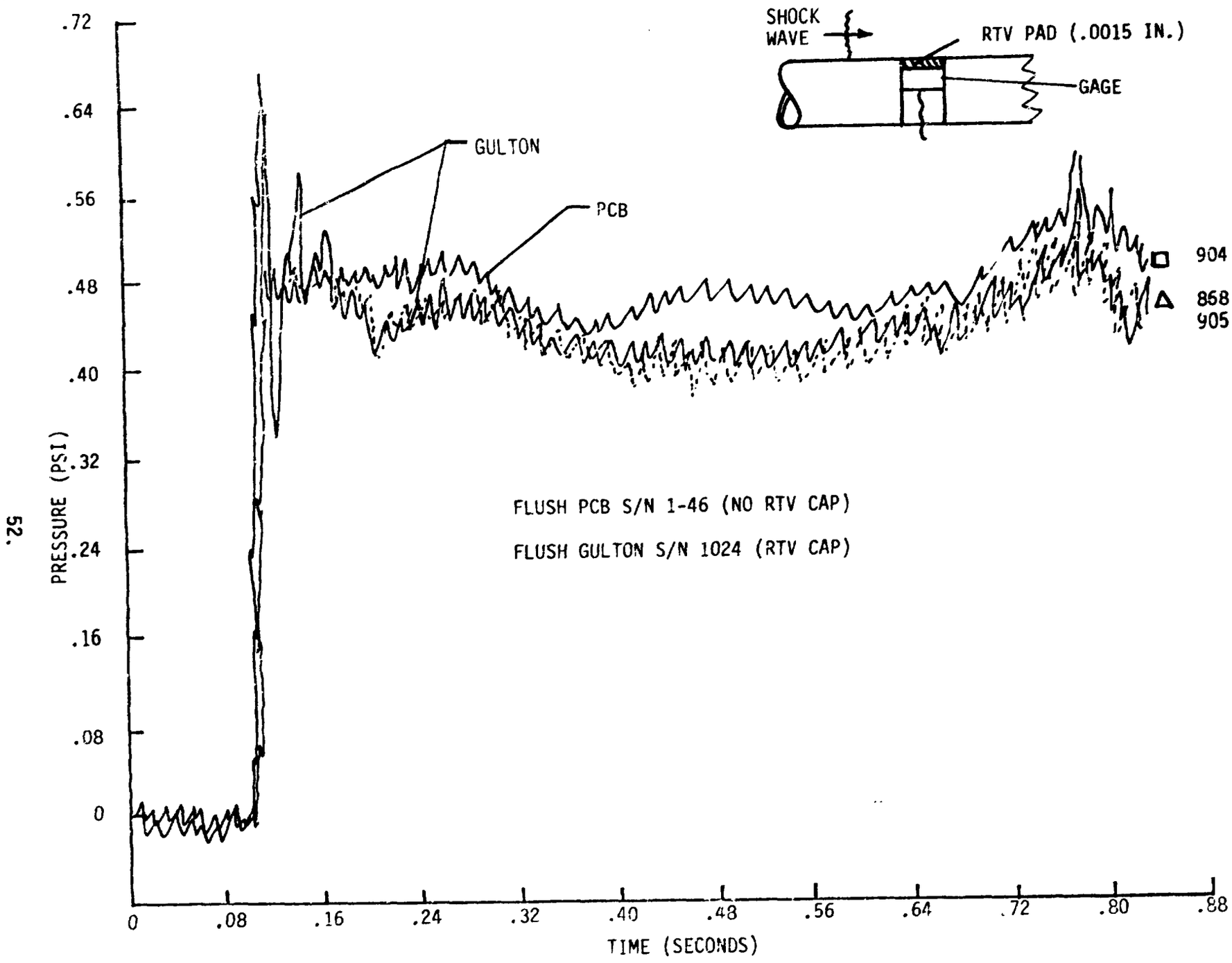

FIGURE 15A. FLUSH-MOUNTED TRANSDUCERS - RESPONSE TO PRESSURE STEP IMPOSED BY SHOCK MOVING PAST SURFACE MOUNTED TRANSDUCERS

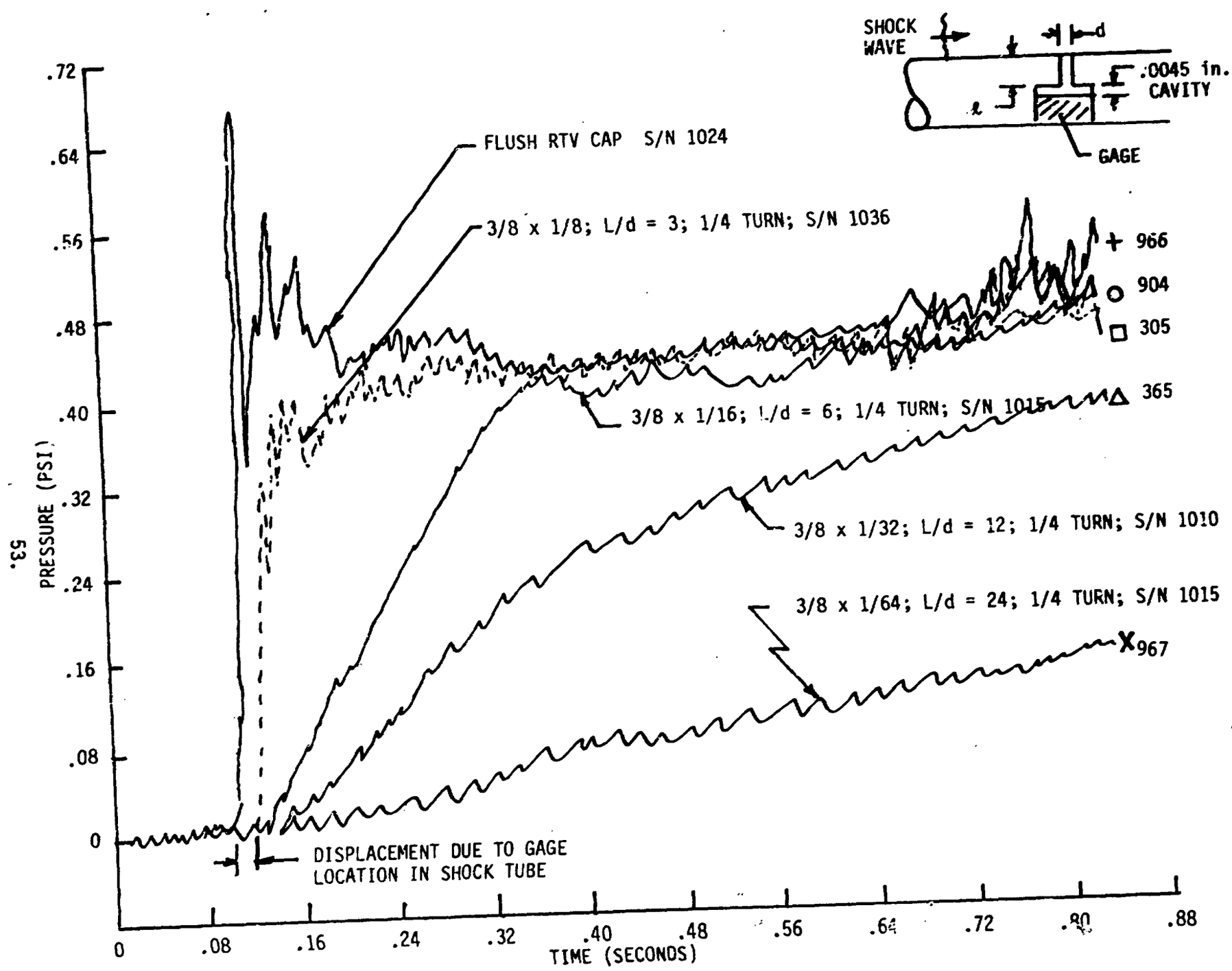

FIGURE 15B. EFFECT OF PORTED HOLE LENGTH TO DIAMETER RATIO

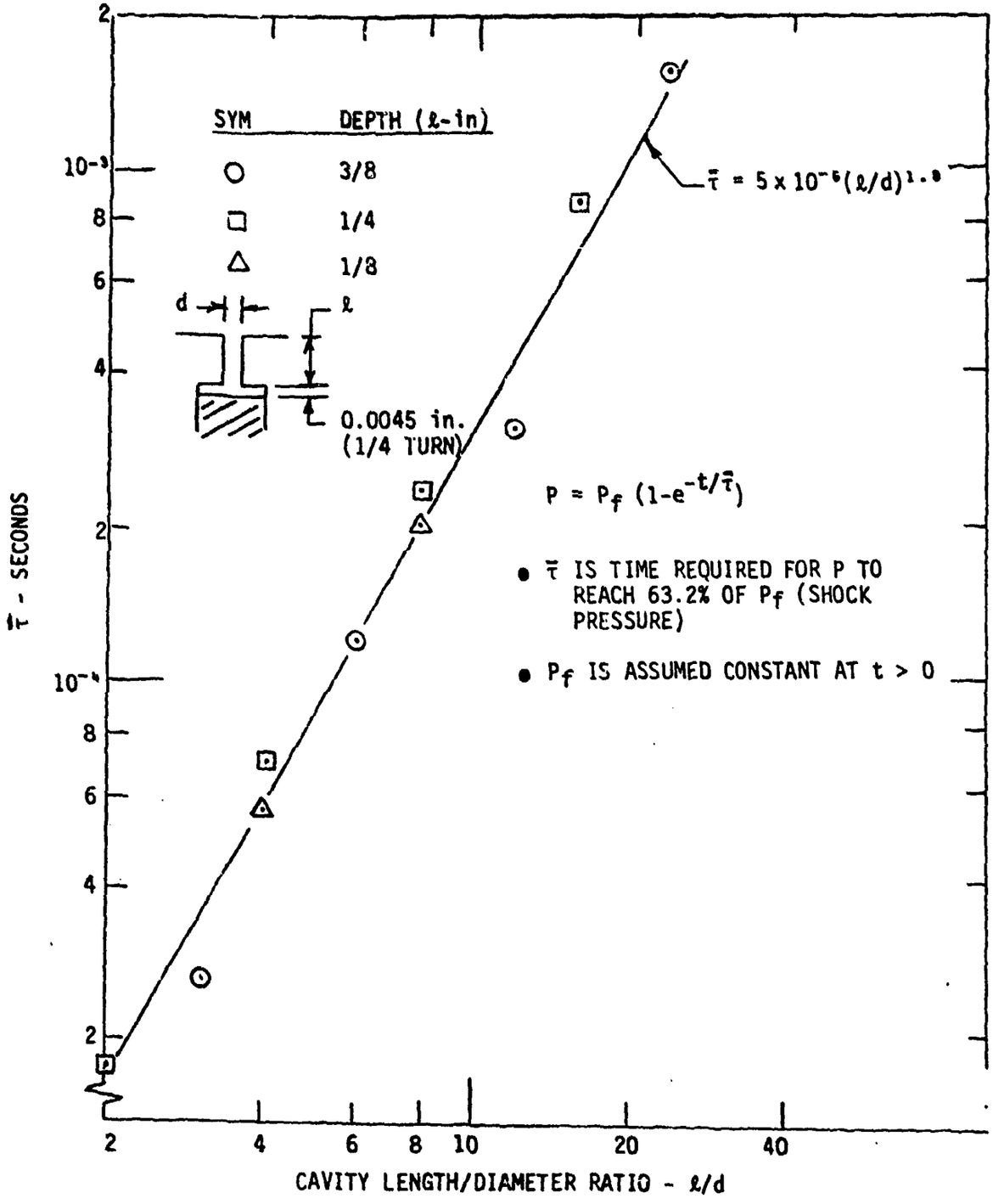

FIGURE 16. DYNAMIC RESPONSE OF PORTED GAGES TESTED IN AEDC SHOCK TUBE

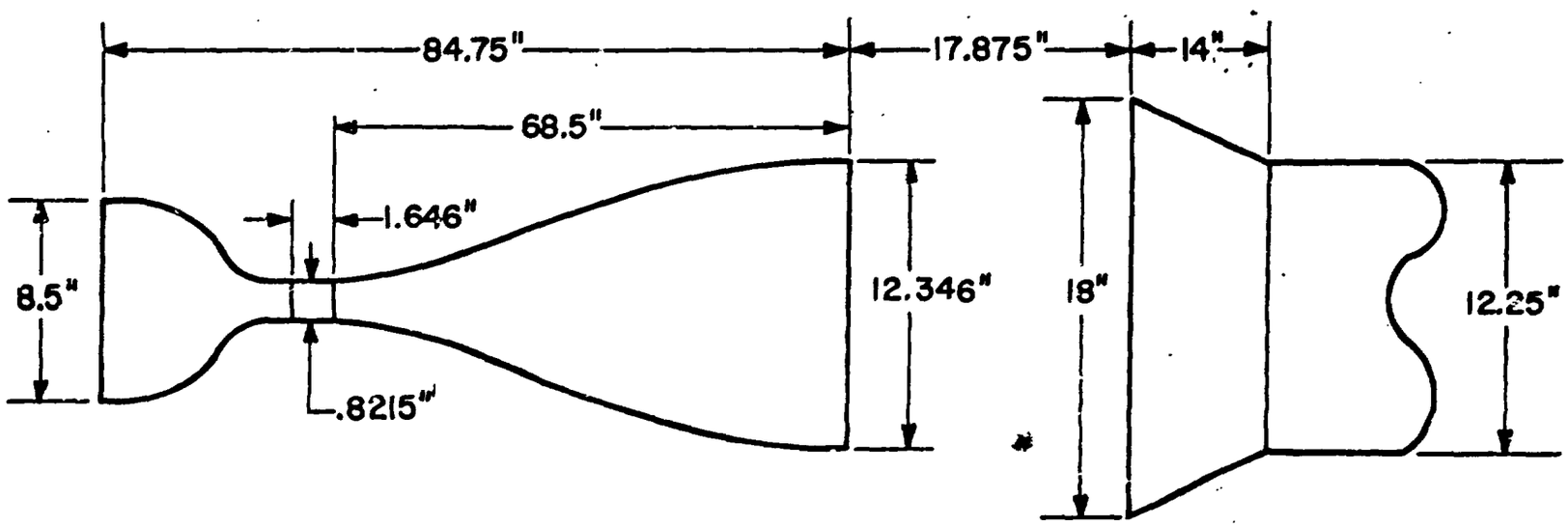

FIGURE 17. M = 6 WIND TUNNEL NOZZLE, JET, AND COLLECTOR CONFIGURATION

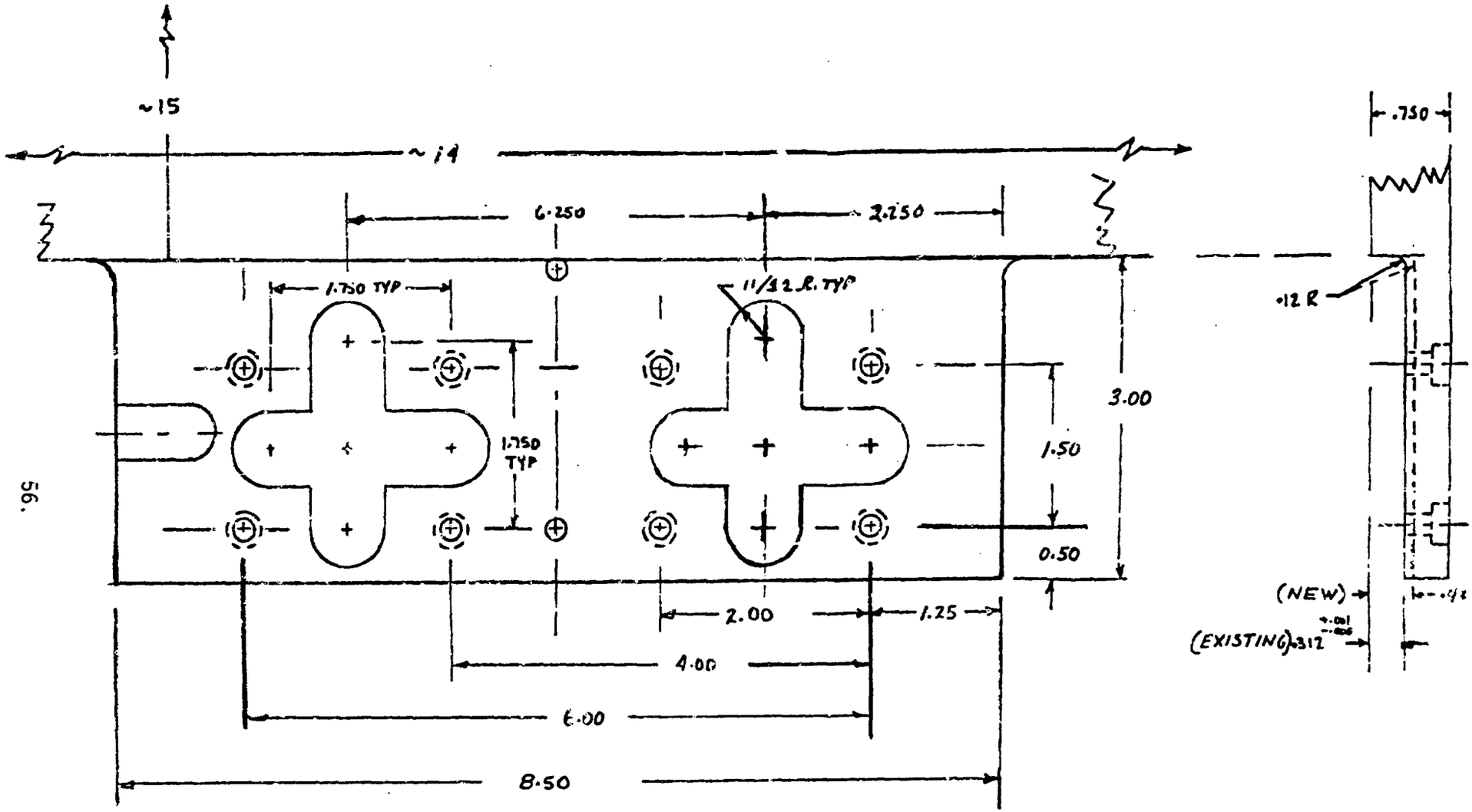

FIGURE 18. TWCP SPECIMEN MOUNTING PLATE

FIGURE 19. AFWAL MACH 6 FACILITY WITH TEST PLATE AND TWCP SPECIMENS

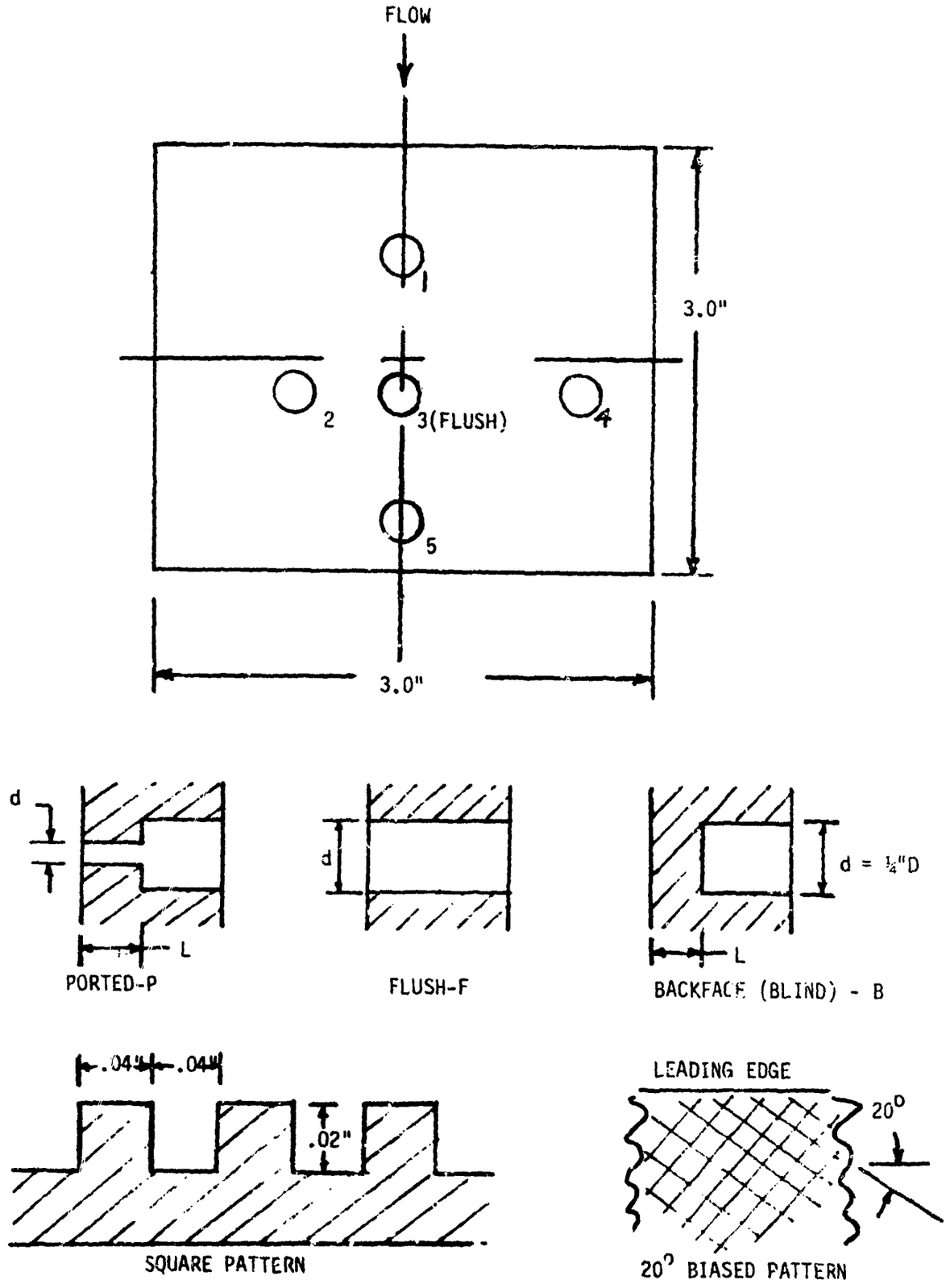

FIGURE 20. TYPICAL GAGE LOCATION/MODEL GEOMETRIC CHARACTERISTICS

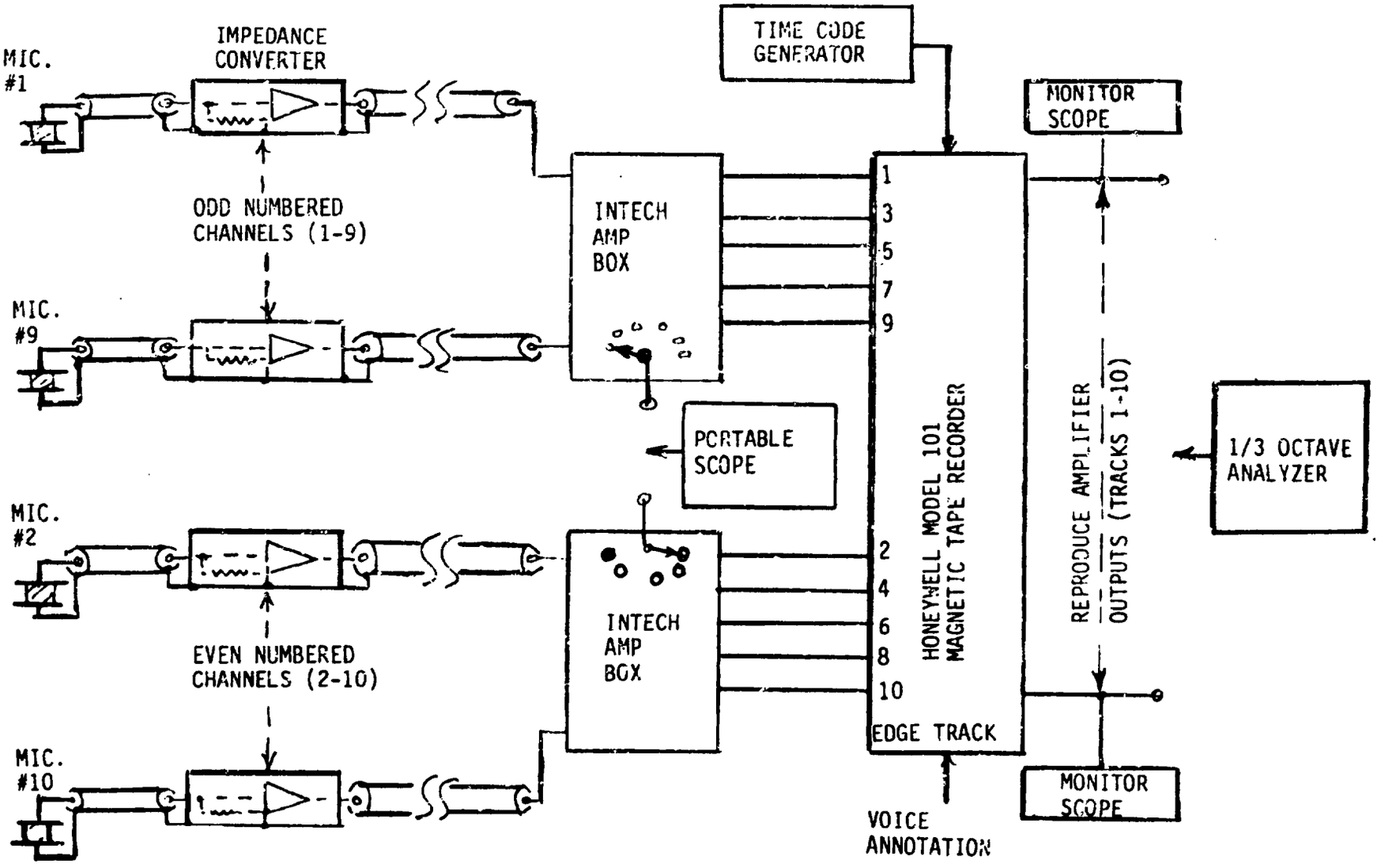

FIGURE 21. SIGNAL CONDITIONING & DATA RECORDING

12
5

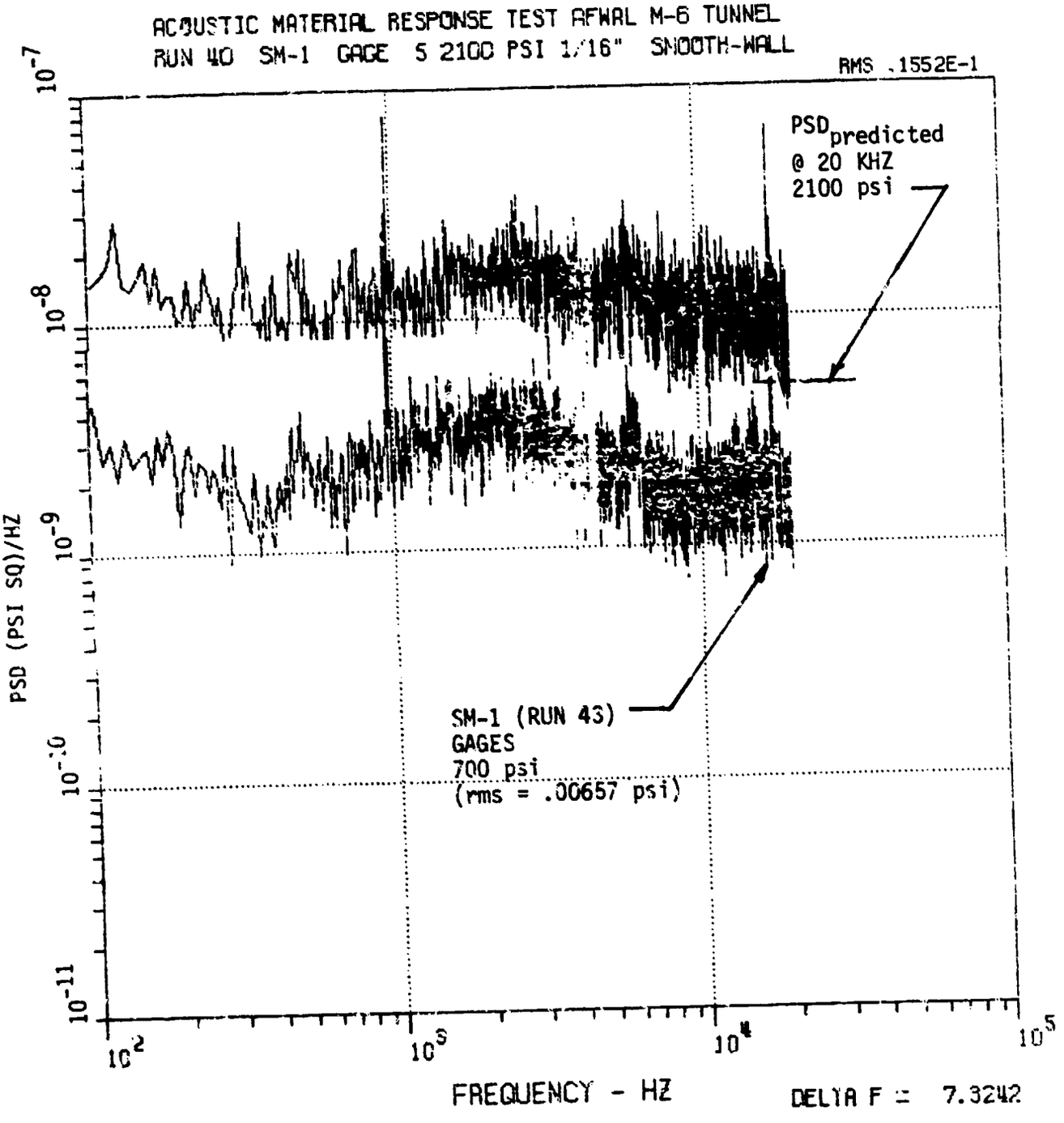

FIGURE 22. SMOOTH WALL POWER SPECTRAL DENSITY FOR FLUSH MOUNTED GAGES

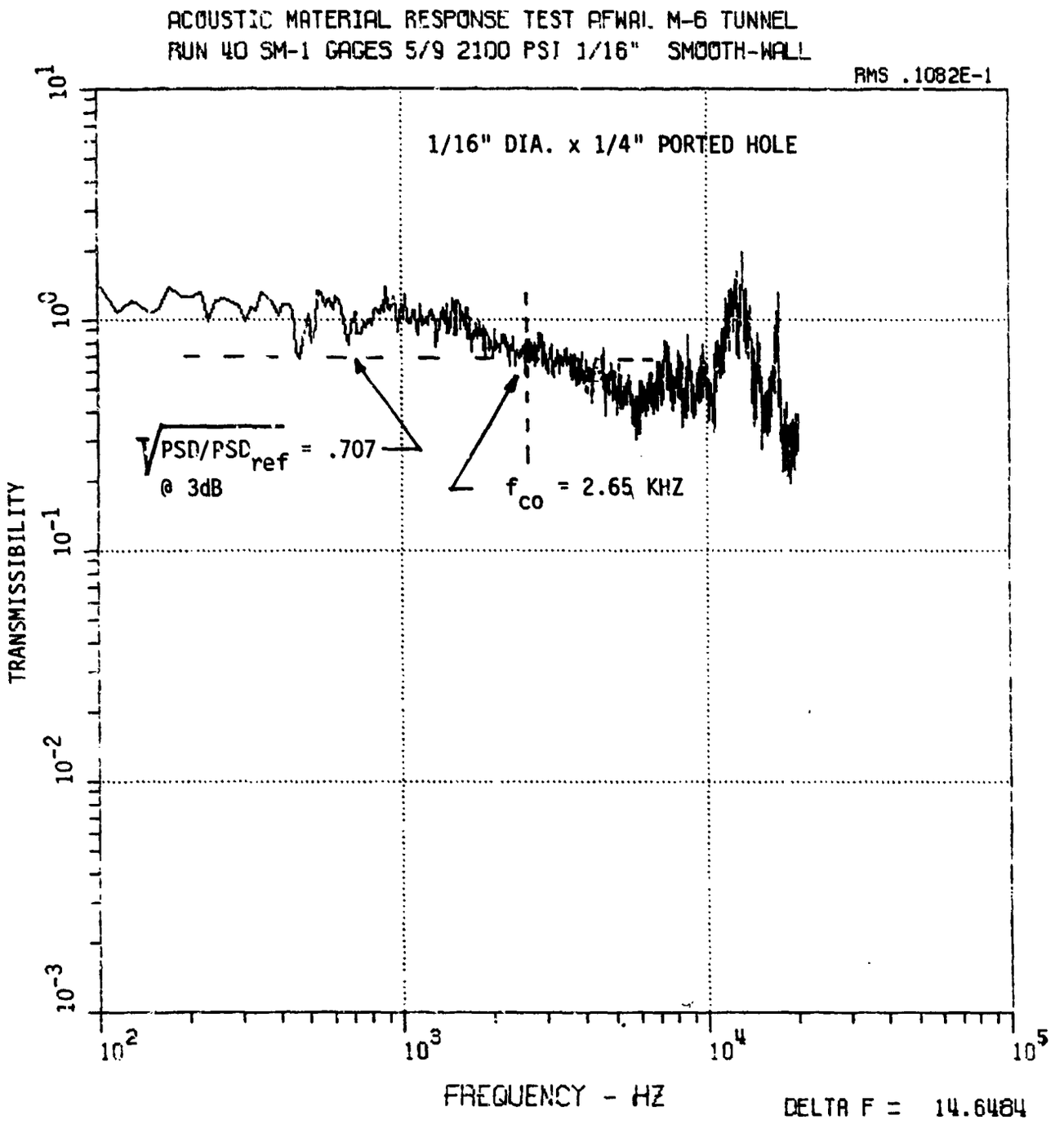

FIGURE 23. TRANSMISSIBILITY CHARACTERISTICS FOR A SMOOTH WALL PORTED HOLE GAGE

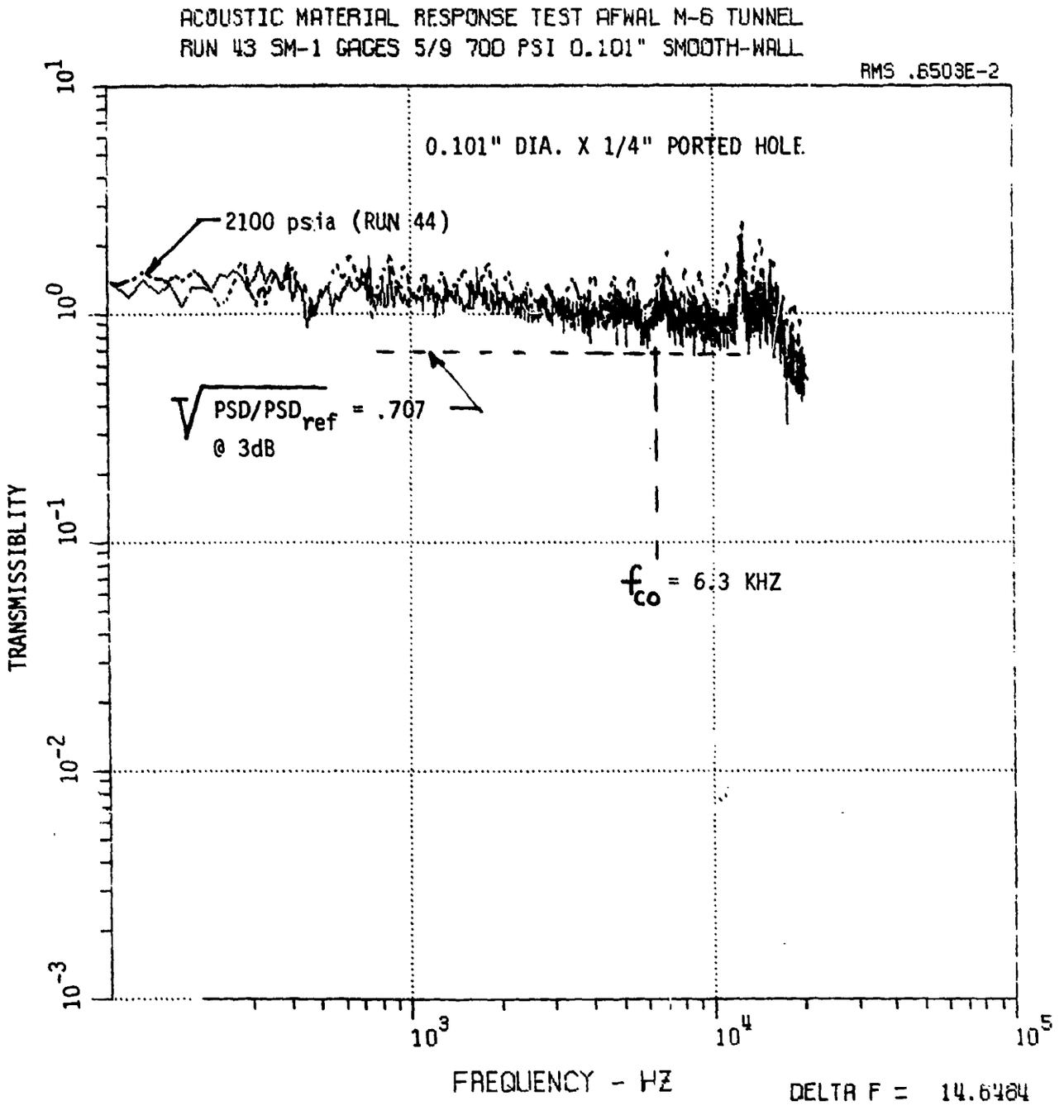

FIGURE 24. COMPARISON OF TRANSMISSIBILITY WITH TUNNEL PRESSURE FOR SMOOTH WALL PORTED HOLE

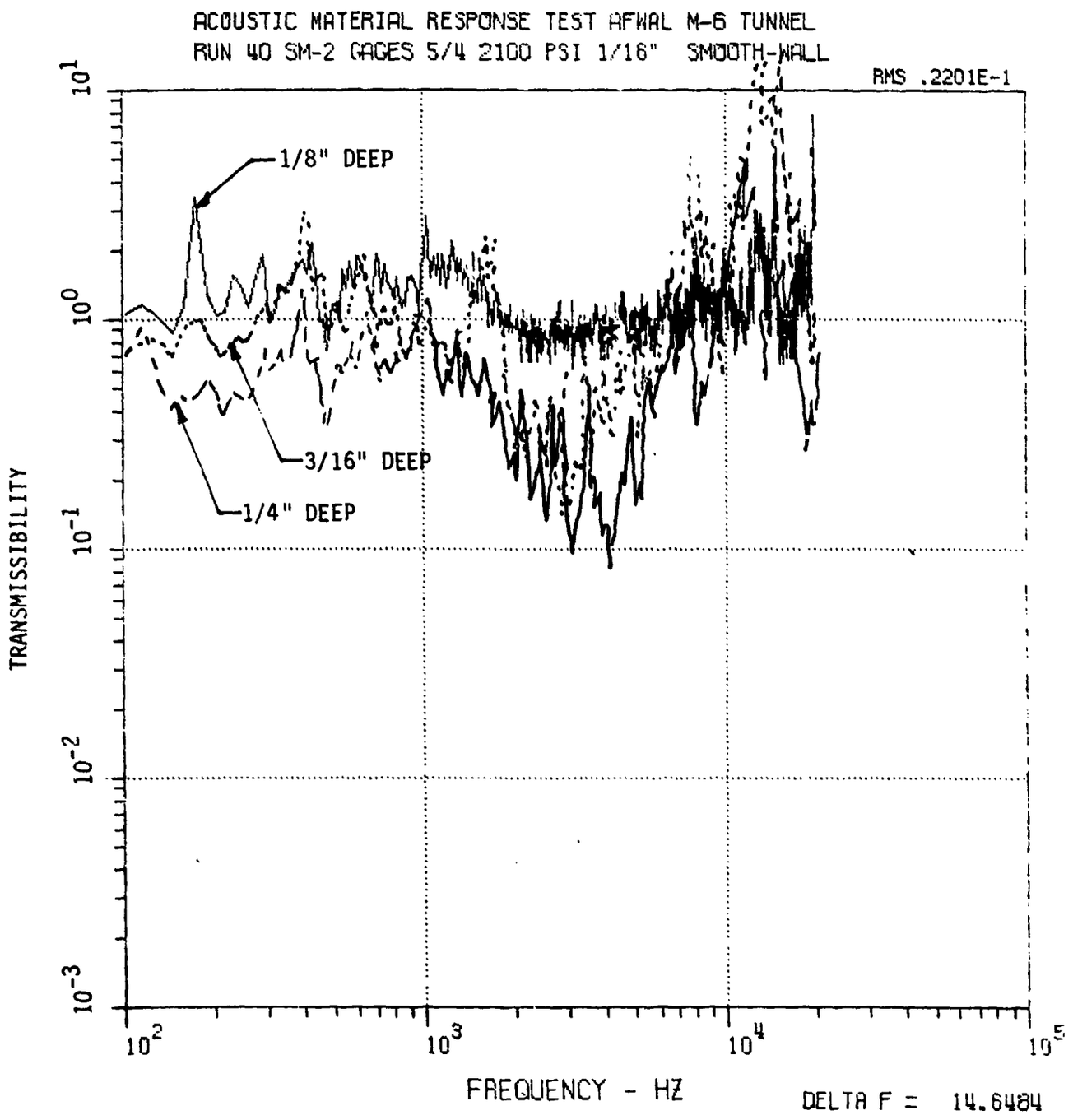

FIGURE 25. BACKFACE (BLIND HOLE) GAGE RESPONSE FOR SMOOTH WALL CONDITIONS

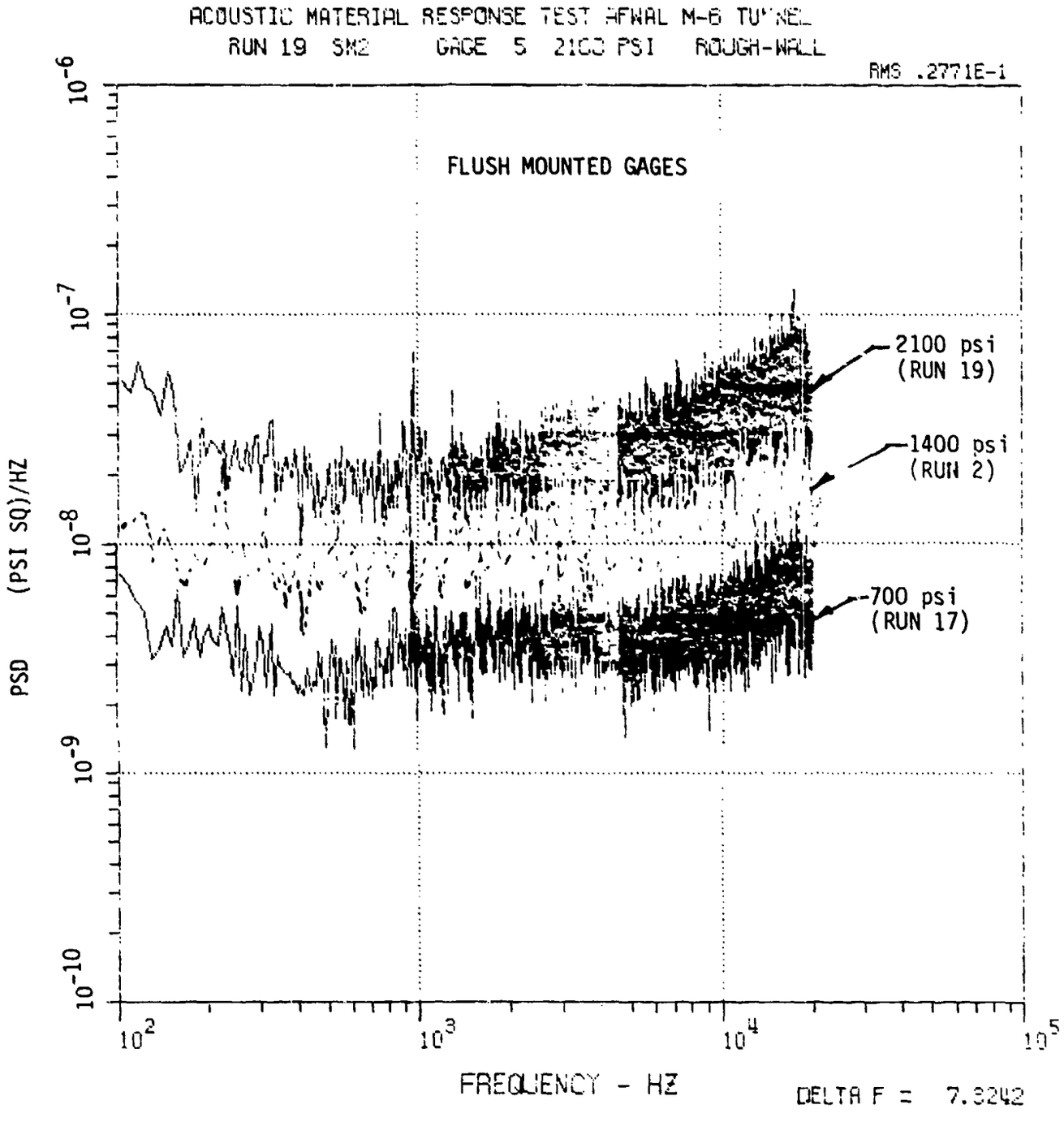

FIGURE 26. ROUGH WALL POWER SPECTRAL DENSITY DISTRIBUTION WITH FLUSH MOUNTED SENSORS

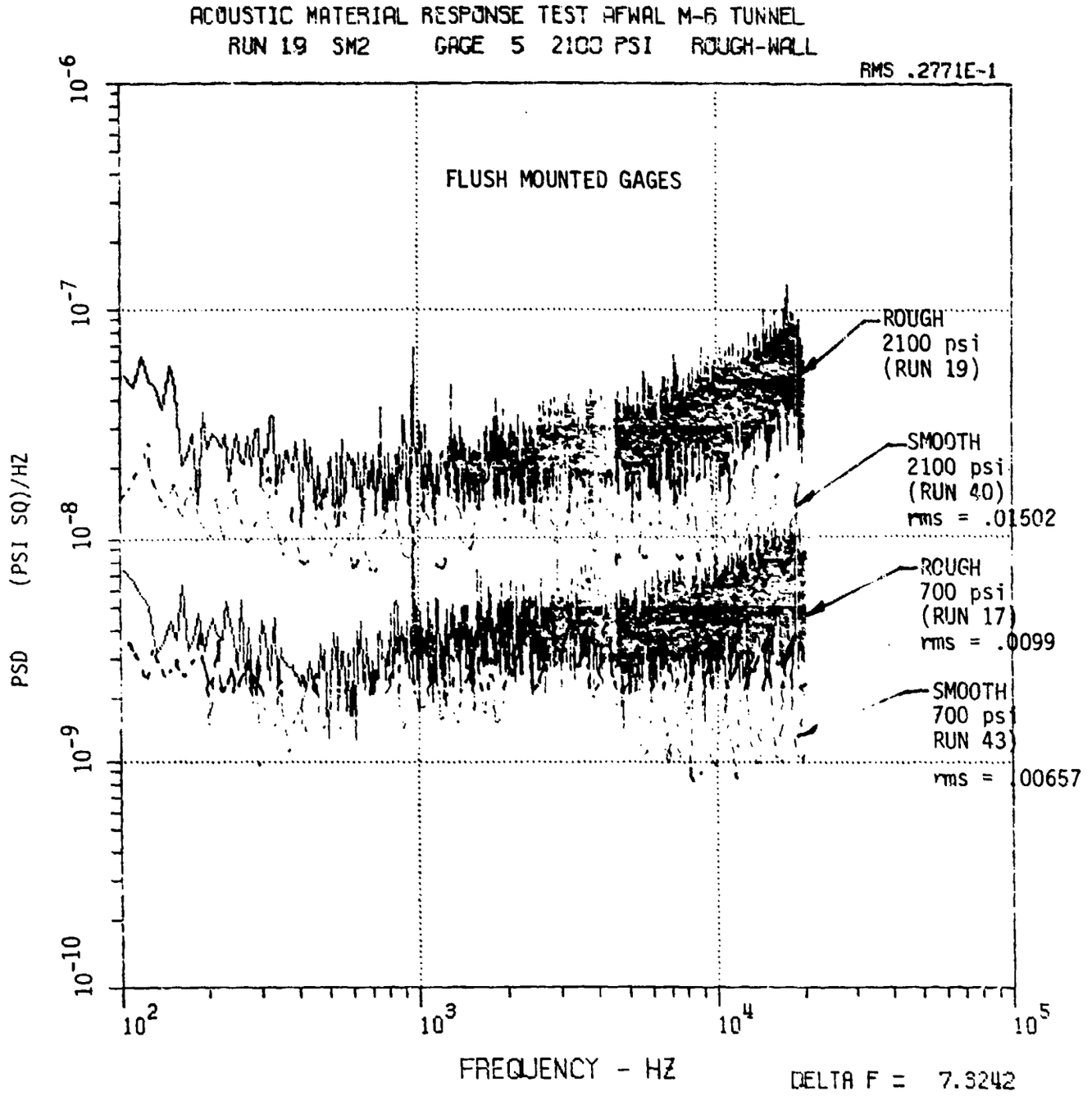

FIGURE 27. COMPARISON OF SMOOTH AND UNIFORM ROUGH WALL FLUSH MOUNTED SENSORS

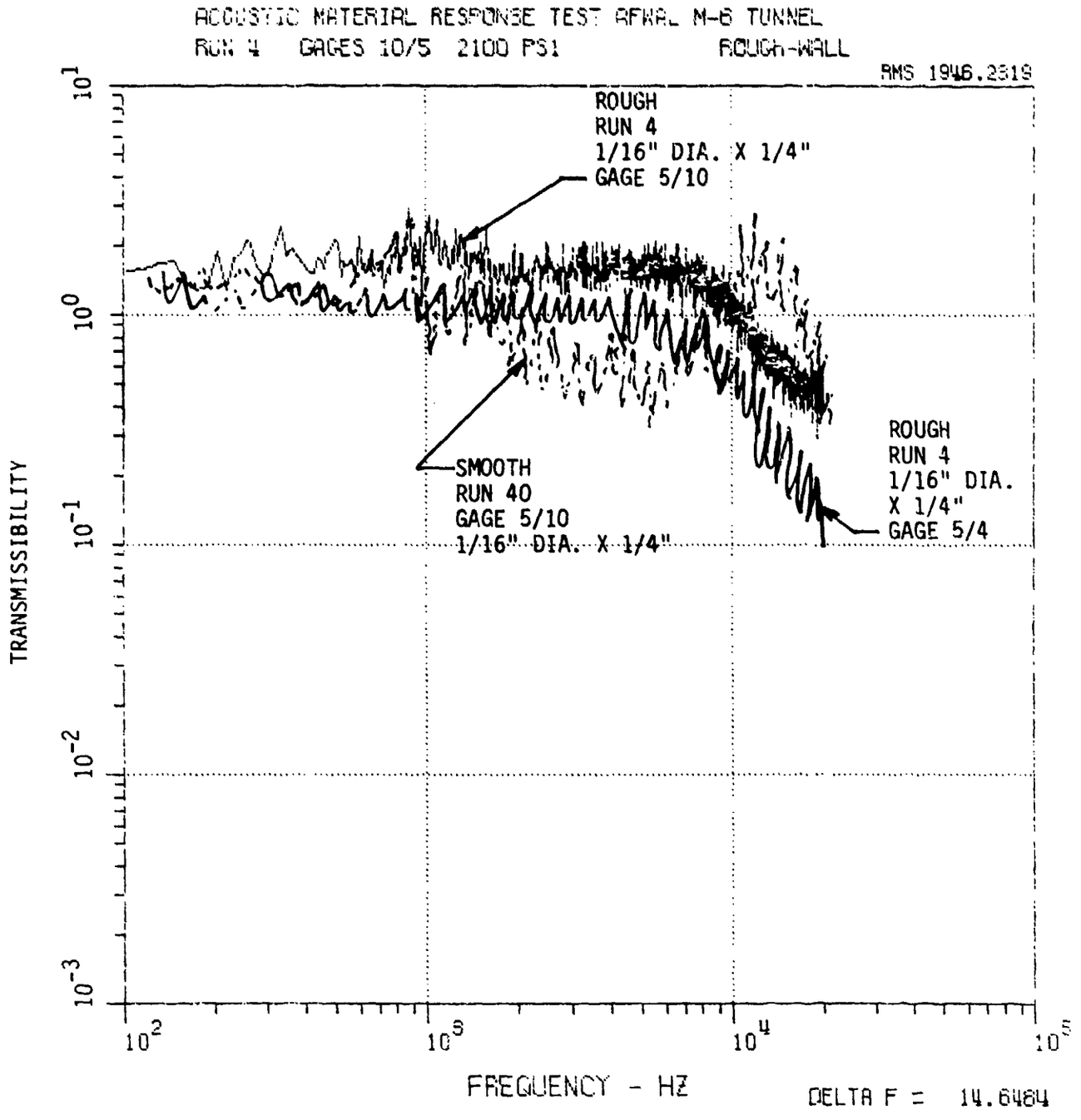

FIGURE 28. COMPARISON OF SMOOTH AND UNIFORM ROUGHNESS PORTED GAGES

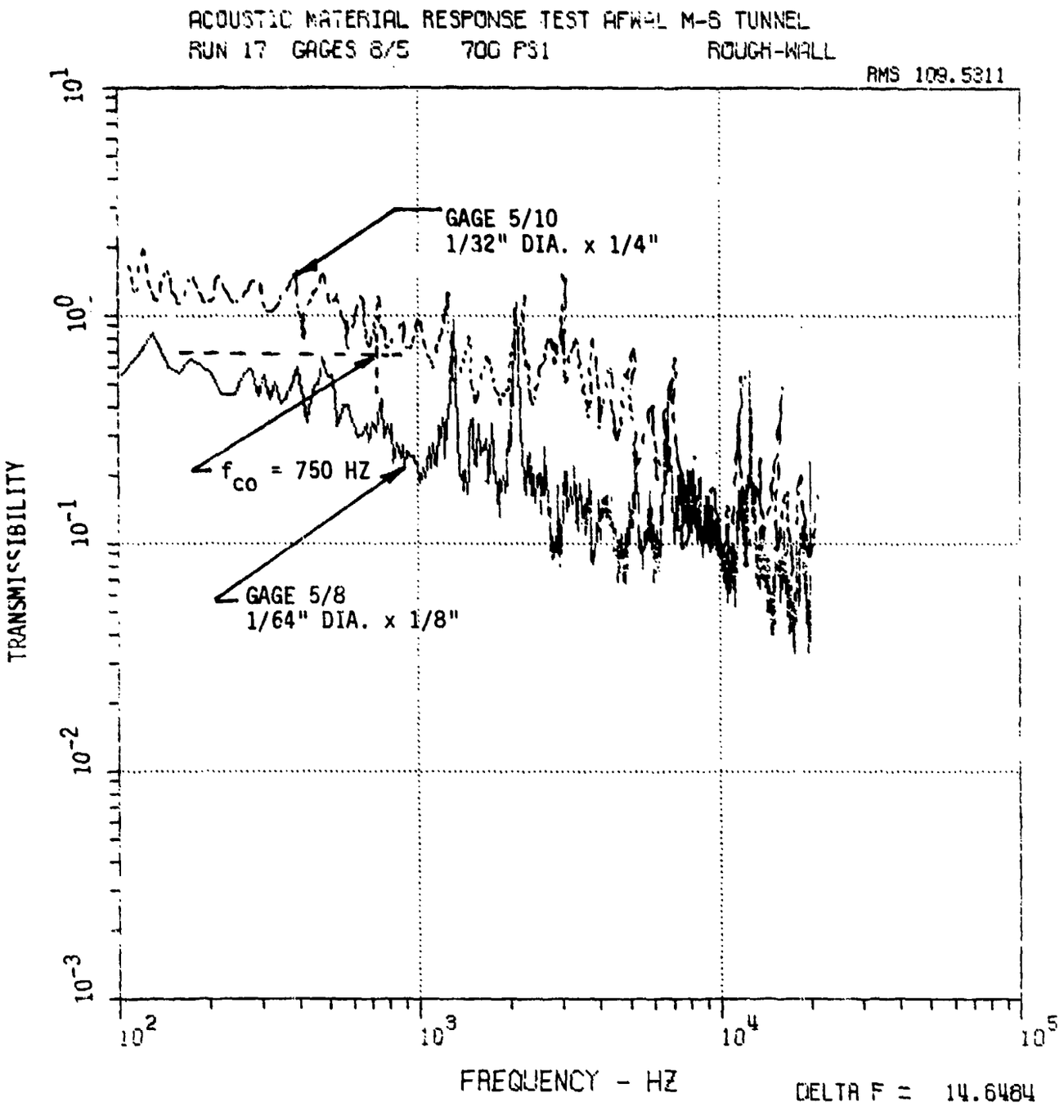

FIGURE 29. CUT-OFF FREQUENCY CHARACTERISTICS FOR PORTED GAGES ON ROUGH SURFACES

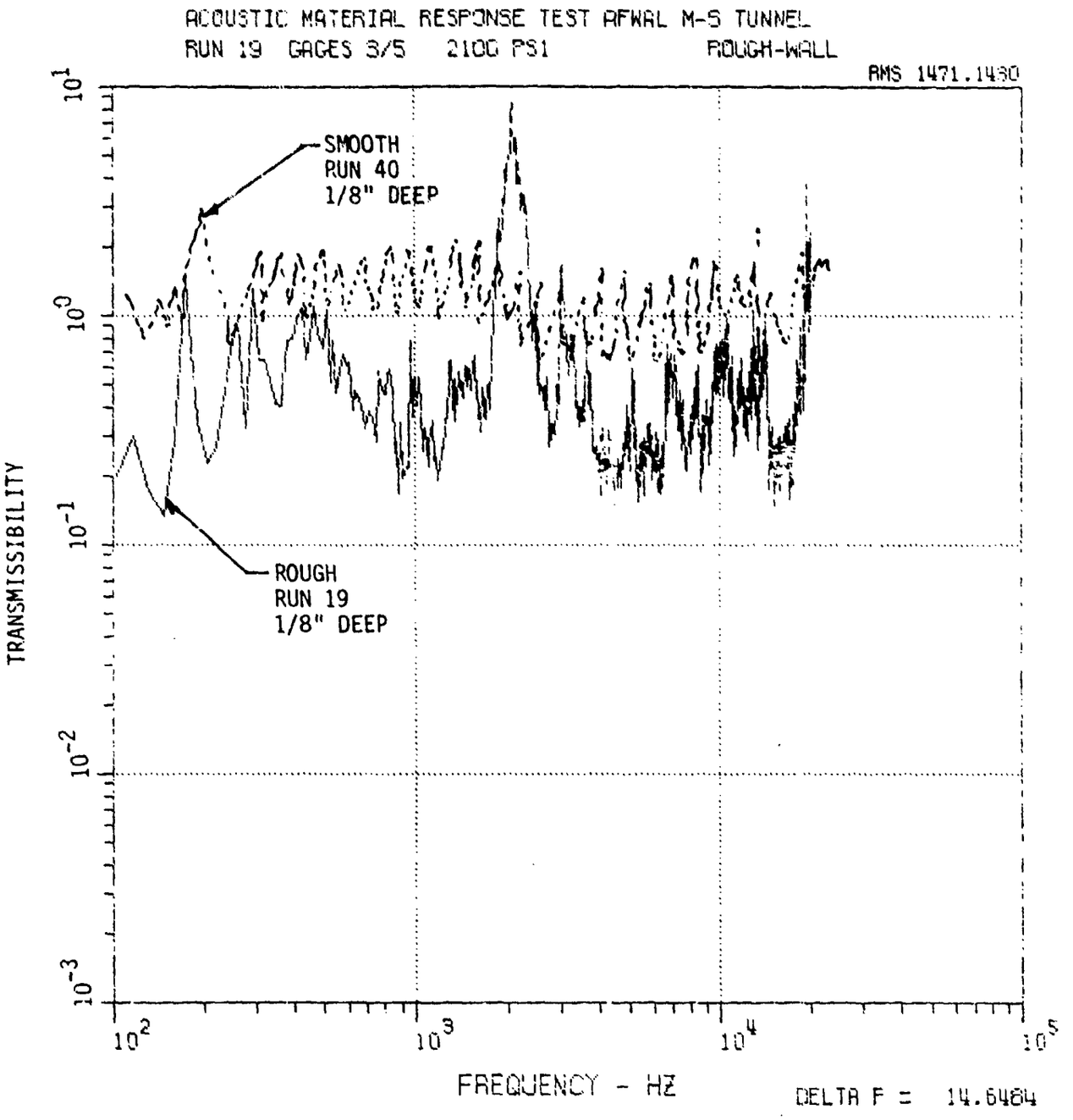

FIGURE 30. BACKFACE (BLIND GAGE) ACOUSTIC RESPONSE FOR UNIFORM ROUGH WALL CONDITIONS

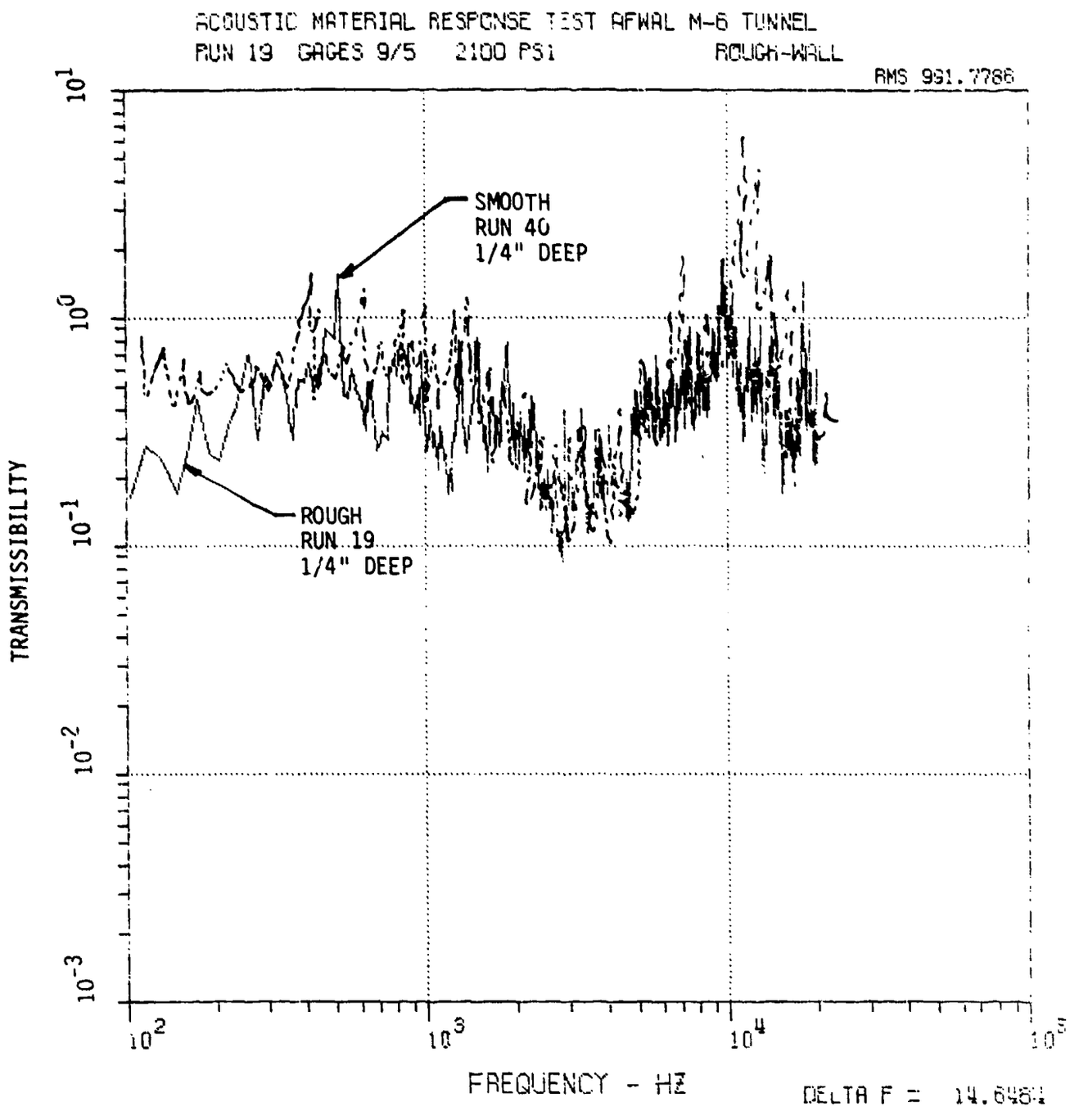

FIGURE 31. BACKFACE (BLIND GAGE) ACOUSTIC RESPONSE FOR UNIFORM ROUGH WALL CONDITIONS

REFERENCES

1 Laganelli, A. L. and Howe, J. R., "Prediction of Pressure Fluctuations Associated with Maneuvering Reentry Weapons," AFFDL-TR-77-59, July 1977.

2. Burton, T. E., "Wall Pressure Fluctuations at Smooth and Rough Surfaces under Turbulent Boundary Layers with Favorable and Adverse Pressure Gradients," Tech. Report 70208-9, M.I.T. also AD772548.

3. Blake, W. K., "Turbulent Boundary Layer Wall Pressure Fluctuations on Smooth and Rough Walls," J. Fluid Mech., Vol. 44, Part 4, December 1970.

4. Peckham, V. D., "Boundary Layer Measurement Program, Volume I - B. L. Acoustic Monitor Development Characterization and Installation," DNA 4873F-1, June 30, 1978.

5. Lilley, G. M., "A Review of Pressure Fluctuations in Turbulent Boundary Layers at Subsonic and Supersonic Speeds," Arc. Mech. Stosow #16, 1964, p. 301 (see also AGARD Report 454, 1963.)

6. Martellucci, et al., "Damaged Heatshield Reentry Performance Evaluation," SAI-067-81R-003, February 1980. Report number to be designated.

7. Bull, M. K., "Properties of the Fluctuating Wall Pressure Field of a Turbulent Boundary Layer," AGARD Report 455, April 1963.

8. Cassanto, J. M. and Rogers, D. A., "An Experiment to Determine Nosetip Transition with Fluctuating Pressure Measurements," AIAA Paper 74-625, July 1974.

9. Houbolt, J. C., "Structural Response of Reentry Vehicles to Boundary Layer Noise," GE TIS-65SD223A, March 1965.

10. Fiore, A. W. and Law, C. H., "Aerodynamic Calibration of the Aerospace Research Laboratories M = 6 High Reynolds Number Facility," ARL TR 75-0028, February 1975.

11. Seidman, M. H., "Rough Wall Heat Transfer in a Compressible Turbulent Boundary Layer," AIAA Paper No. 78-163 presented at the AIAA 16th Aerospace Sciences Meeting, Huntsville, Ala., January 16-18, 1978.

12. Droblenkov, V. D., "The Turbulent Boundary Layer on a Rough Curvilinear Surface," NACA TM 1440, 1955.

13. Laganelli, A. L., Fogaroli, R., and Martellucci, A., "The Effect of Mach Number and Wall Temperature on Turbulent Heat Blockage Resulting from Mass Injection," presented at AIAA 12th Thermophysics Conference, Albuquerque, New Mexico, June 1977, Paper No. 77-784. Published in Progress in Astronautics and Aeronautics, Vol, 59, L. S. Fletcher Editor, 1978.

14. Spadling, D. B., Auslander, D. M., and Sundaram, T. R., "The Calculation of Heat and Mass Transfer Through the Turbulent Boundary Layer on a Flat Plate at High Mach Numbers, with and without Chemical Reaction," AGARD Combustion and Propulsion Colloquium, London, 1963.

15. Fenter, F. W., "The Turbulent Boundary Layer on Uniform Rough Surfaces at Supersonic Speeds," University of Texas Report DRL-437, January 1960.

16. Winter, K. G. and Gaudet, L., "Some Recent Work on Compressible Turbulent Boundary Layers and Excerscence Drag," NSAA SP-216, December 1968.

17. Laganelli, A. L. and Scntowski, J., "Prediction of Skin Friction with Coupled Roughness and Blowing Based on Transformation Functions," Presented at AIAA 20th Aerospace Sciences Meeting, January 11, 1982, Paper No. 82-0033.

18. Dirling, R. B., "A Method for Computing Rough Wall Heat Transfer Rates on Reentry Nosetips," AIAA Paper No. 73-763, Presented at AIAA 8th Thermophysics Conference, July 16, 1973.

APPENDIX A
SHOCK TUBE DATA

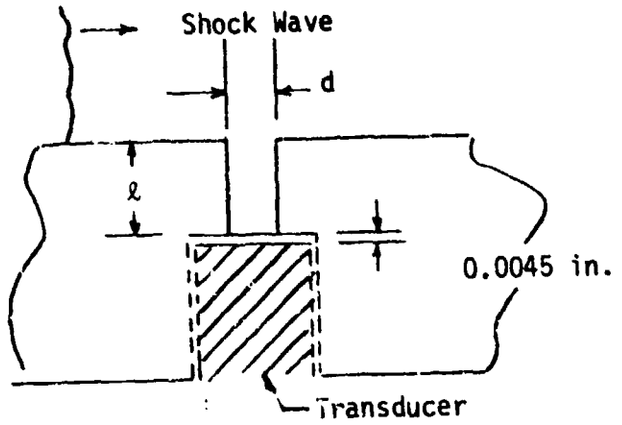

Notation: ℓxd

a. Ported Gage:

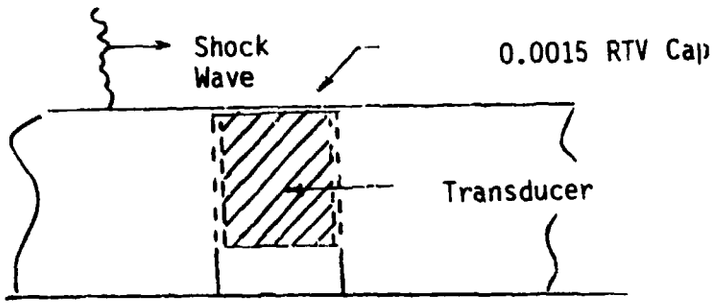

b. Flush-Mounted Gage

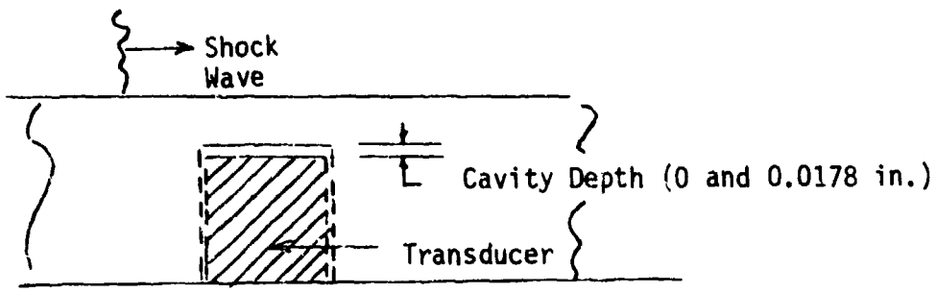

FIGURE A-1. BACKFACED MOUNTED (BLIND) GAGE

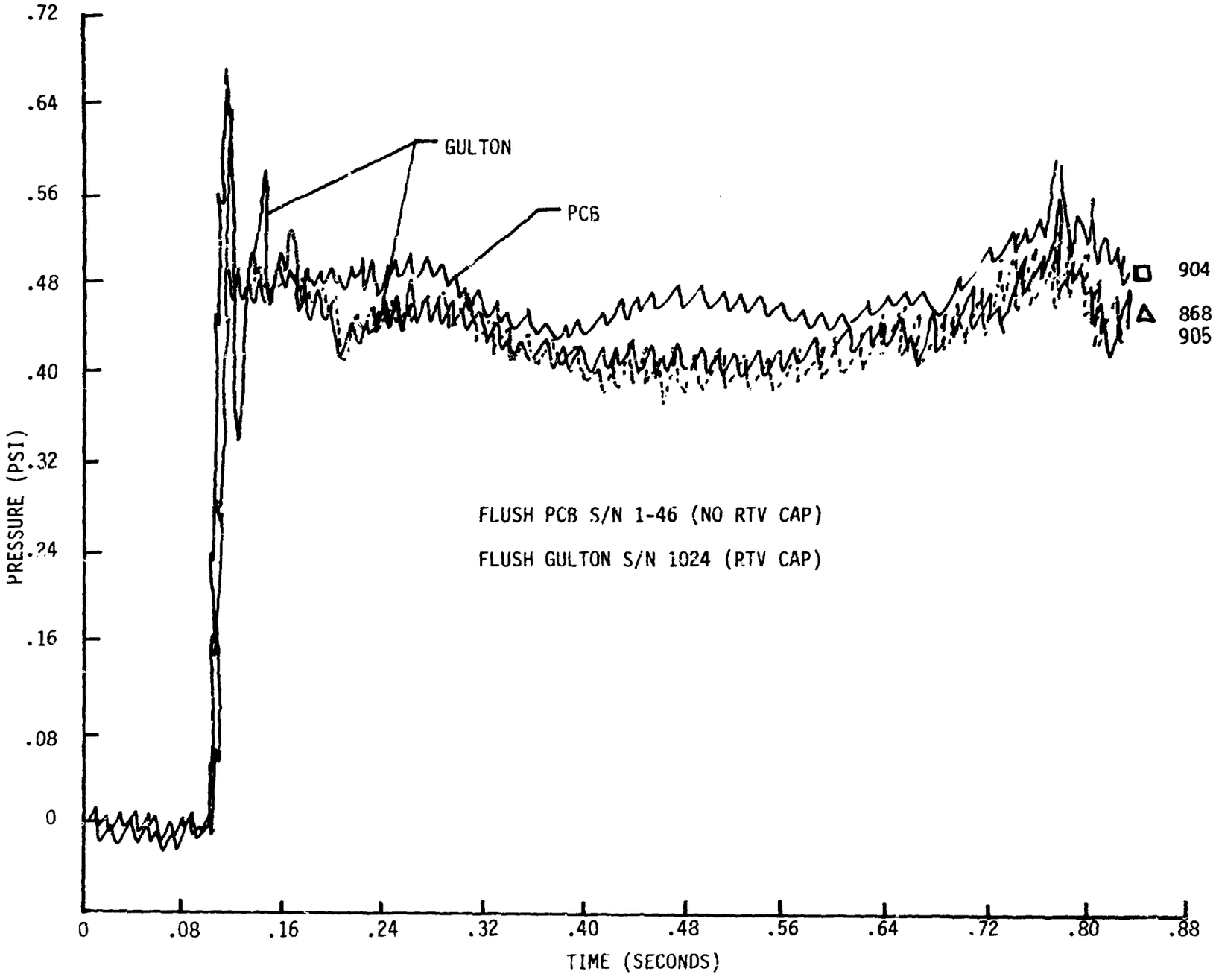

FIGURE A-2. FLUSH-MOUNTED TRANSDUCERS - RESPONSE TO PRESSURE STEP IMPOSED BY SHOCK MOVING PAST SURFACE MOUNTED TRANSDUCERS

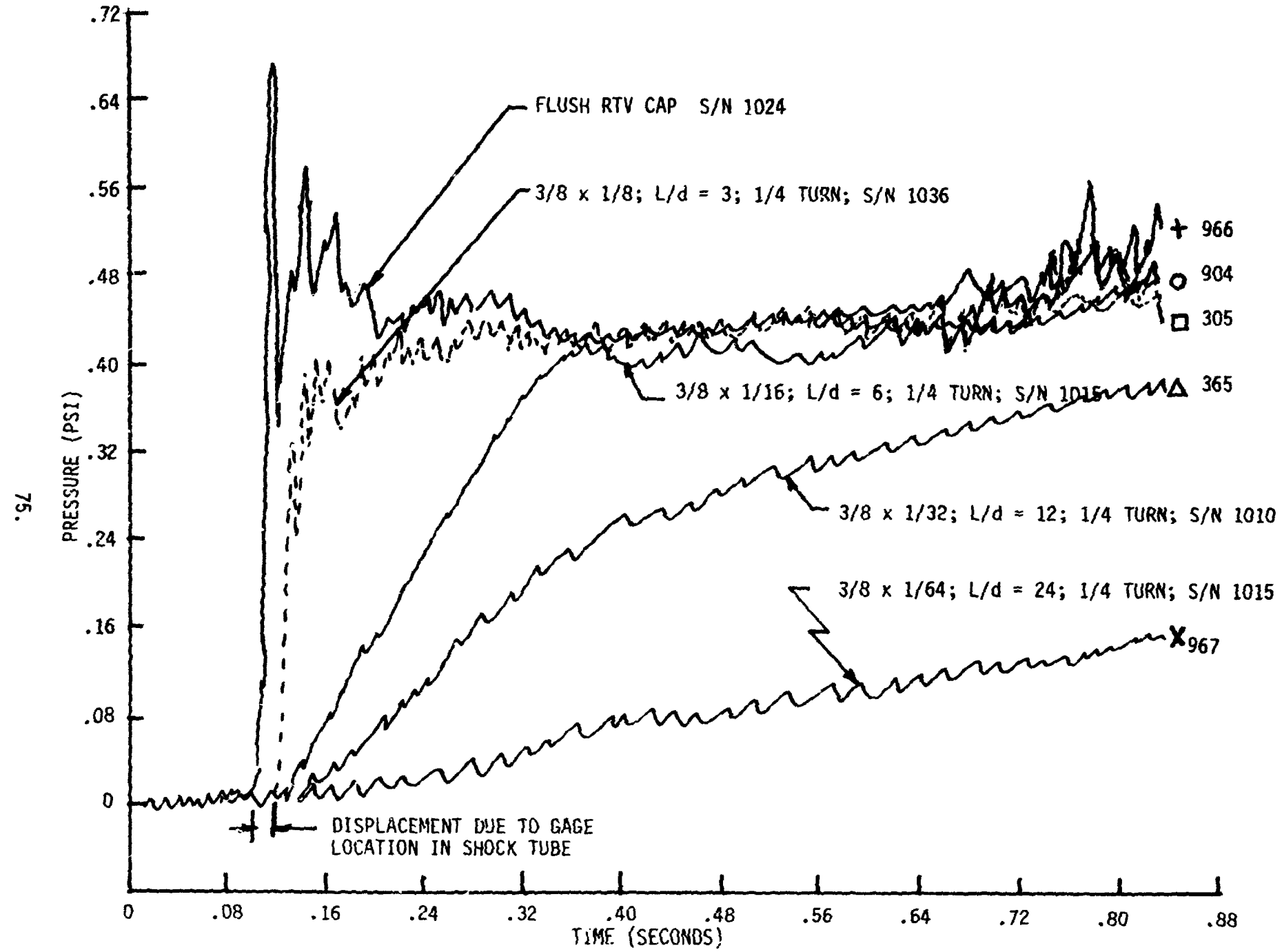

FIGURE A-3. EFFECT OF PORTED HOLE DEPTH - HOLE DEPTH 0.375 IN.

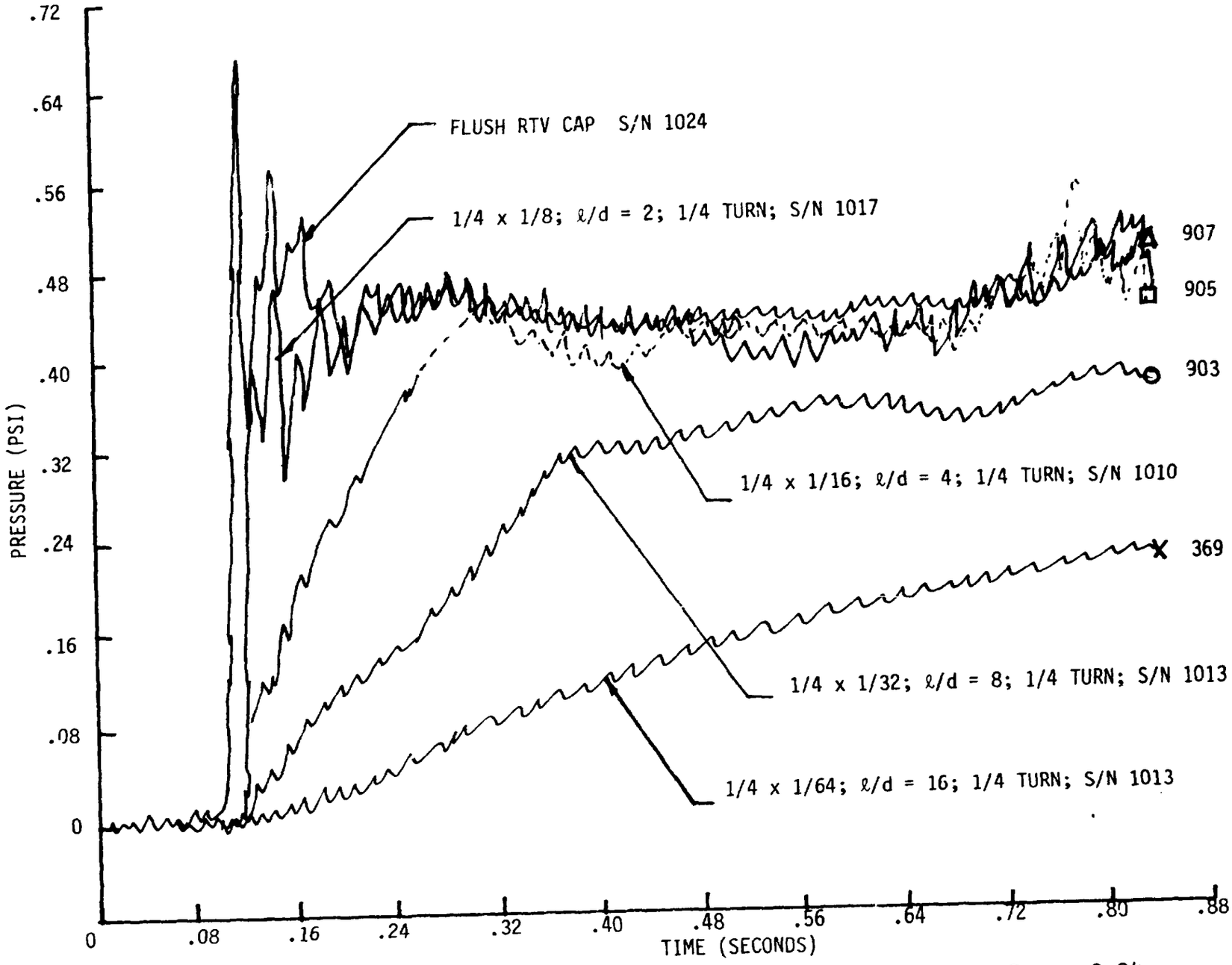

FIGURE A-4. EFFECT OF PORTED HOLE DEPTH - HOLE DEPTH 0.24 IN.

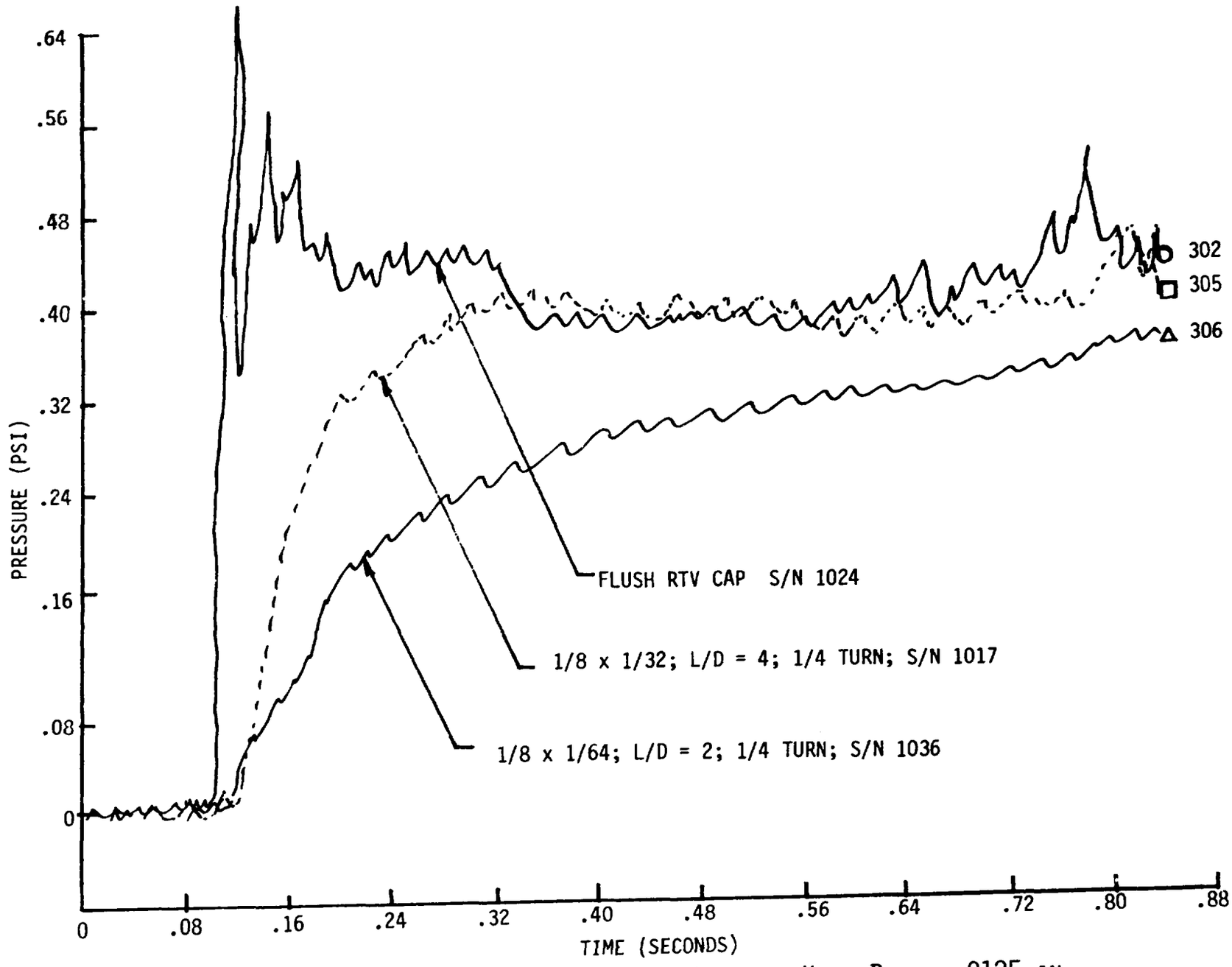

FIGURE A-5. EFFECT OF PORTED HOLE DEPTH - HOLE DEPTH .0125 IN.

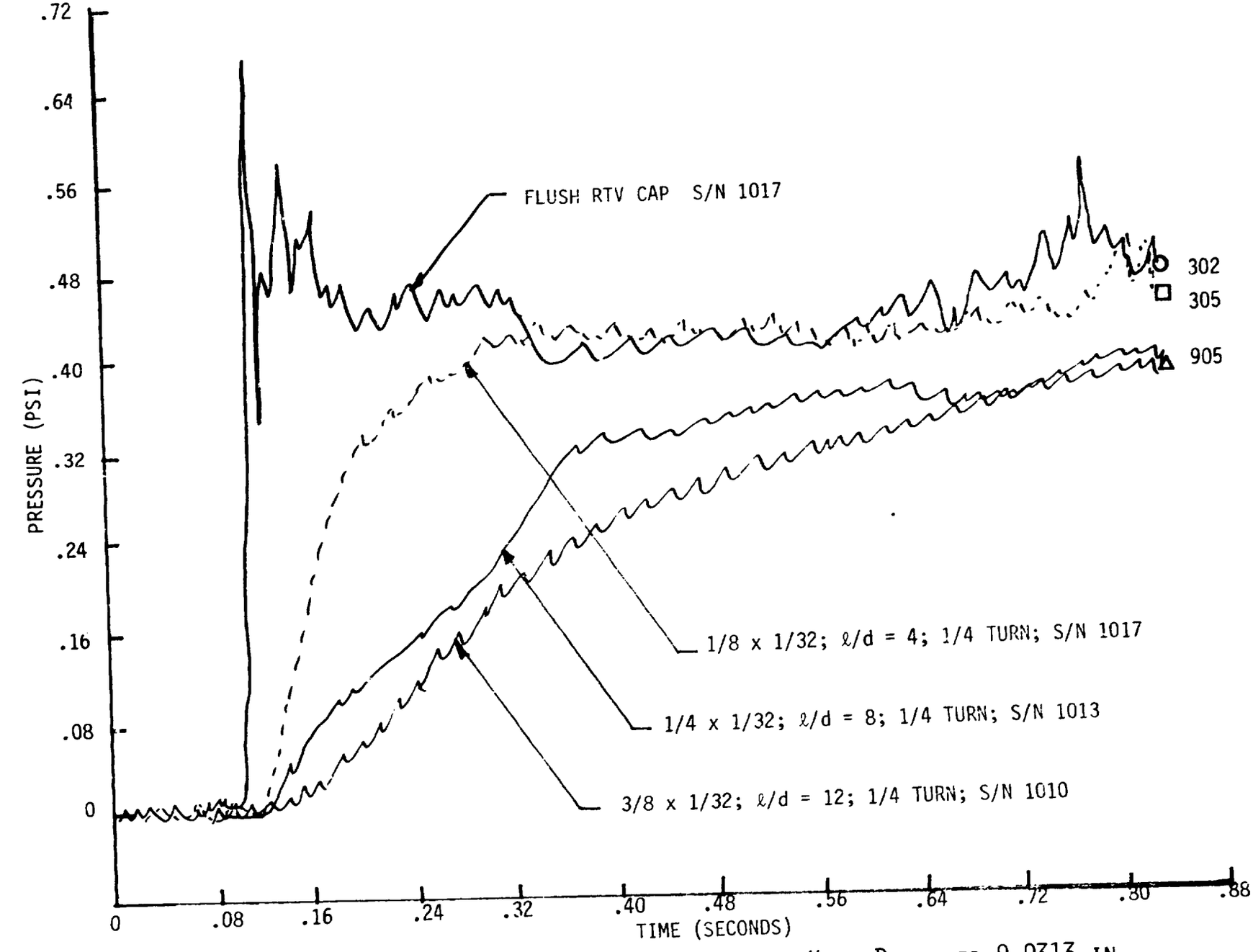

FIGURE A-6. EFFECT OF PORTED HOLE DEPTH - HOLE DIAMETER 0.0313 IN.

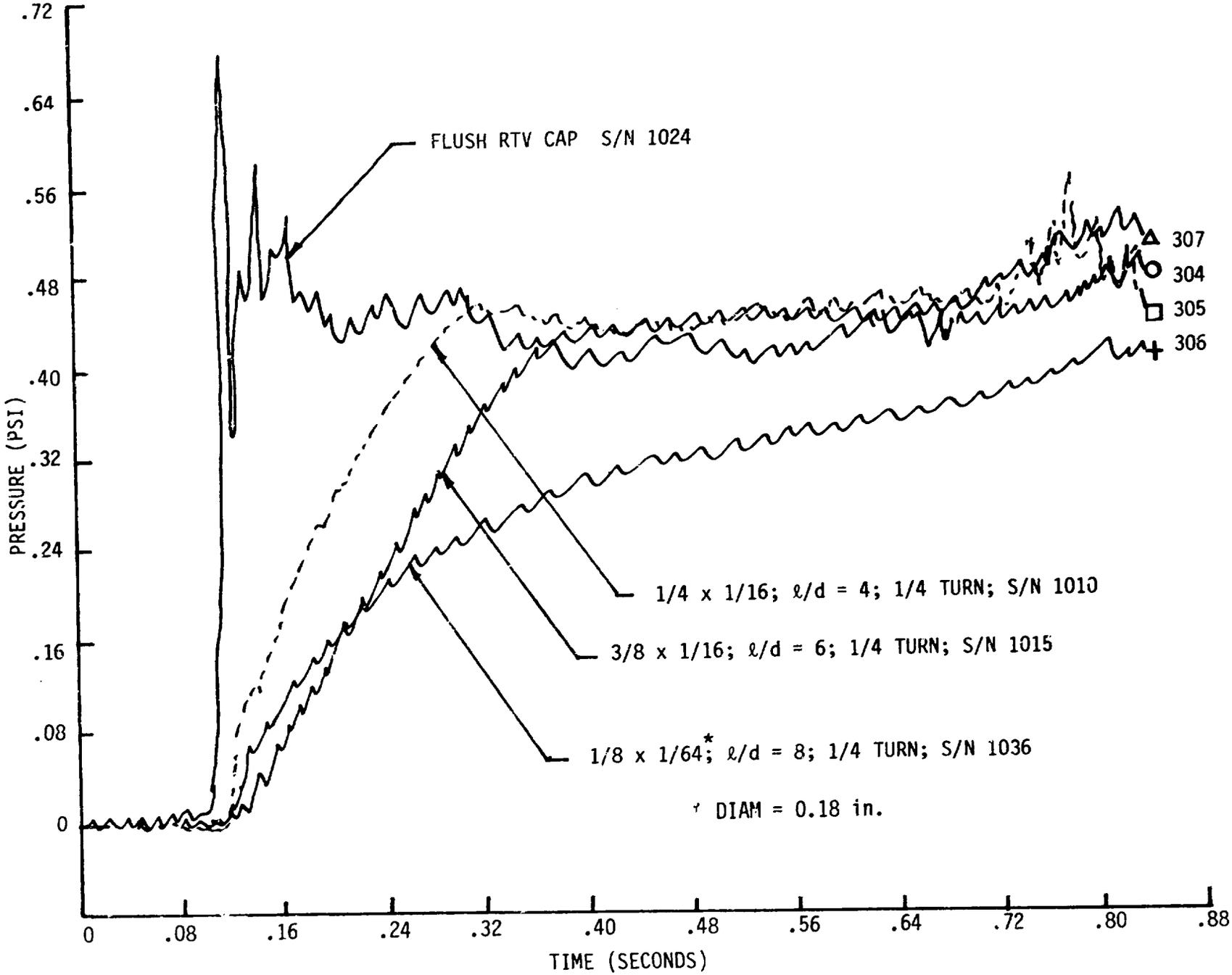

FIGURE A-7. EFFECT OF PORTED HOLE DEPTH - HOLE DIAMETER 0.0625 IN.

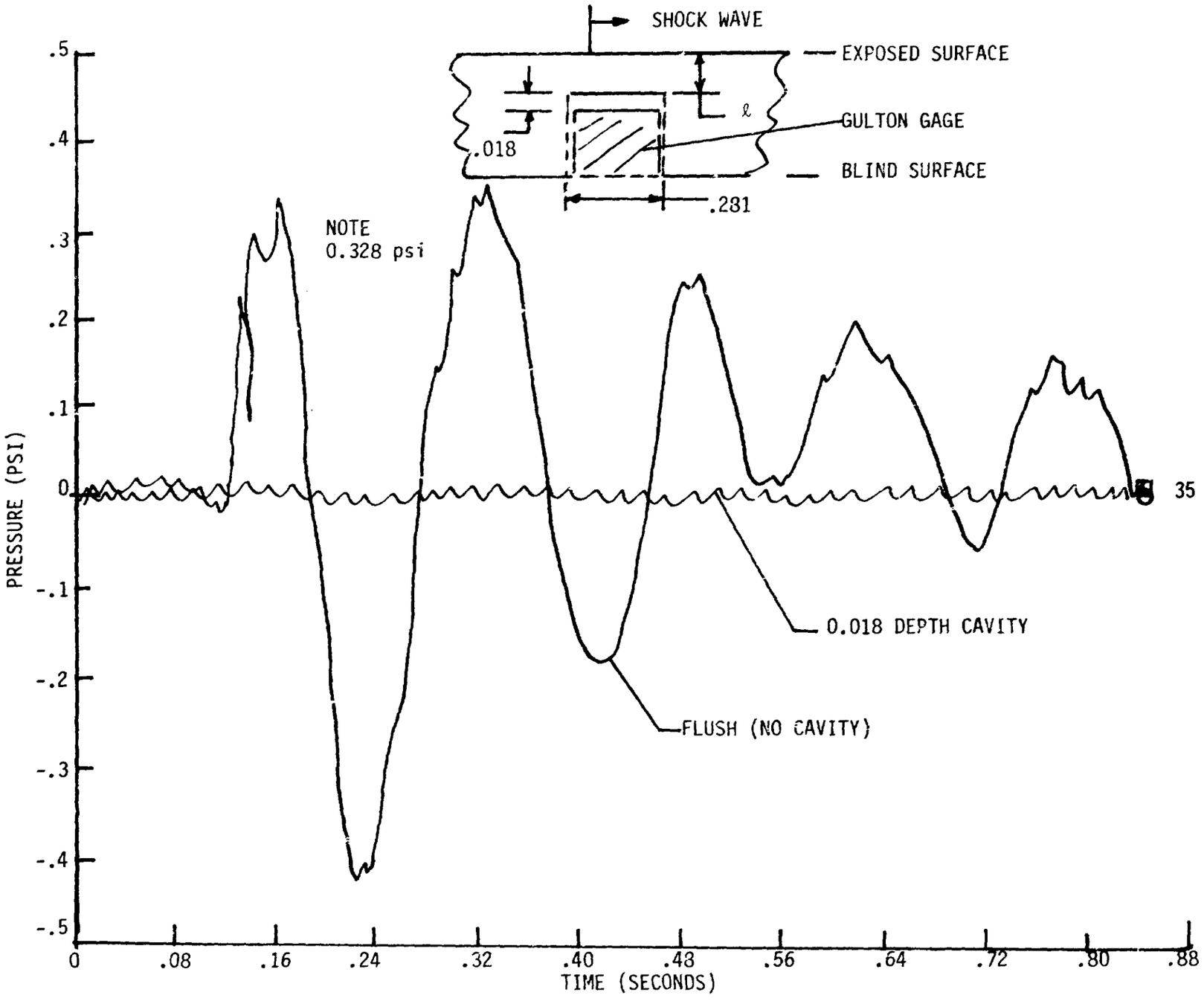

FIGURE A-8. BACKFACE MOUNTED TRANSDUCERS - CAVITY EFFECTS

APPENDIX B
SMOOTH WALL DATA

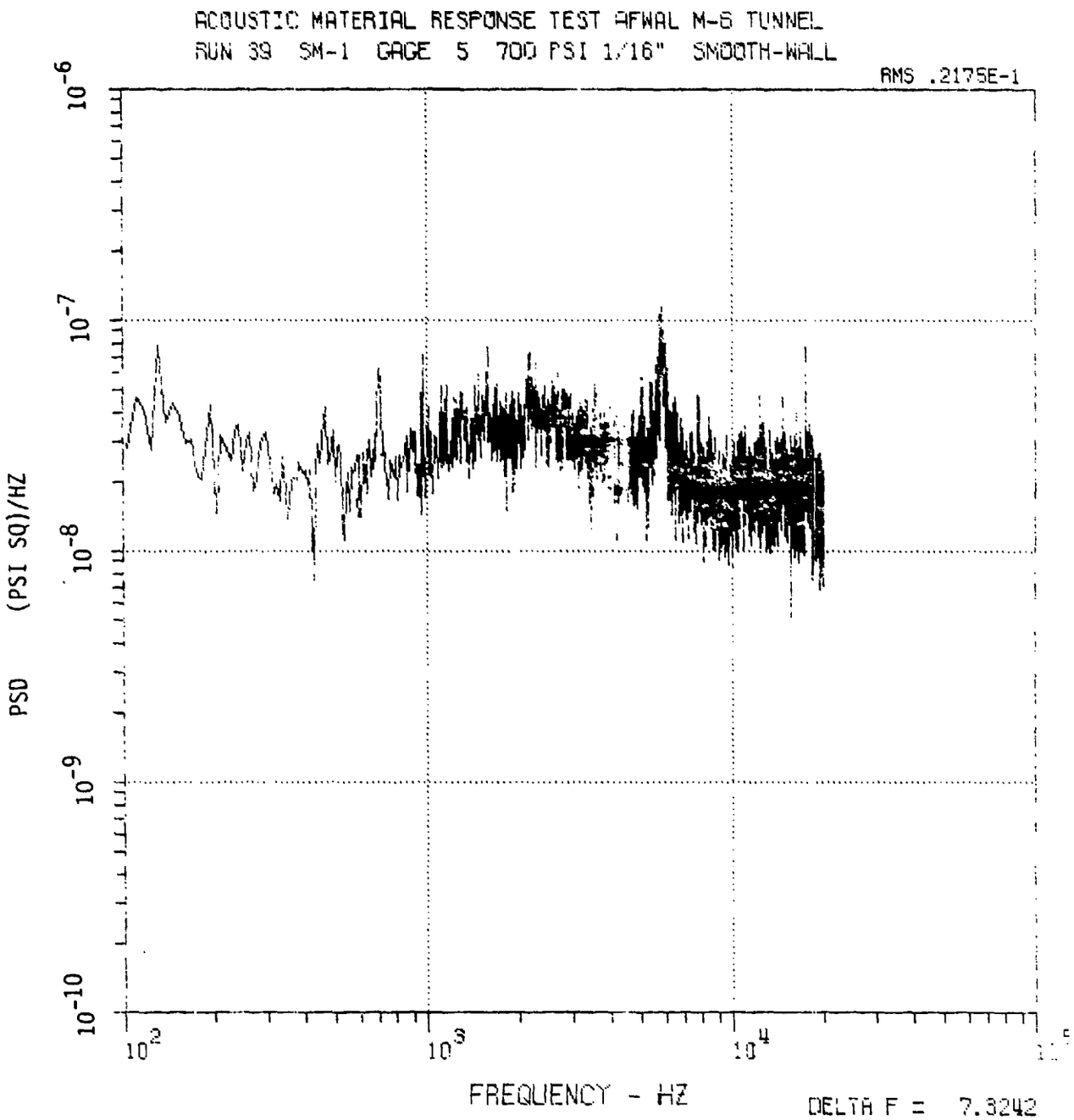
ACOUSTIC MATERIAL RESPONSE TEST AFWAL M-6 TUNNEL
RUN 39 SM-1 GAGE 5 700 PSI 1/16" SMOOTH-WALL
RMS .2175E-1
PSD (PSI SQ)/HZ
10^{-6}
10^{-7}
10^{-8}
10^{-9}
10^{-10}
10^{2}
10^{3}
10^{4}
FREQUENCY - HZ
DELTA F = 7.3242

FIGURE B-1

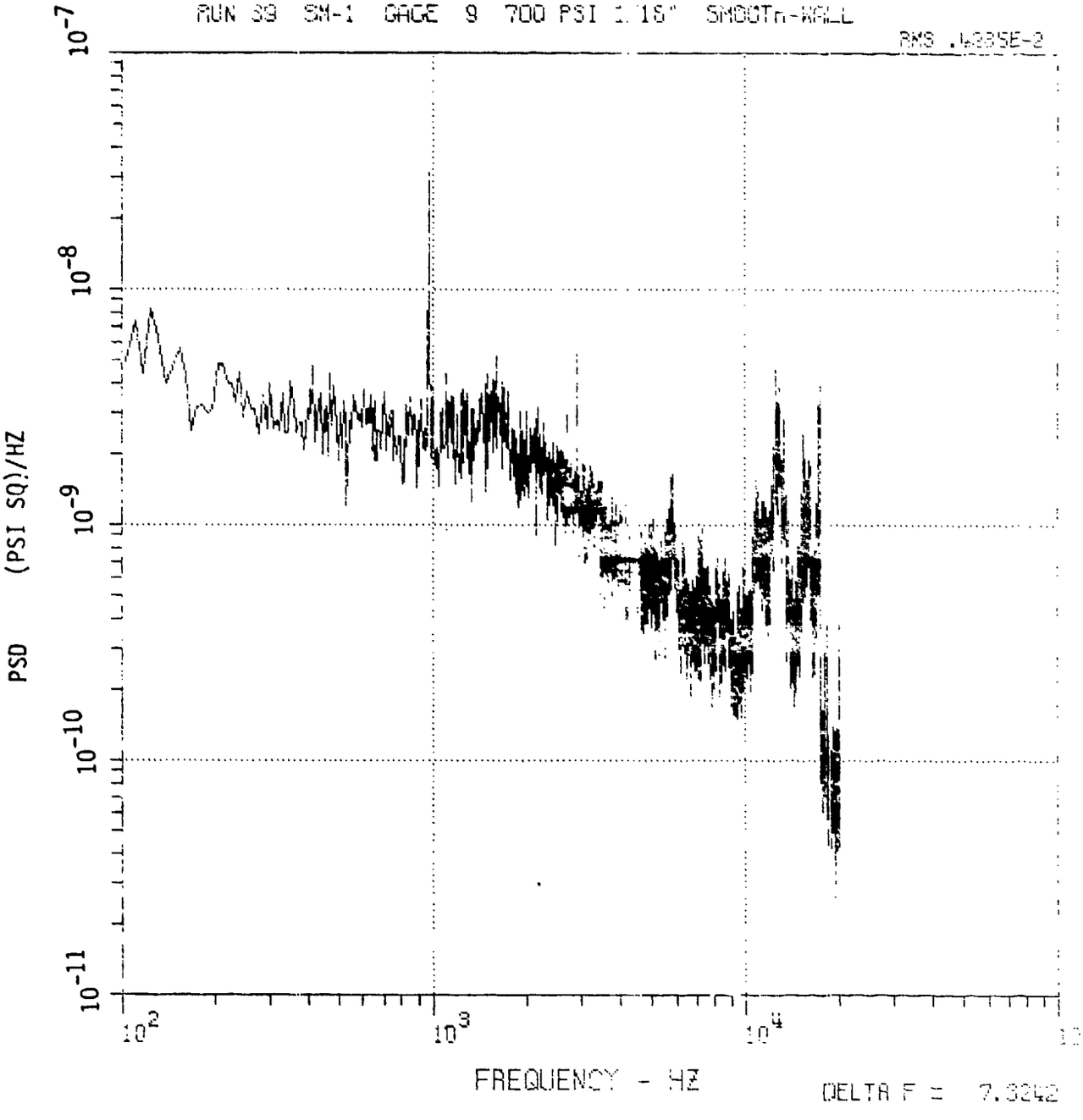
ACOUSTIC MATERIAL RESPONSE TEST TFWAL M-6 TUNNEL
RUN 39 SM-1 GAGE 9 700 PSI 1.15" SMOOTH-WALL
RMS .4385E-2
PSD (PSI SQ)/HZ
10^{-7}
10^{-8}
10^{-9}
10^{-10}
10^{-11}
10^{2}
10^{3}
10^{4}
FREQUENCY - HZ
DELTA F = 7.3242

FIGURE B-2

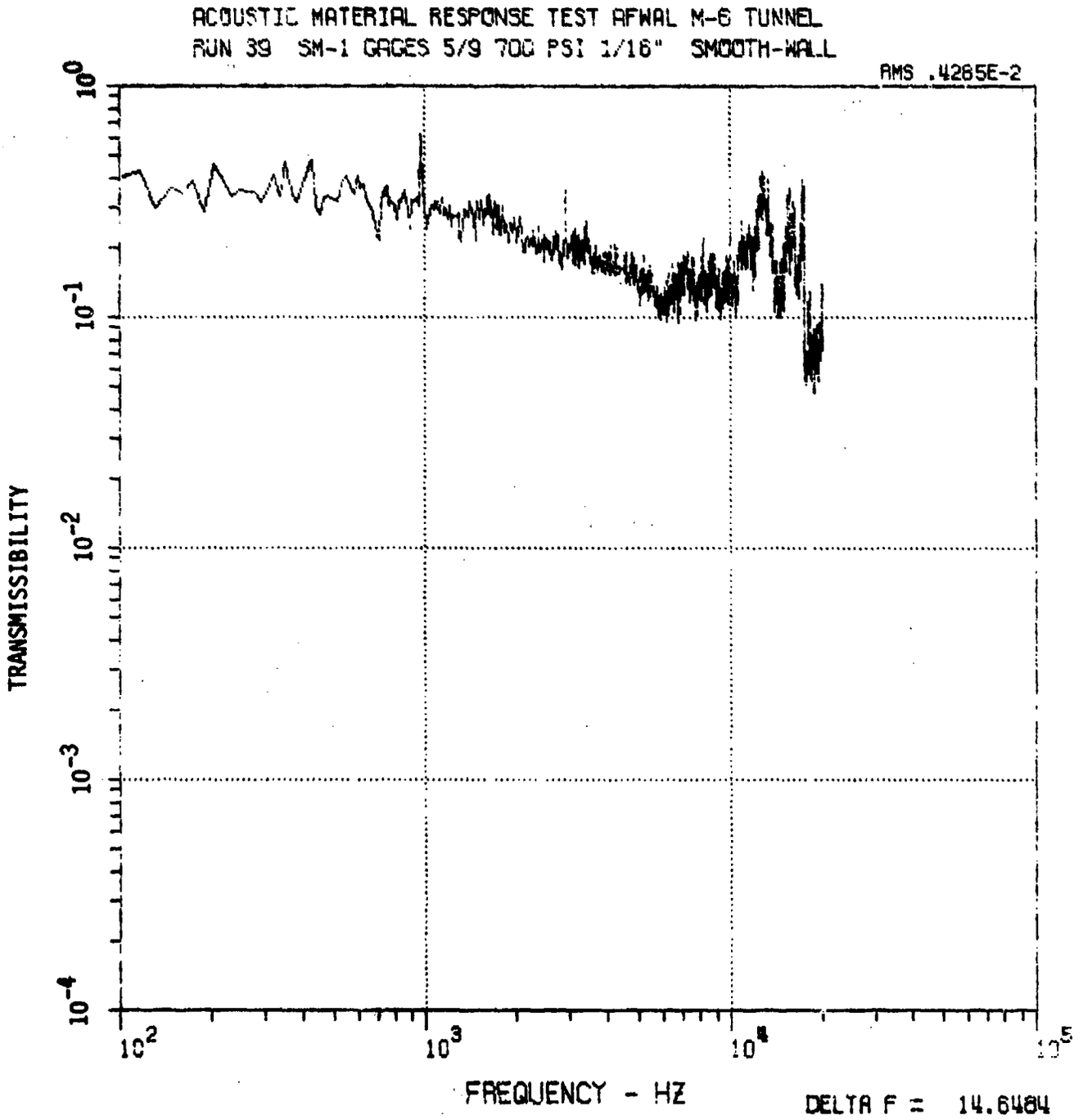
ACOUSTIC MATERIAL RESPONSE TEST AFWAL M-6 TUNNEL
RUN 39 SM-1 GAGES 5/9 700 PSI 1/16" SMOOTH-WALL
RMS .4265E-2
TRANSMISSIBILITY
10^{0}
10^{-1}
10^{-2}
10^{-3}
10^{-4}
10^{2}
10^{3}
10^{4}
10^{5}
FREQUENCY - HZ
DELTA F = 14.6484

FIGURE B-3

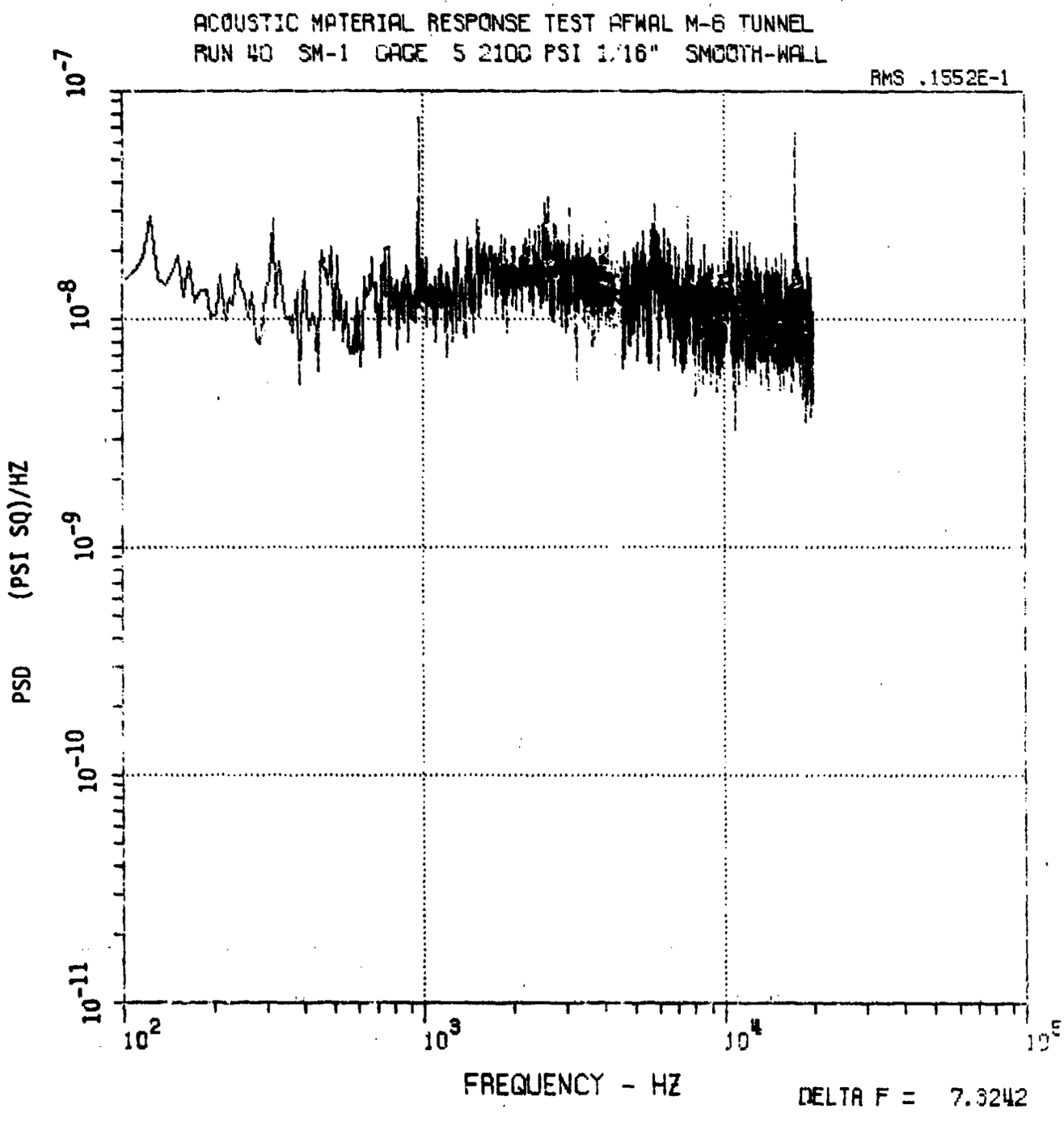
ACOUSTIC MATERIAL RESPONSE TEST AFWAL M-6 TUNNEL
RUN 40 SM-1 GAGE 5 2100 PSI 1/16" SMOOTH-WALL
RMS .1552E-1
PSD (PSI SQ)/HZ
10^{-7}
10^{-8}
10^{-9}
10^{-10}
10^{-11}
10^{2}
10^{3}
10^{4}
10^{5}
FREQUENCY - HZ
DELTA F = 7.3242

FIGURE B-4

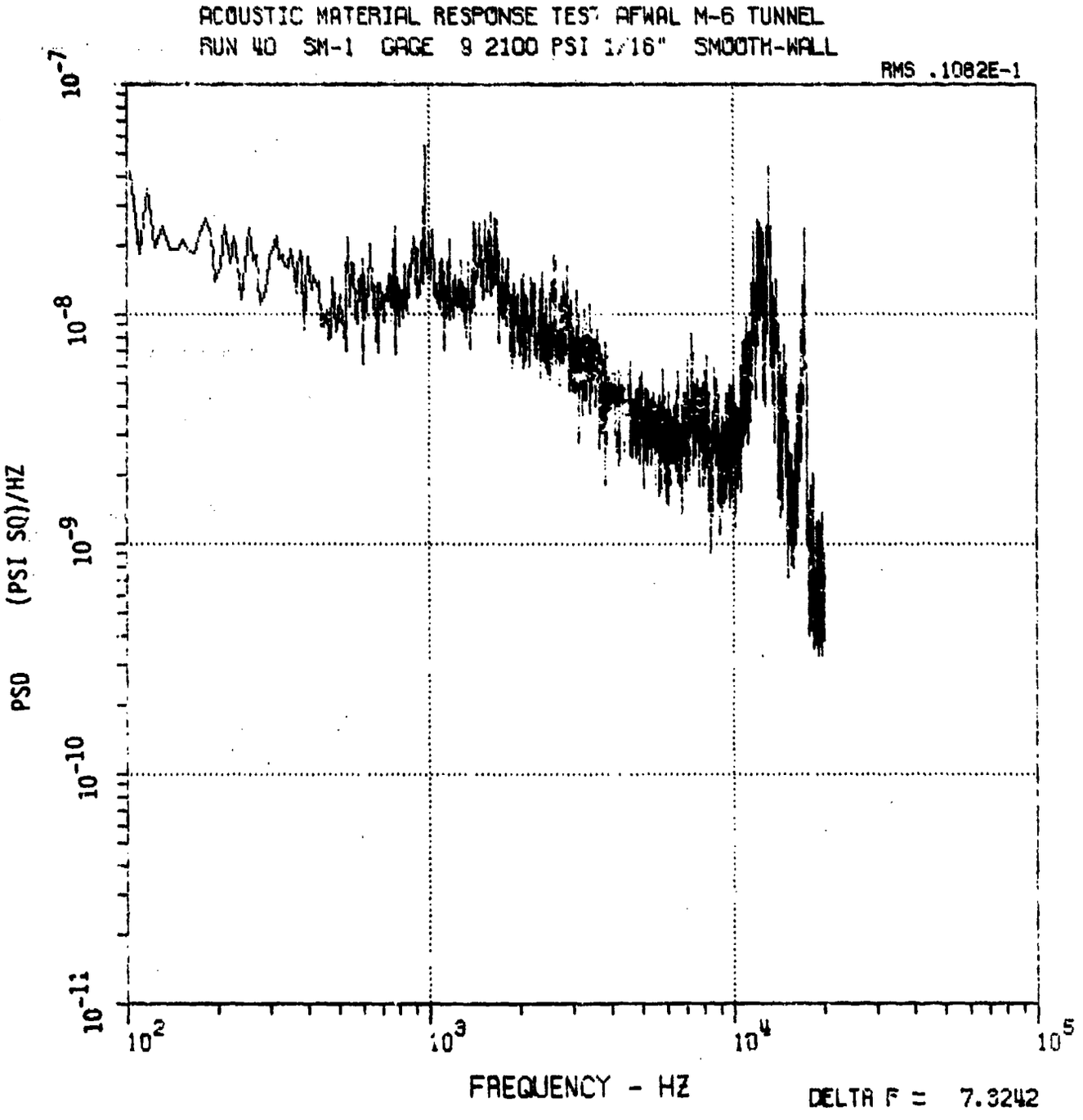
ACOUSTIC MATERIAL RESPONSE TEST AFWAL M-6 TUNNEL
RUN 40 SM-1 GAGE 9 2100 PSI 1/16" SMOOTH-WALL
RMS .1082E-1
PSD (PSI SQ)/HZ
10^{-7}
10^{-8}
10^{-9}
10^{-10}
10^{-11}
10^{2}
10^{3}
10^{4}
10^{5}
FREQUENCY - HZ
DELTA F = 7.3242

FIGURE B-5

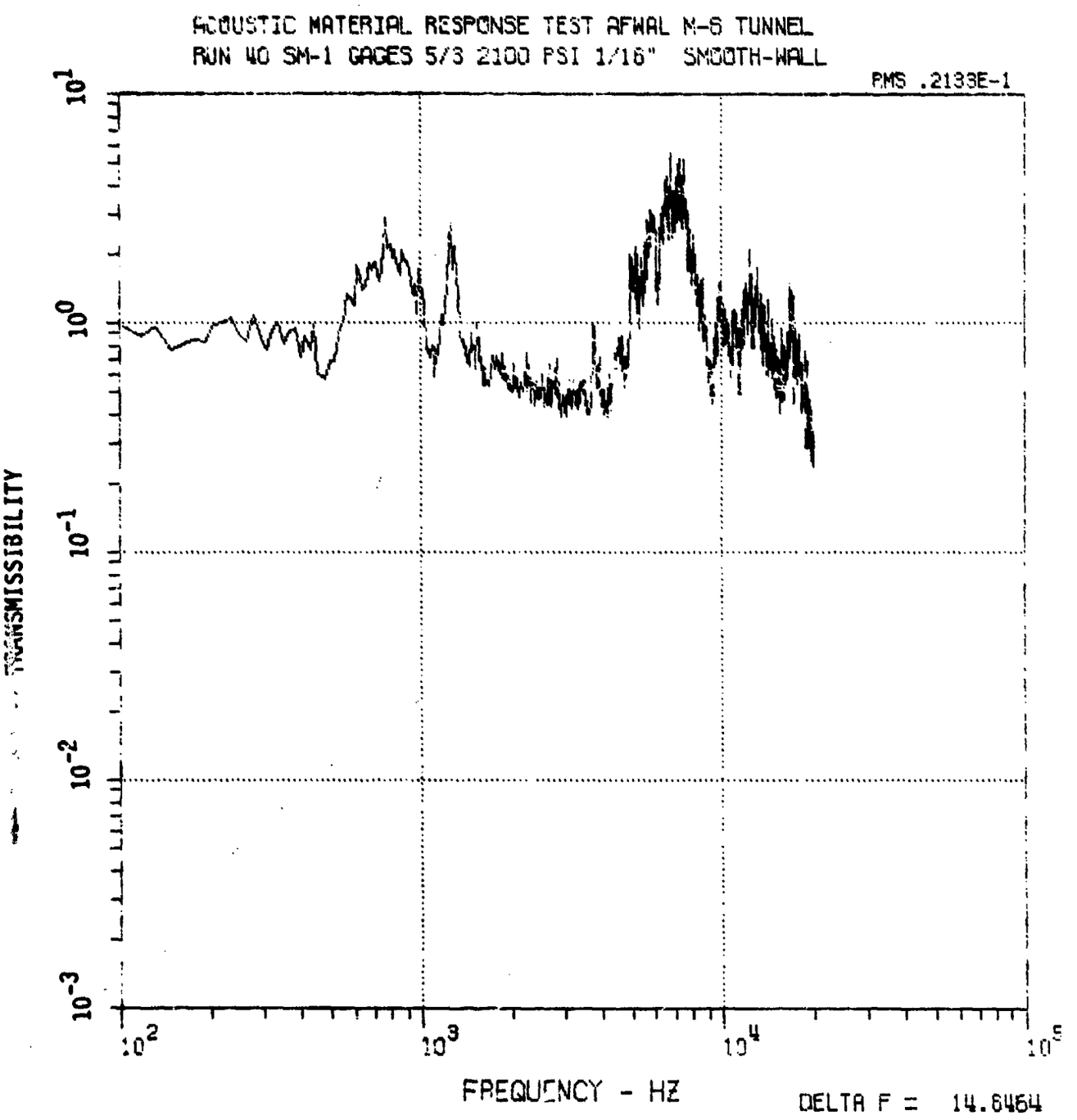
ACOUSTIC MATERIAL RESPONSE TEST AFWAL M-6 TUNNEL
RUN 40 SM-1 GAGES 5/3 2100 PSI 1/16" SMOOTH-WALL
RMS .2133E-1
TRANSMISSIBILITY
10^{1}
10^{0}
10^{-1}
10^{-2}
10^{-3}
10^{2}
10^{3}
10^{4}
10^{5}
FREQUENCY - HZ
DELTA F = 14.6464

FIGURE B-6

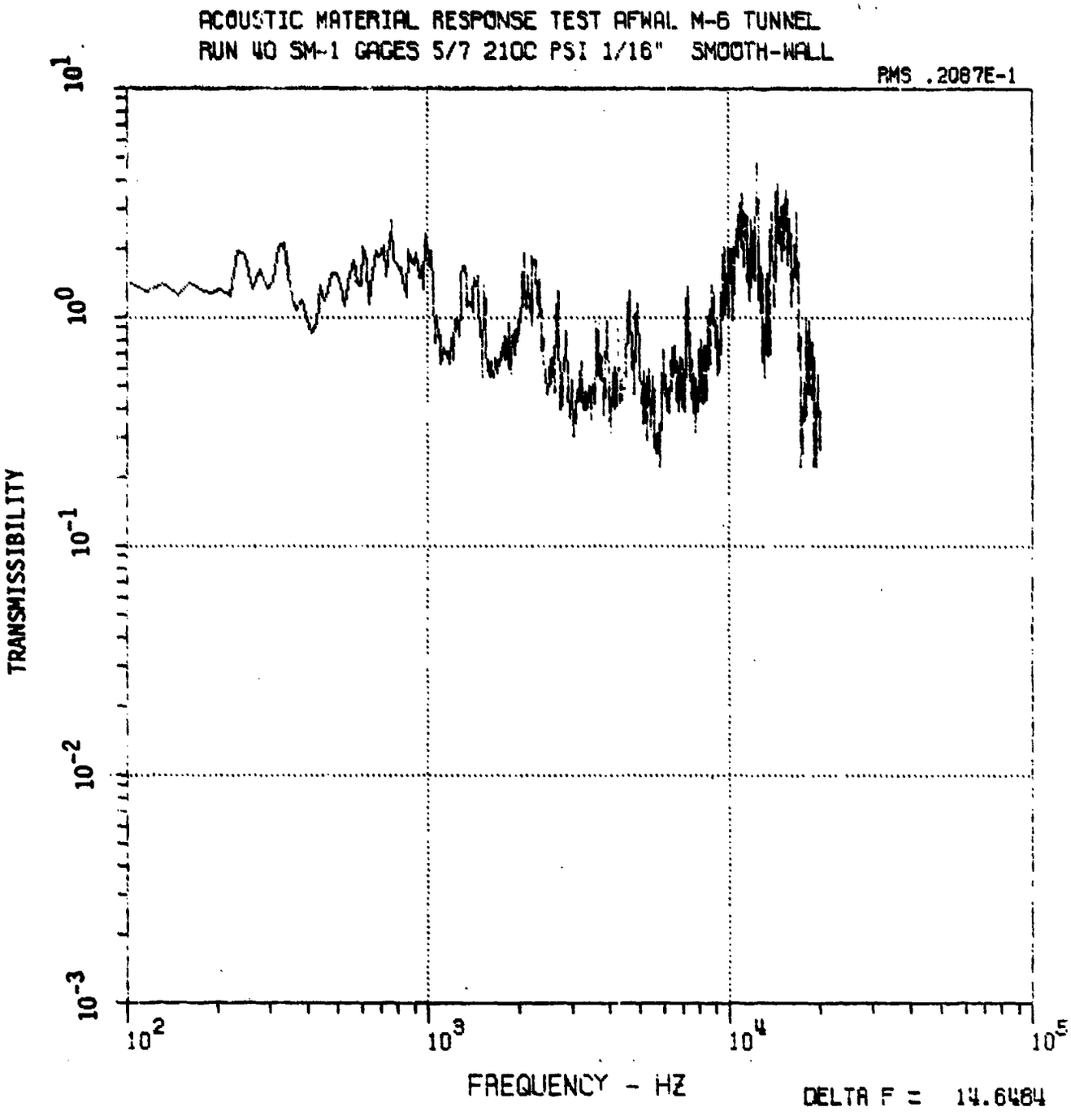
ACOUSTIC MATERIAL RESPONSE TEST AFWAL M-6 TUNNEL
RUN 40 SM-1 GAGES 5/7 210C PSI 1/16" SMOOTH-WALL
RMS .2087E-1
TRANSMISSIBILITY
10^{1}
10^{0}
10^{-1}
10^{-2}
10^{-3}
10^{2}
10^{3}
10^{4}
10^{5}
FREQUENCY - HZ
DELTA F = 14.6484

FIGURE B-7

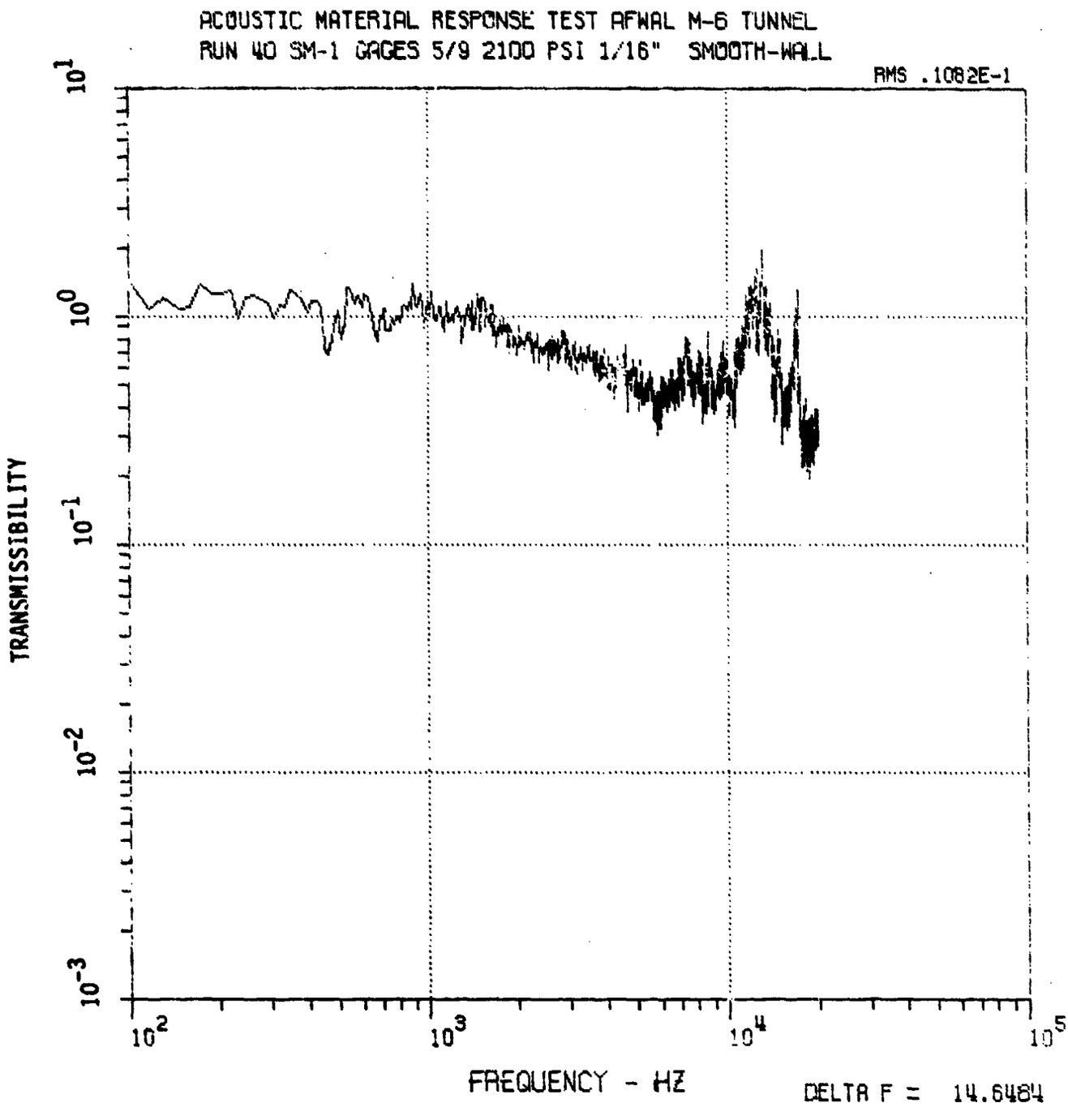
ACOUSTIC MATERIAL RESPONSE TEST AFWAL M-6 TUNNEL
RUN 40 SM-1 GAGES 5/9 2100 PSI 1/16" SMOOTH-WALL
RMS .1082E-1
TRANSMISSIBILITY
10^{1}
10^{0}
10^{-1}
10^{-2}
10^{-3}
10^{2}
10^{3}
10^{4}
10^{5}
FREQUENCY - HZ
DELTA F = 14.6484

FIGURE B-8

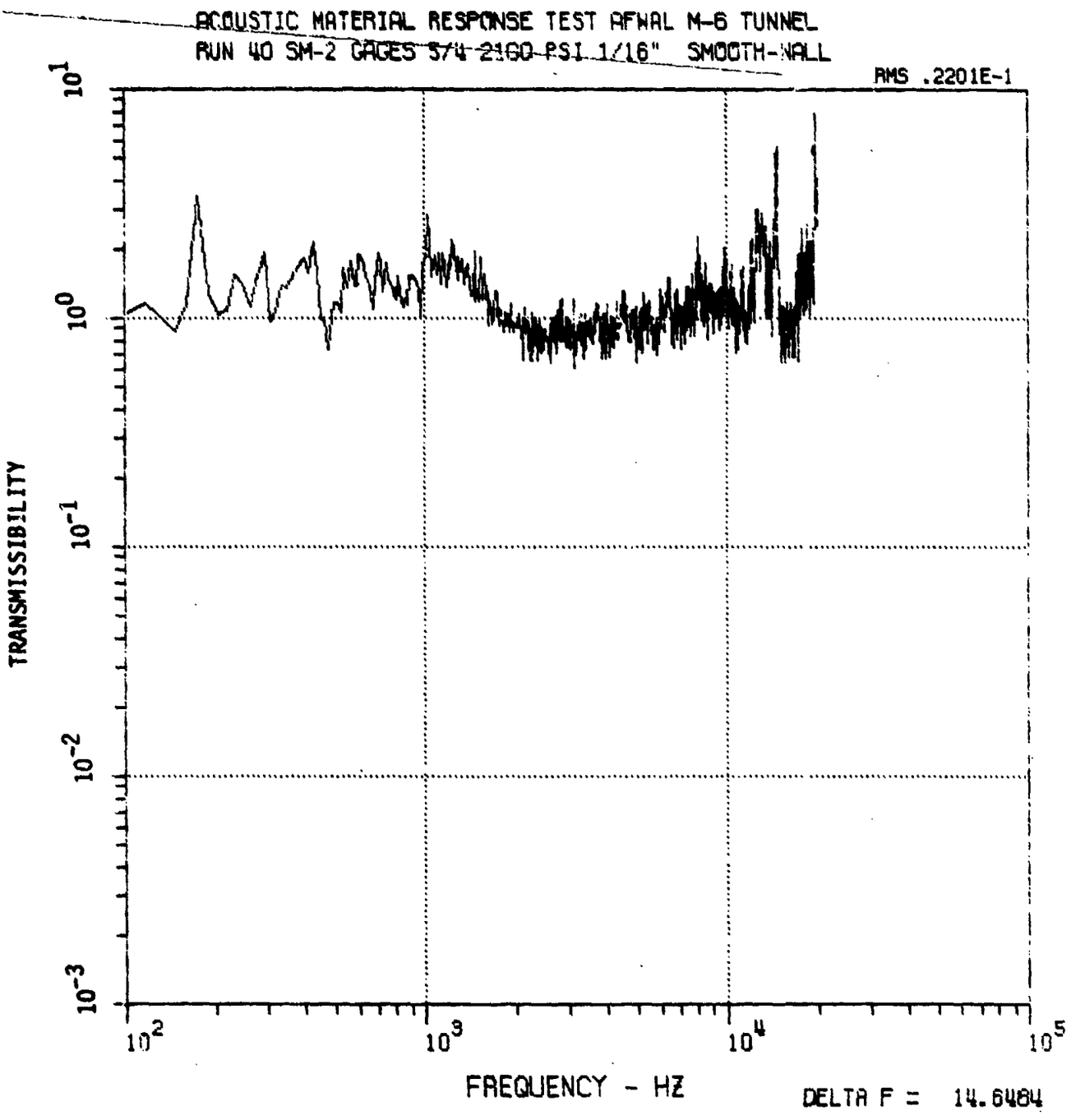
ACOUSTIC MATERIAL RESPONSE TEST AFWAL M-6 TUNNEL
RUN 40 SM-2 GAGES 5?4 2160 PSI 1/16" SMOOTH-WALL
RMS .2201E-1
TRANSMISSIBILITY
10^{1}
10^{0}
10^{-1}
10^{-2}
10^{-3}
10^{2}
10^{3}
10^{4}
10^{5}
FREQUENCY - HZ
DELTA F = 14.6484

FIGURE B-9

16
8

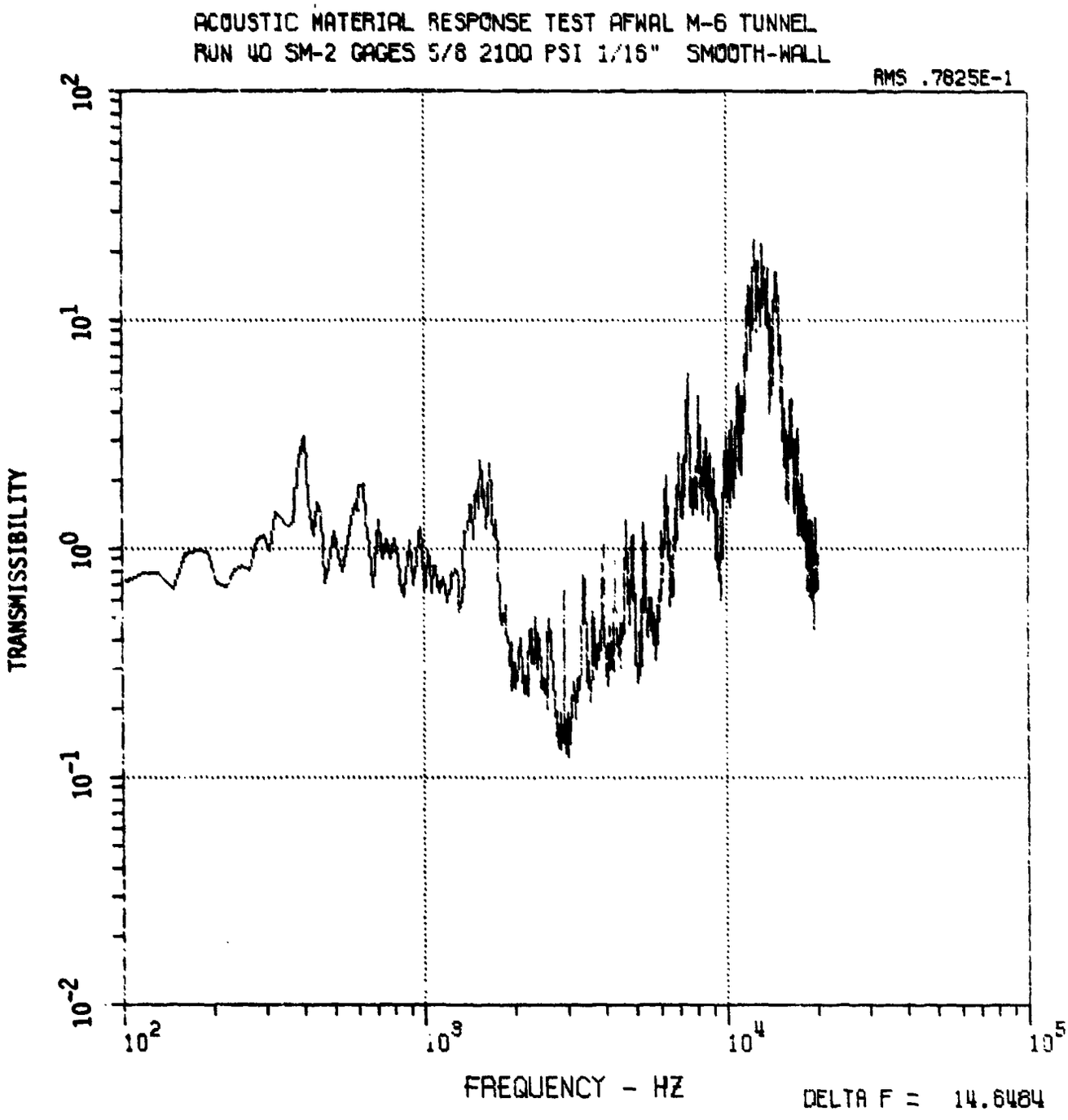

FIGURE B-10

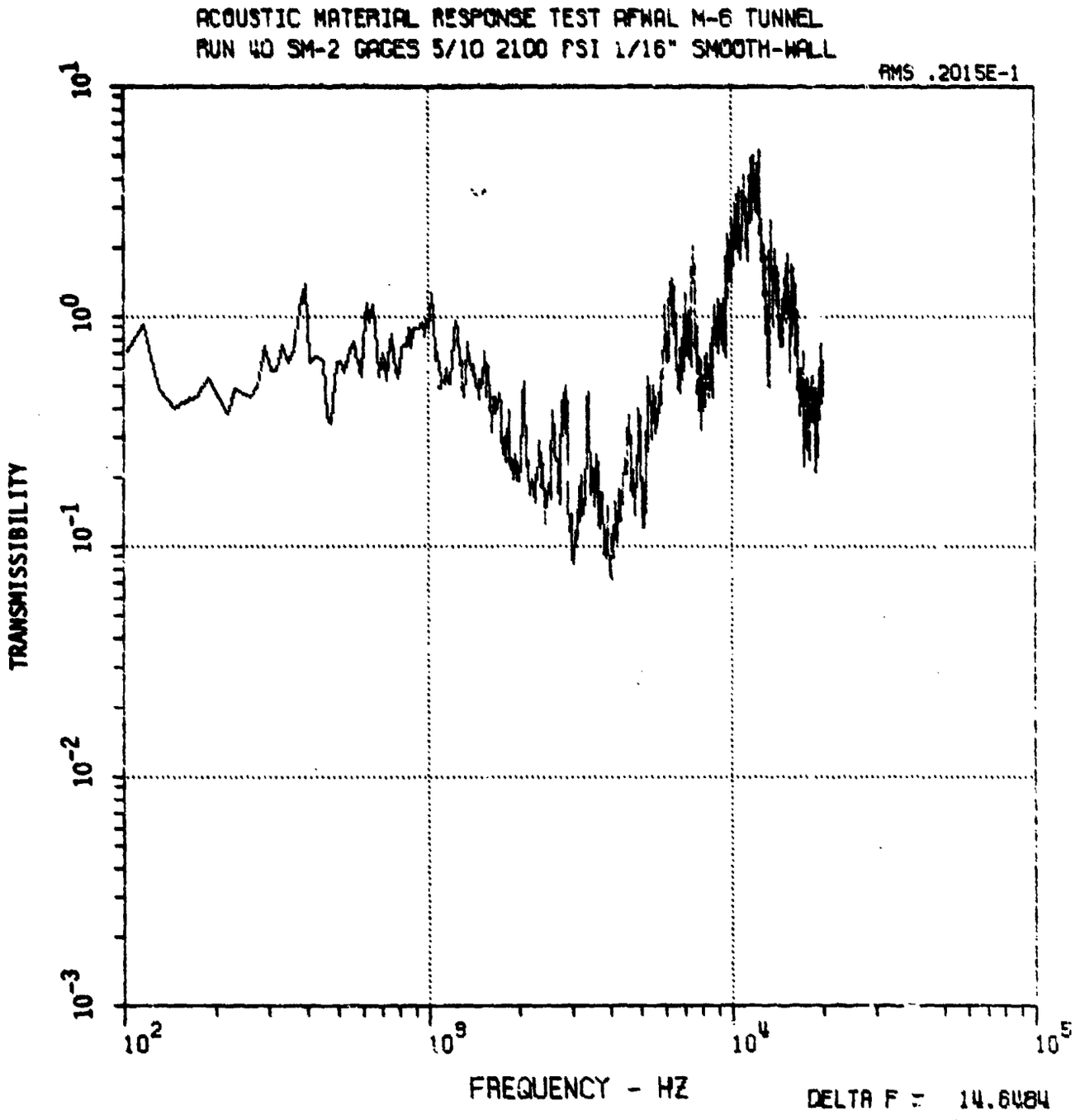
ACOUSTIC MATERIAL RESPONSE TEST AFWAL M-6 TUNNEL
RUN 40 SM-2 GAGES 5/10 2100 PSI 1/16" SMOOTH-WALL
RMS .2015E-1
TRANSMISSIBILITY
10^{-1}
10^{0}
10^{-1}
10^{-2}
10^{-3}
10^{2}
10^{3}
10^{4}
10^{5}
FREQUENCY - HZ
DELTA F = 14.6484

FIGURE B-11

12
5

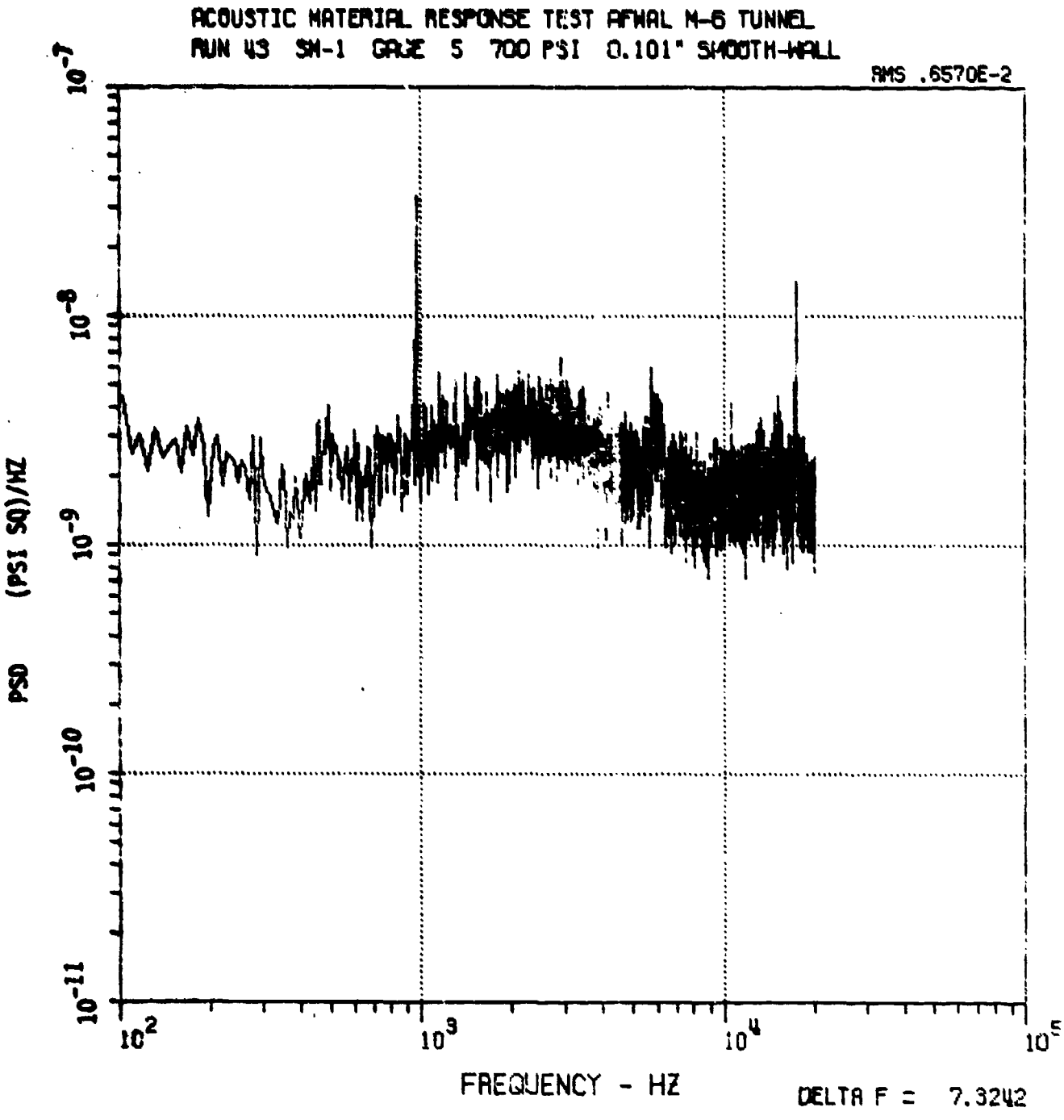

FIGURE B-12

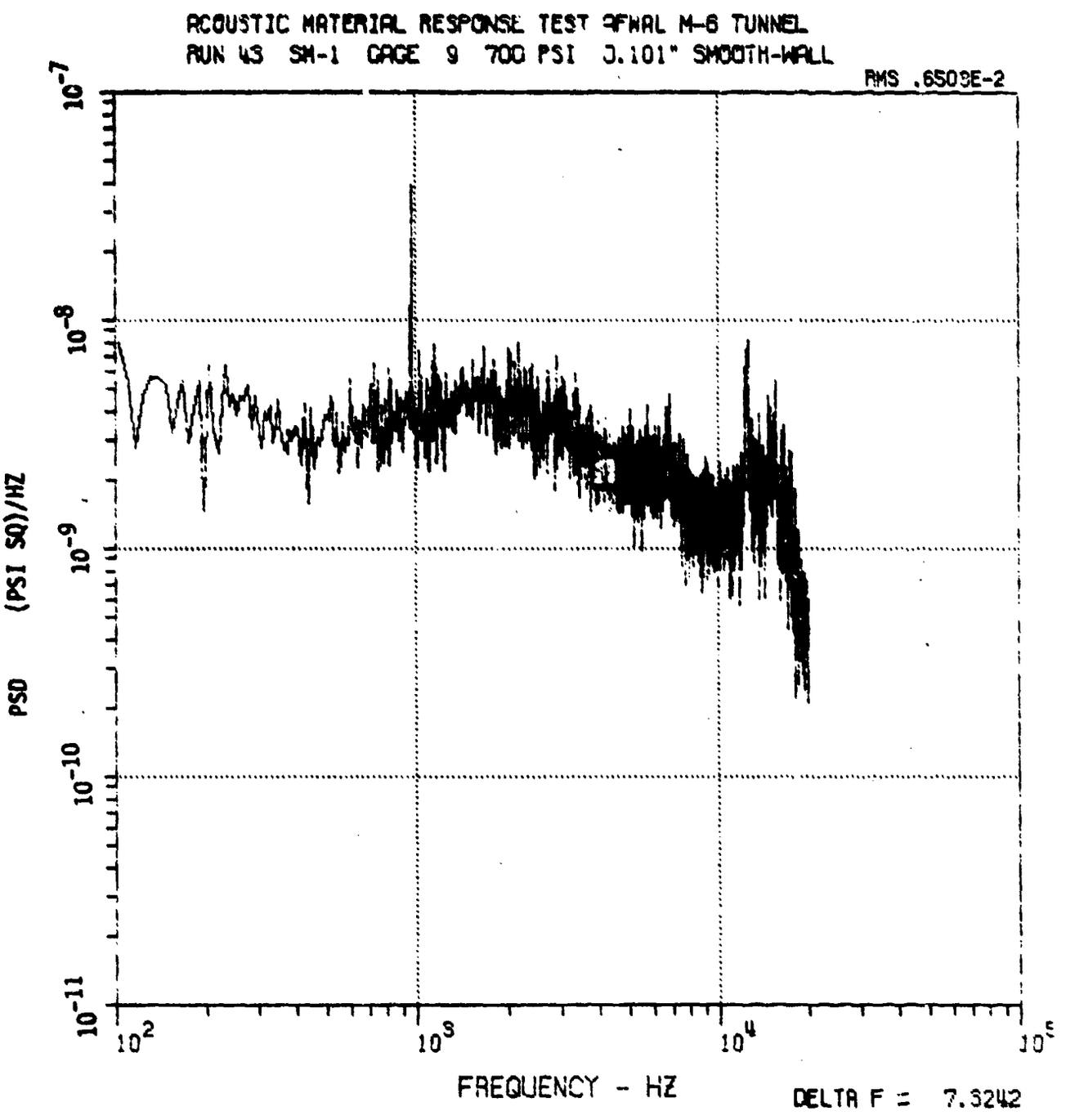
ACOUSTIC MATERIAL RESPONSE TEST 9FWAL M-6 TUNNEL
RUN 43 SM-1 GAGE 9 700 PSI 3.101" SMOOTH-WALL
RMS .6503E-2
PSD (PSI SQ)/HZ
10^{-7}
10^{-8}
10^{-9}
10^{-10}
10^{-11}
10^{2}
10^{3}
10^{4}
10^{5}
FREQUENCY - HZ
DELTA F = 7.3242

FIGURE B-13

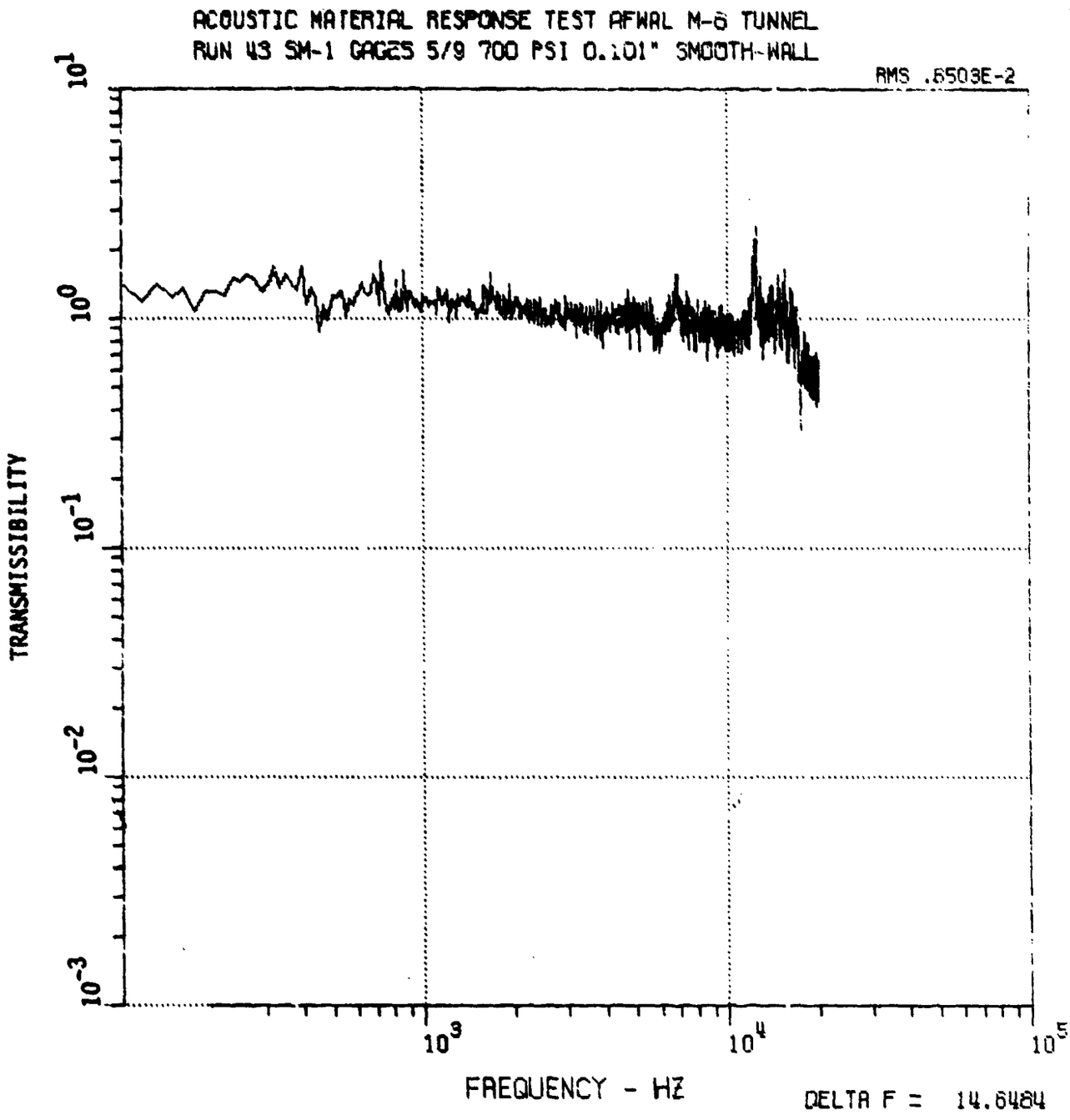
ACOUSTIC MATERIAL RESPONSE TEST AFWAL M-6 TUNNEL
RUN 43 SM-1 GAGES 5/9 700 PSI 0.101" SMOOTH-WALL
RMS .6503E-2
TRANSMISSIBILITY
10^{1}
10^{0}
10^{-1}
10^{-2}
10^{-3}
10^{3}
10^{4}
10^{5}
FREQUENCY - HZ
DELTA F = 14.6484

FIGURE B-14

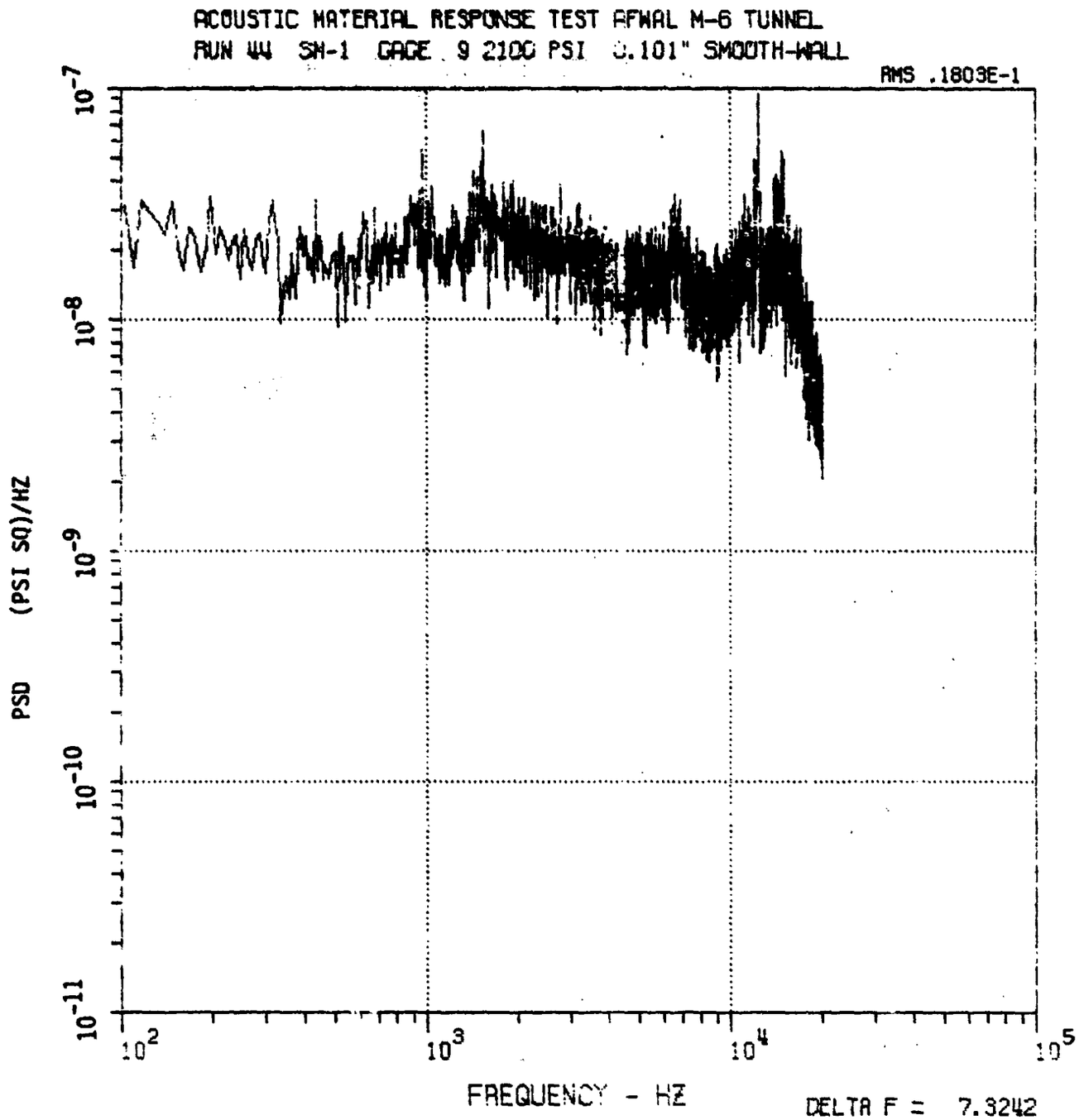
ACOUSTIC MATERIAL RESPONSE TEST AFWAL M-6 TUNNEL
RUN 44 SM-1 GAGE 9 2100 PSI .101" SMOOTH-WALL
RMS .1803E-1
PSD (PSI SQ)/HZ
10^{-7}
10^{-8}
10^{-9}
10^{-10}
10^{-11}
10^{2}
10^{3}
10^{4}
10^{5}
FREQUENCY - HZ
DELTA F = 7.3242

FIGURE B-15

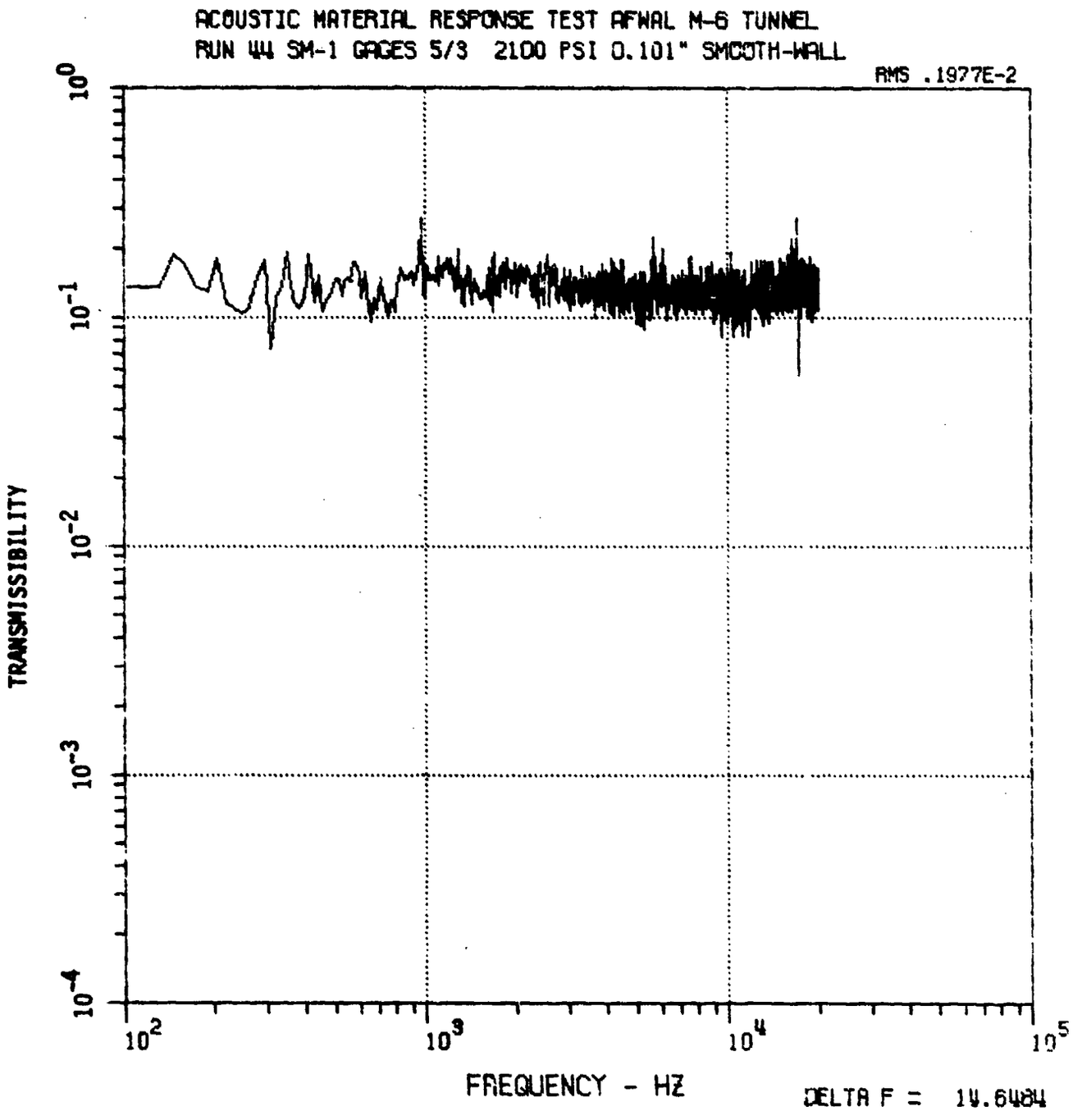
ACOUSTIC MATERIAL RESPONSE TEST AFWAL M-6 TUNNEL
RUN 44 SM-1 GAGES 5/3 2100 PSI 0.101" SMOOTH-WALL
RMS .1977E-2
TRANSMISSIBILITY
10^{0}
10^{-1}
10^{-2}
10^{-3}
10^{-4}
10^{2}
10^{3}
10^{4}
10^{5}
FREQUENCY - HZ
DELTA F = 14.6484

FIGURE B-16

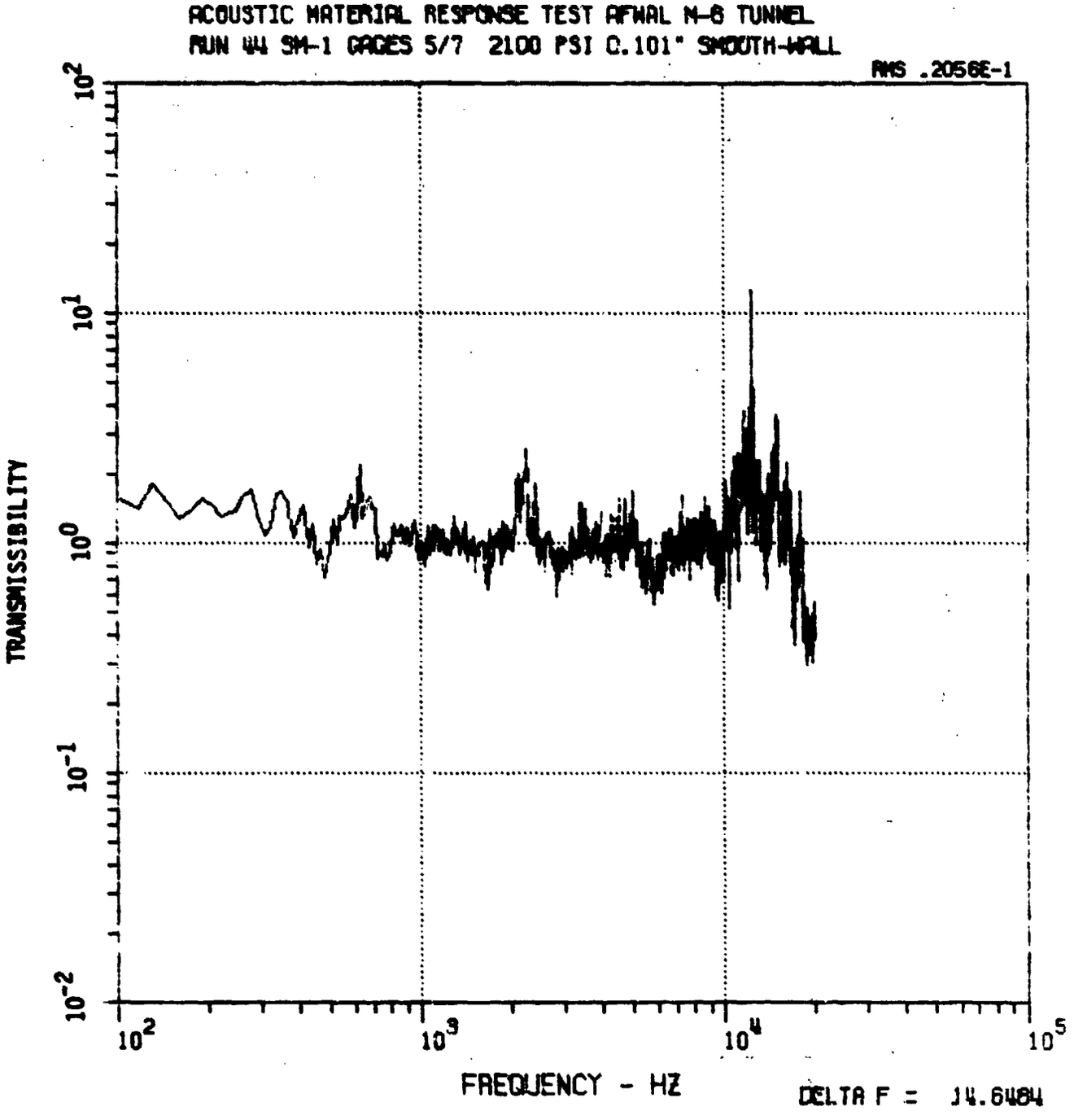
ACOUSTIC MATERIAL RESPONSE TEST AFWAL M-6 TUNNEL
RUN 44 SM-1 GAGES 5/7 2100 PSI 0.101" SMOOTH-WALL
RMS .2056E-1
TRANSMISSIBILITY
10^{2}
10^{1}
10^{0}
10^{-1}
10^{-2}
10^{2}
10^{3}
10^{4}
10^{5}
FREQUENCY - HZ
DELTA F = 14.6484

FIGURE B-17

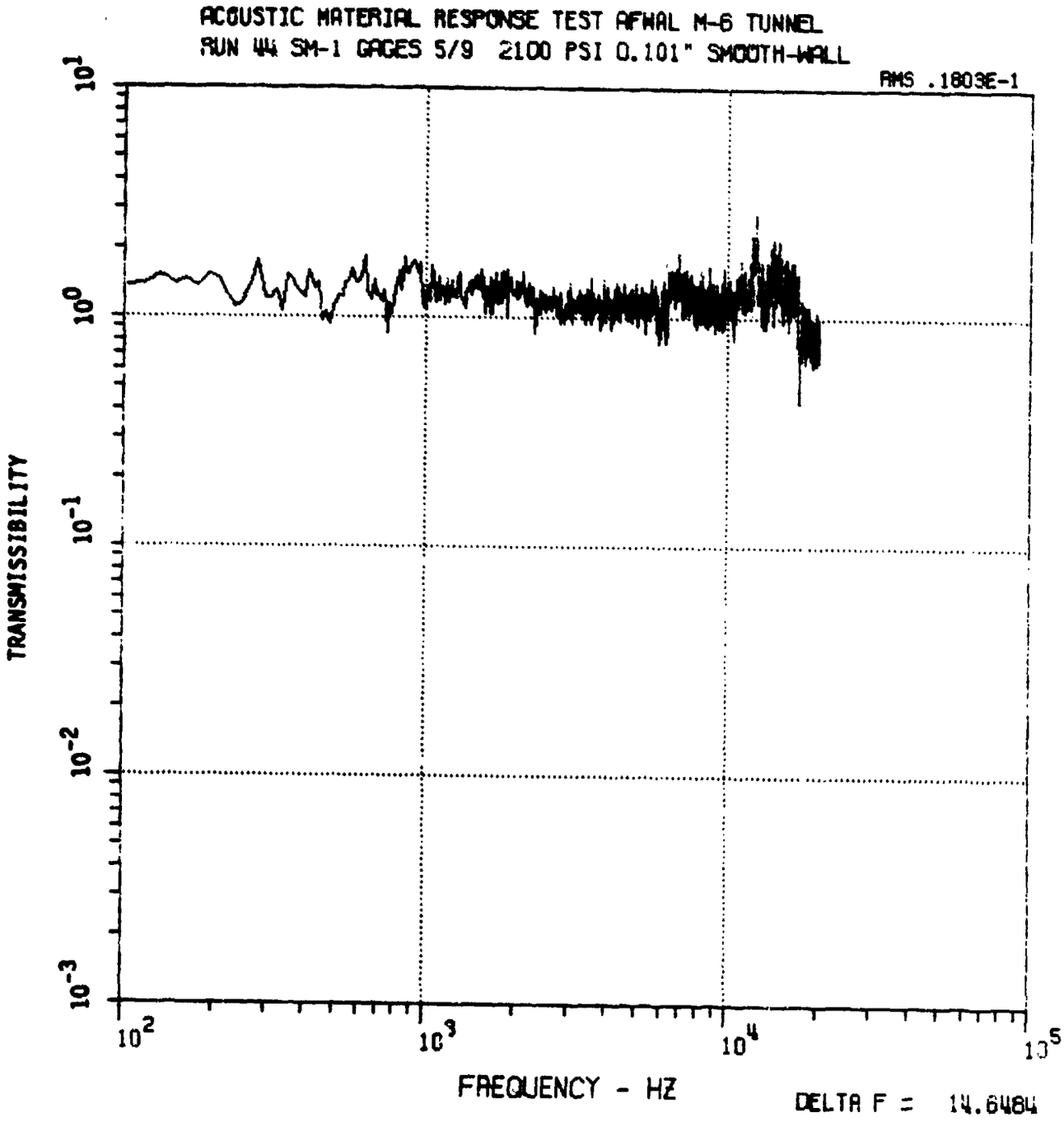
ACOUSTIC MATERIAL RESPONSE TEST AFWAL M-6 TUNNEL
RUN 44 SM-1 GAGES 5/9 2100 PSI 0.101" SMOOTH-WALL
RMS .1803E-1
TRANSMISSIBILITY
10^{1}
10^{0}
10^{-1}
10^{-2}
10^{-3}
10^{2}
10^{3}
10^{4}
10^{5}
FREQUENCY - HZ
DELTA F = 14.6484

FIGURE B-18

APPENDIX B
ROUGH WALL DATA

27
5

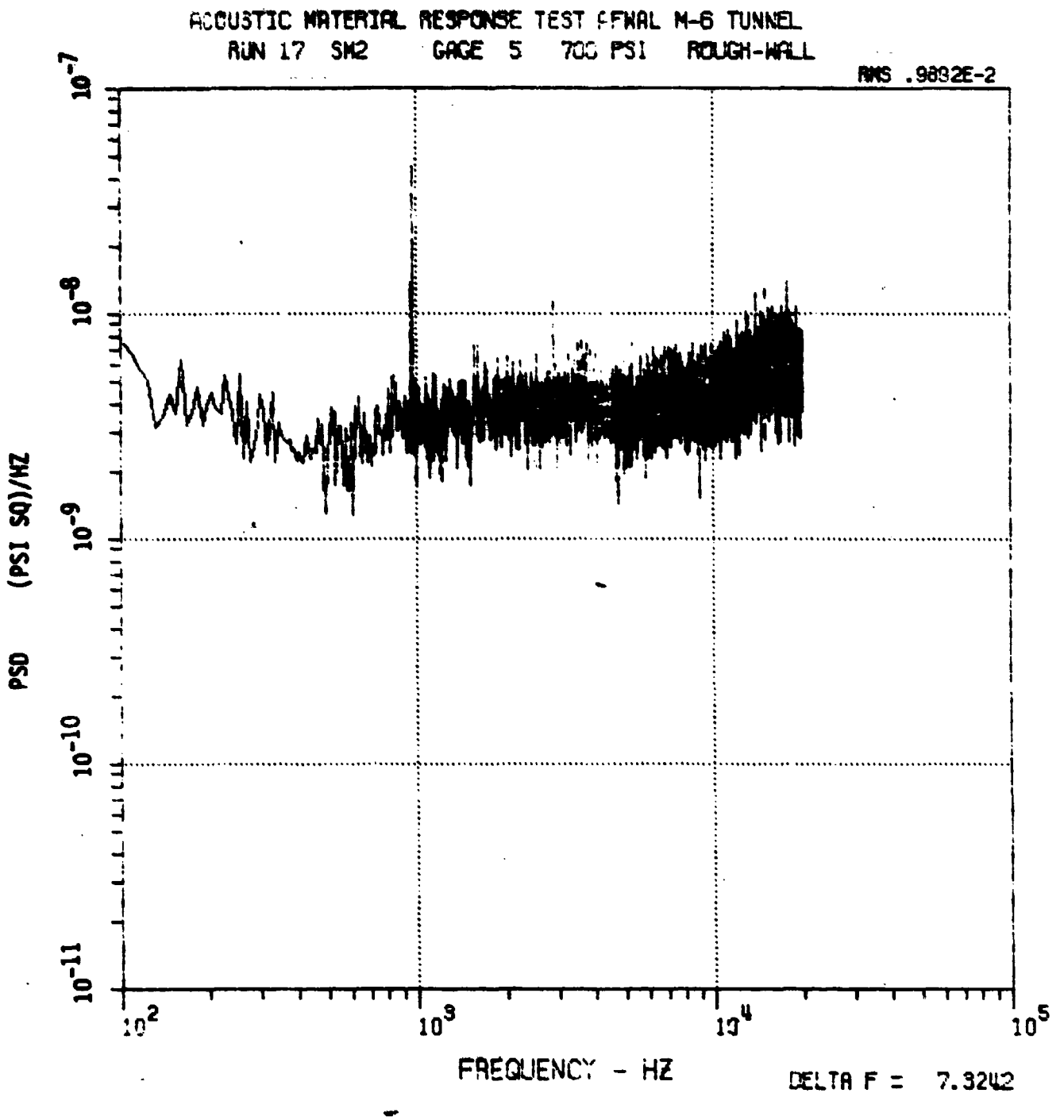

FIGURE B-19

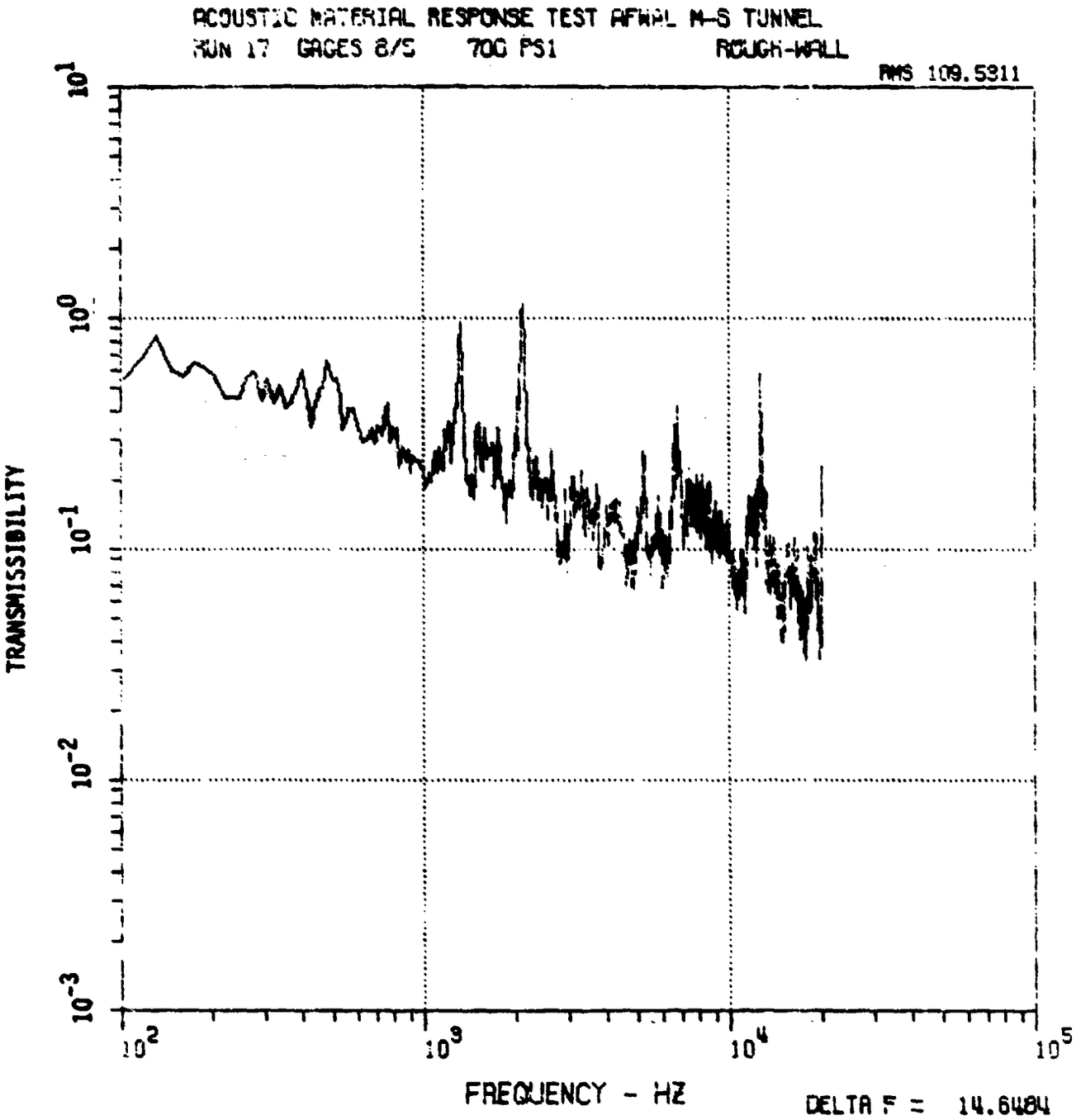
ACOUSTIC MATERIAL RESPONSE TEST AFWAL M-S TUNNEL
RUN 17 GAGES 8/5 700 PSI ROUGH-WALL
RMS 109.5311
TRANSMISSIBILITY
10^{1}
10^{0}
10^{-1}
10^{-2}
10^{-3}
10^{2}
10^{3}
10^{4}
10^{5}
FREQUENCY - HZ
DELTA F = 14.6484

FIGURE B-20

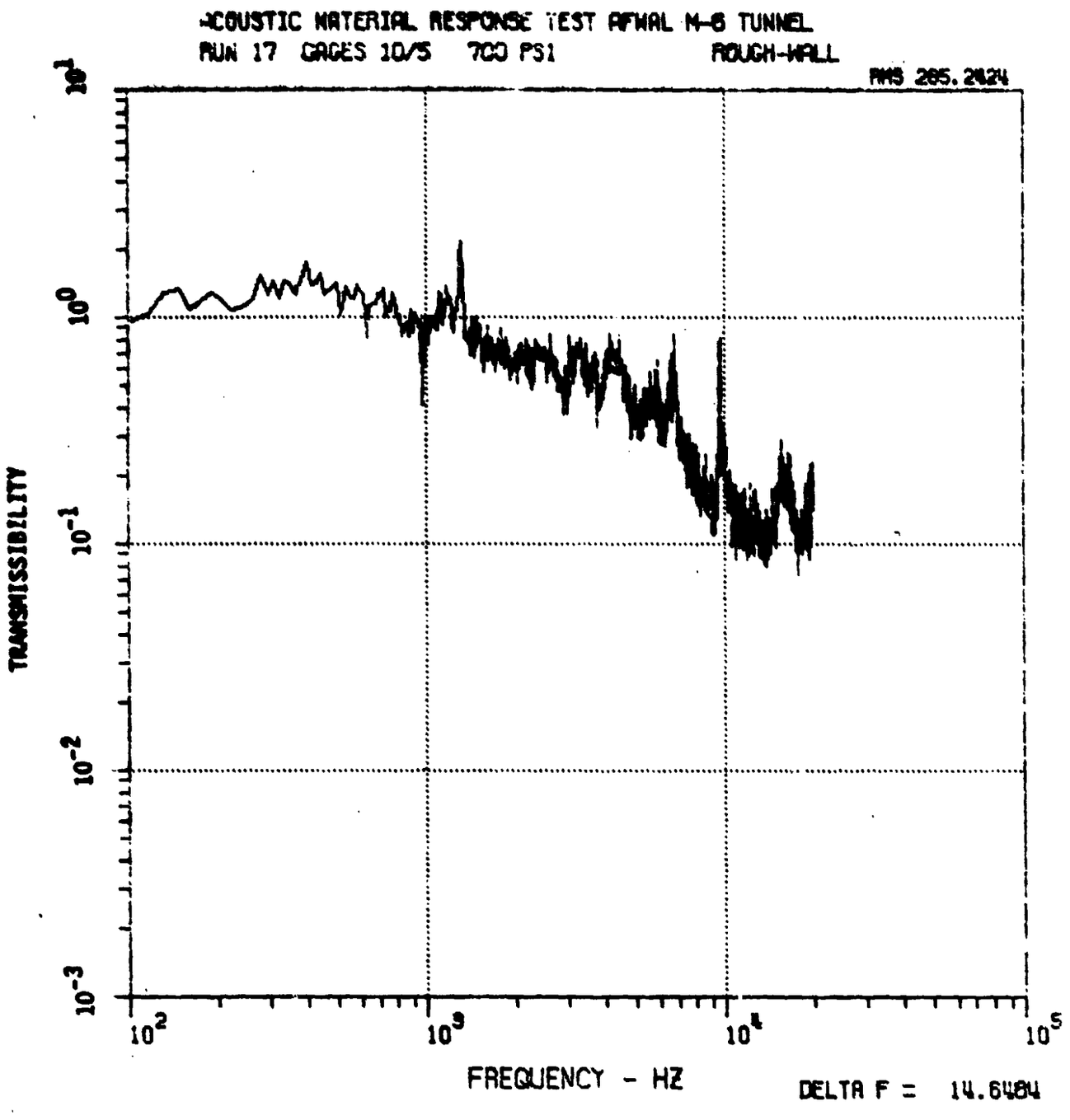
ACOUSTIC MATERIAL RESPONSE TEST AFWAL M-6 TUNNEL
RUN 17 GAGES 10/5 700 PSI ROUGH-WALL
RMS 265.2824
TRANSMISSIBILITY
10^{1}
10^{0}
10^{-1}
10^{-2}
10^{-3}
10^{2}
10^{3}
10^{4}
10^{5}
FREQUENCY - HZ
DELTA F = 14.6484

FIGURE B-21

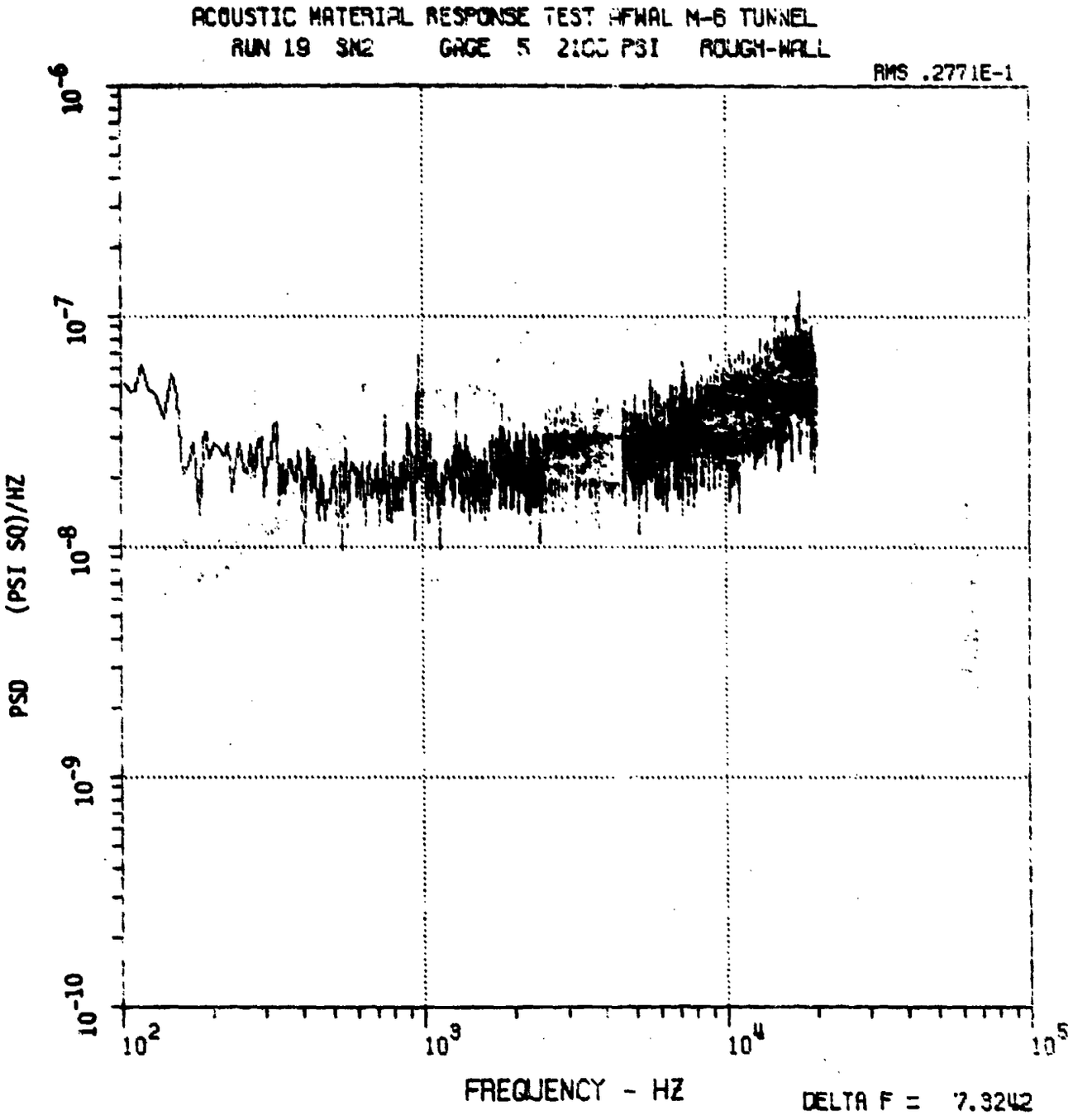
ACOUSTIC MATERIAL RESPONSE TEST AFWAL M-6 TUNNEL
RUN 19 SM2 GAGE 5 2100 PSI ROUGH-WALL
RMS .2771E-1
PSD (PSI SQ)/HZ
10^{-6}
10^{-7}
10^{-8}
10^{-9}
10^{-10}
10^{2}
10^{3}
10^{4}
10^{5}
FREQUENCY - HZ
DELTA F = 7.3242

FIGURE B-22

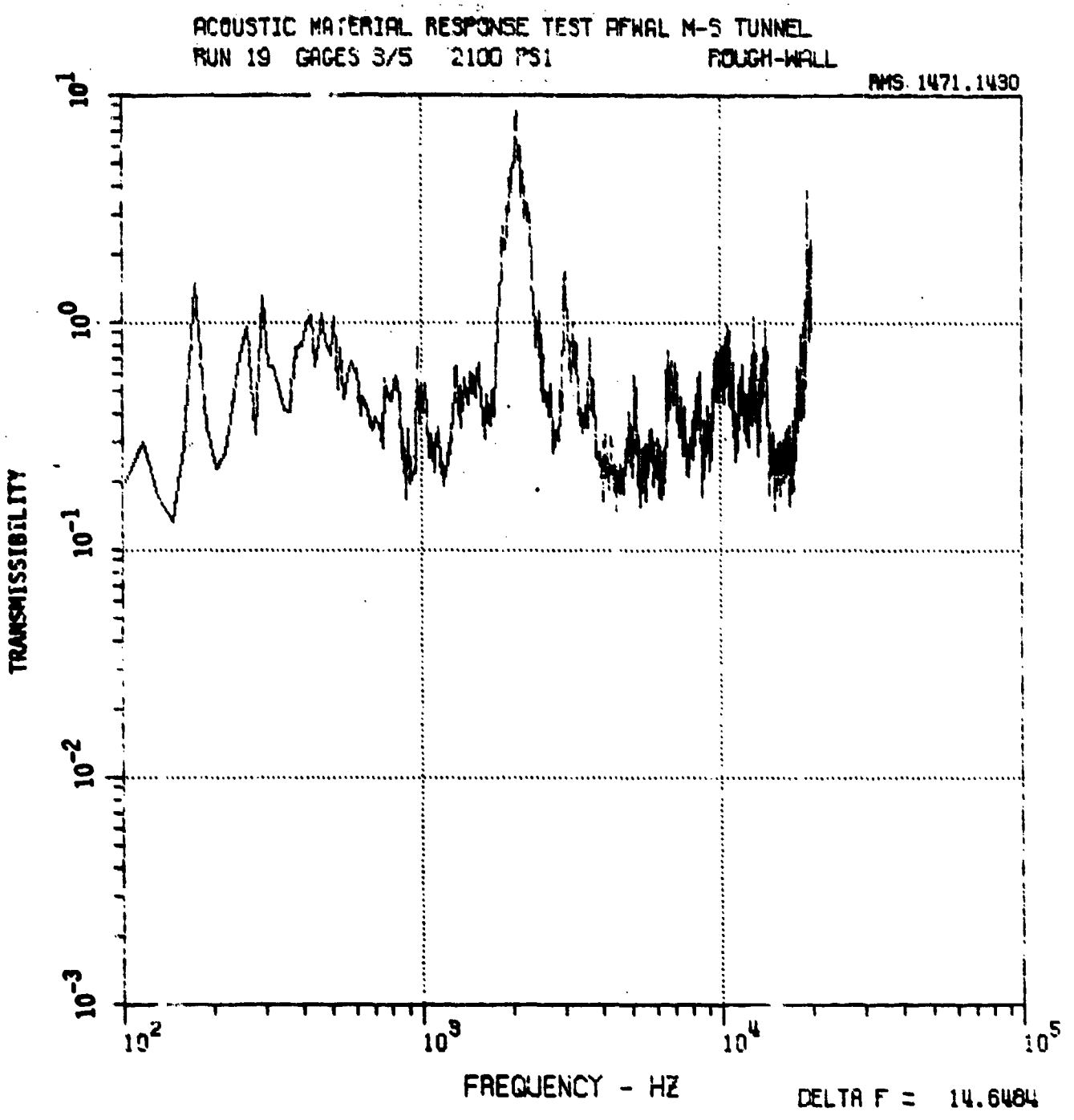
ACOUSTIC MATERIAL RESPONSE TEST AFWAL M-5 TUNNEL
RUN 19 GAGES 3/5 2100 PSI ROUGH-WALL
RMS 1471.1430
TRANSMISSIBILITY
10^{1}
10^{0}
10^{-1}
10^{-2}
10^{-3}
10^{2}
10^{3}
10^{4}
10^{5}
FREQUENCY - HZ
DELTA F = 14.6484

FIGURE B-23

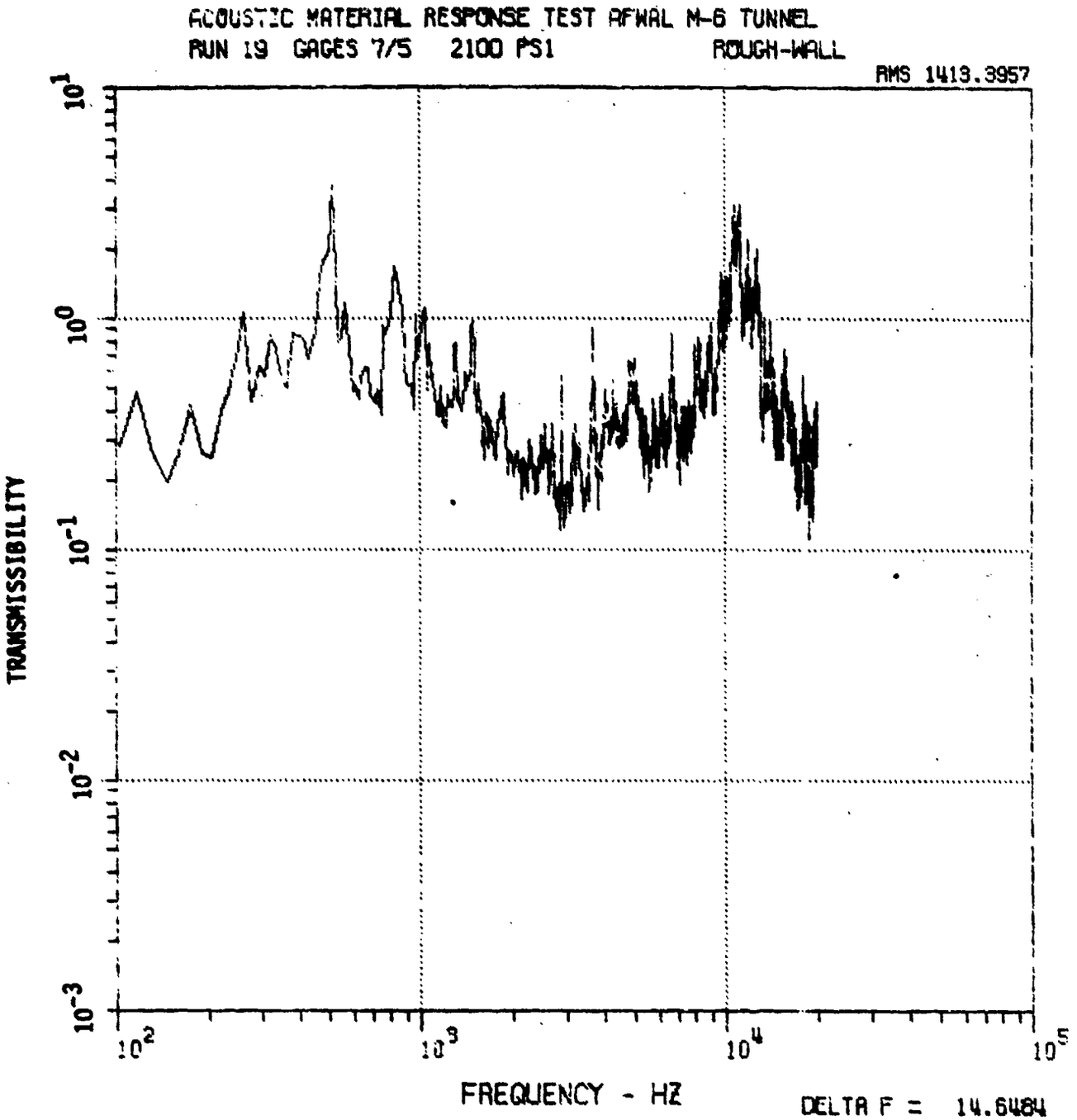
ACOUSTIC MATERIAL RESPONSE TEST AFWAL M-6 TUNNEL
RUN 19 GAGES 7/5 2100 PSI ROUGH-WALL
RMS 1413.3957
TRANSMISSIBILITY
10^{1}
10^{0}
10^{-1}
10^{-2}
10^{-3}
10^{2}
10^{3}
10^{4}
10^{5}
FREQUENCY - HZ
DELTA F = 14.6484

FIGURE B-24

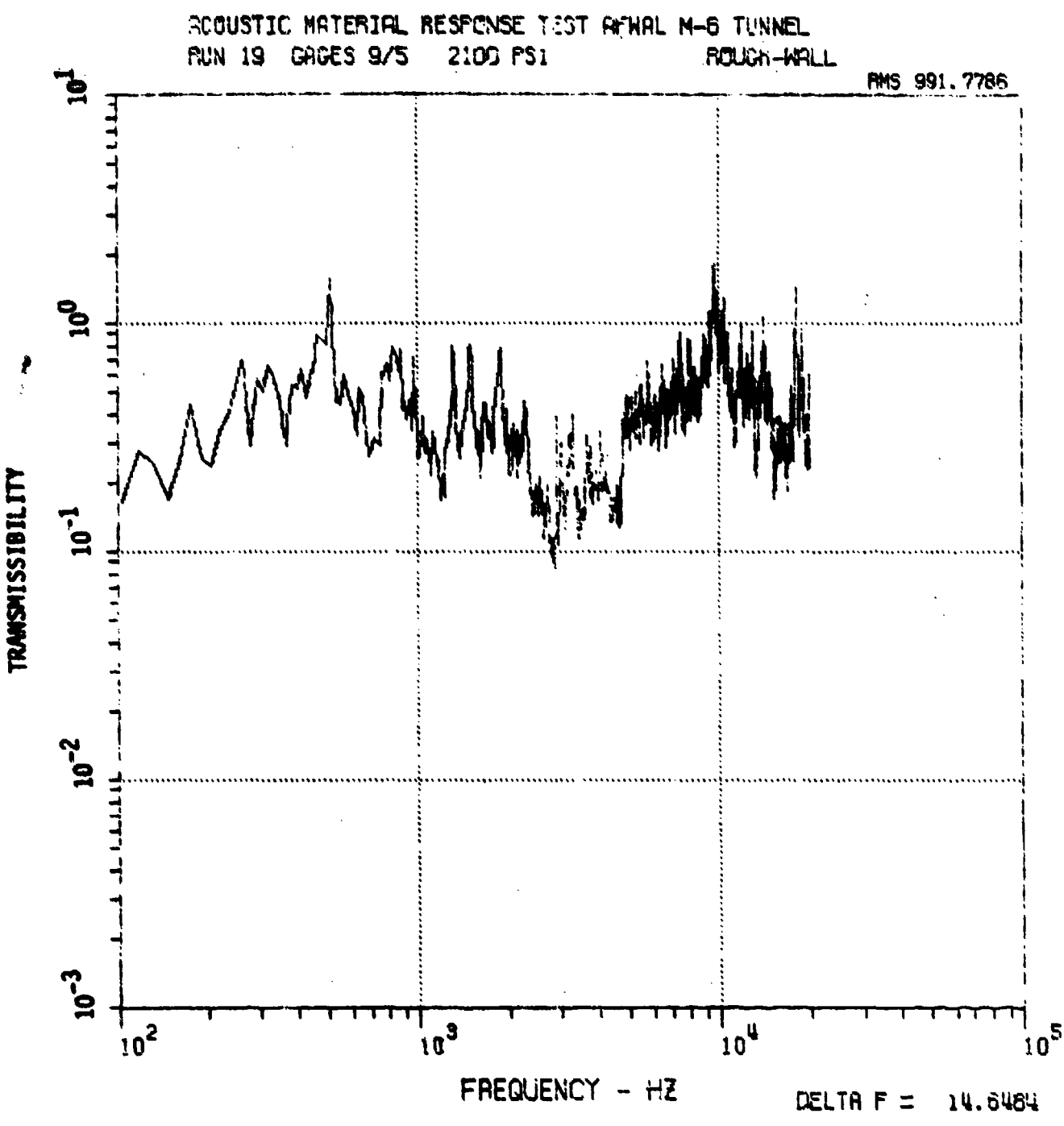
ACOUSTIC MATERIAL RESPONSE TEST AFWAL M-6 TUNNEL
RUN 19 GAGES 9/5 2100 PSI ROUGH-WALL
RMS 991.7786
TRANSMISSIBILITY
10^{1}
10^{0}
10^{-1}
10^{-2}
10^{-3}
10^{2}
10^{3}
10^{4}
10^{5}
FREQUENCY - HZ
DELTA F = 14.6484

FIGURE B-25

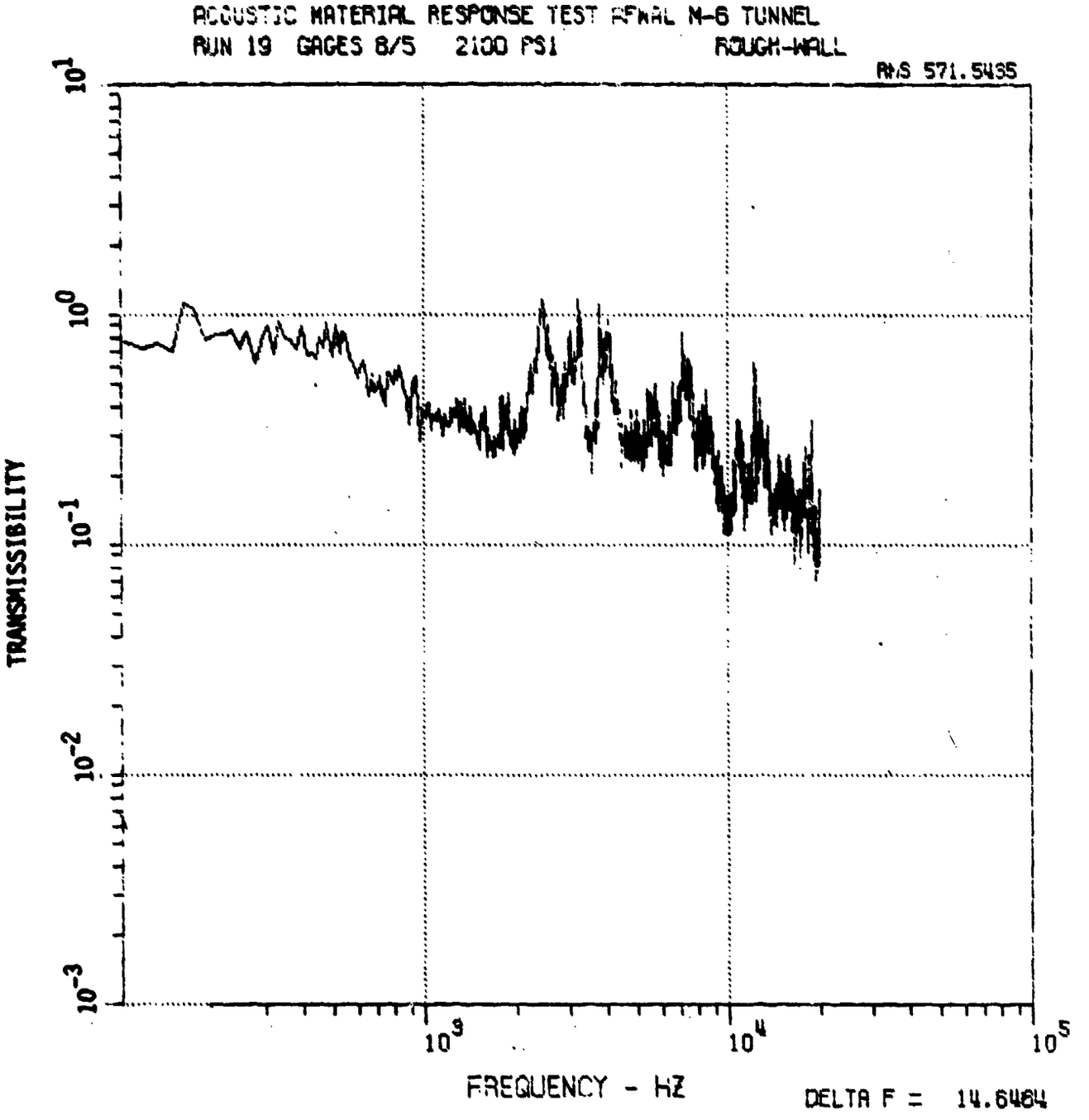
ACOUSTIC MATERIAL RESPONSE TEST AEDC VKF M-6 TUNNEL
RUN 19 GAGES 8/5 2100 PSI ROUGH-WALL
RMS 571.5435
TRANSMISSIBILITY
10^{1}
10^{0}
10^{-1}
10^{-2}
10^{-3}
10^{3}
10^{4}
10^{5}
FREQUENCY - HZ
DELTA F = 14.6484

FIGURE B-26

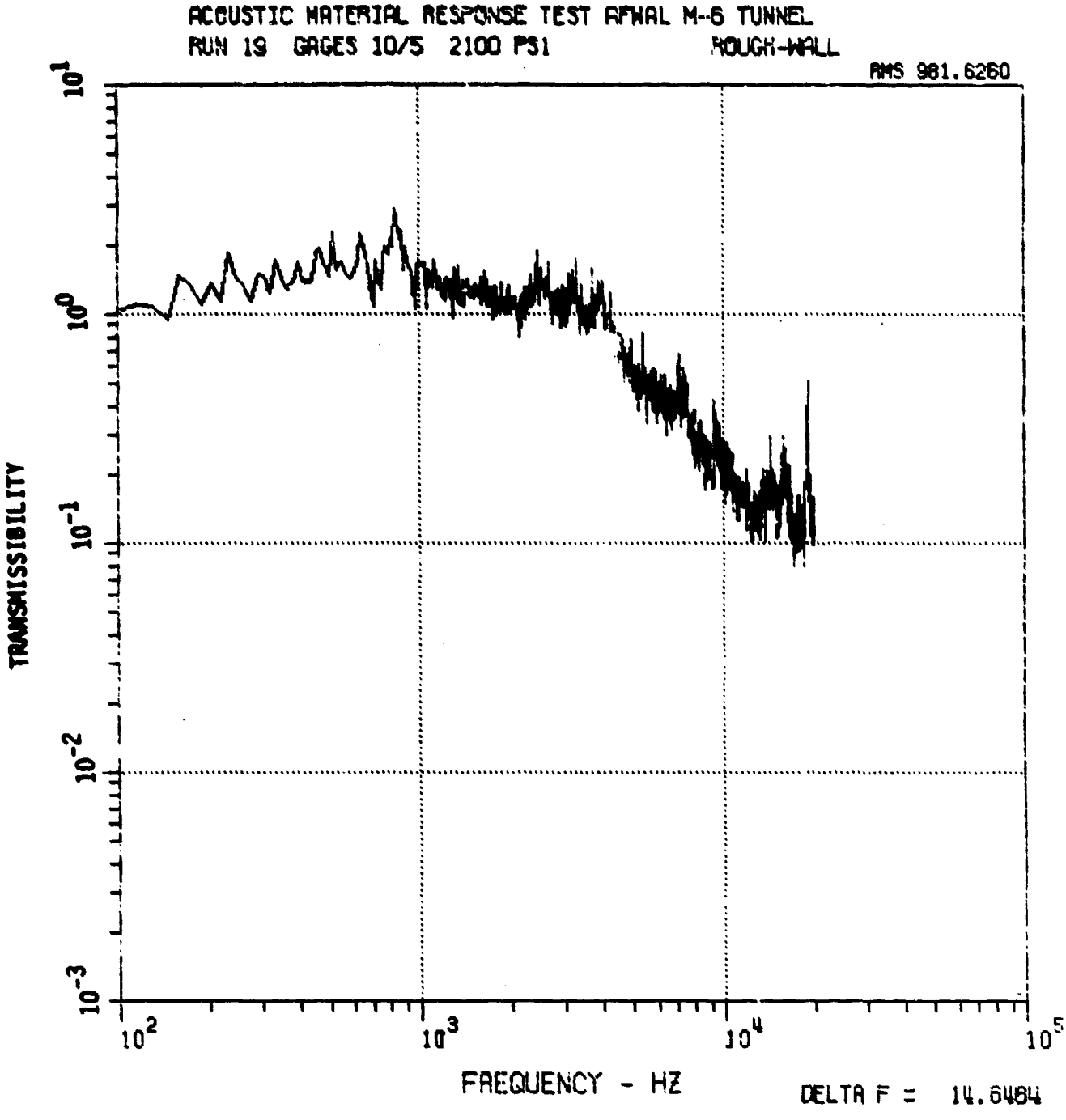
ACOUSTIC MATERIAL RESPONSE TEST AFWAL M-6 TUNNEL
RUN 19 GAGES 10/5 2100 PSI
ROUGH-WALL
RMS 981.6260
TRANSMISSIBILITY
10^{1}
10^{0}
10^{-1}
10^{-2}
10^{-3}
10^{2}
10^{3}
10^{4}
10^{5}
FREQUENCY - HZ
DELTA F = 14.6484

FIGURE B-27

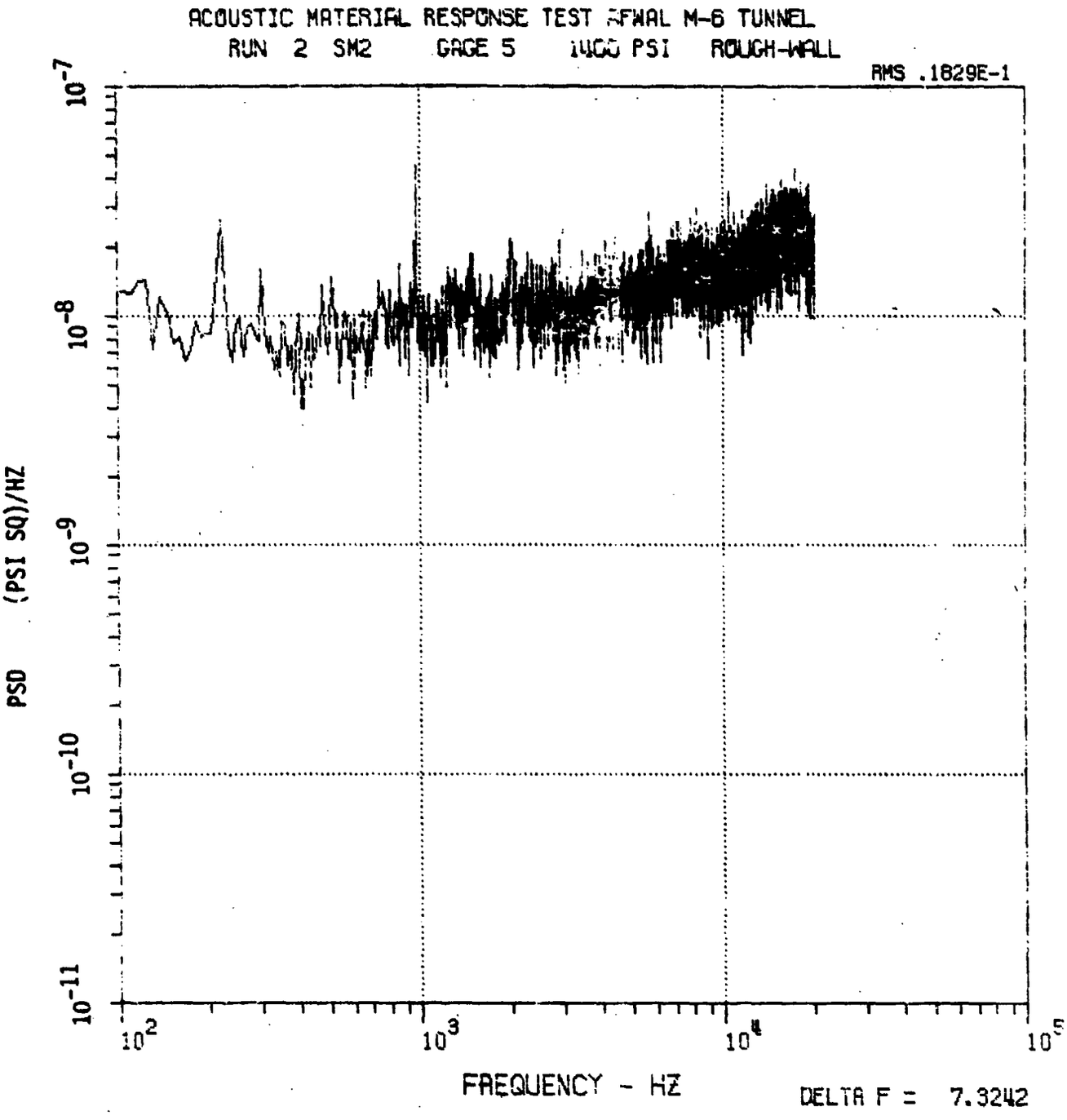
ACOUSTIC MATERIAL RESPONSE TEST AFWAL M-6 TUNNEL
RUN 2 SM2 GAGE 5 1400 PSI ROUGH-WALL
RMS .1829E-1
PSD (PSI SQ)/HZ
10^{-7}
10^{-8}
10^{-9}
10^{-10}
10^{-11}
10^{2}
10^{3}
10^{4}
10^{5}
FREQUENCY - HZ
DELTA F = 7.3242

FIGURE B-28

6
10

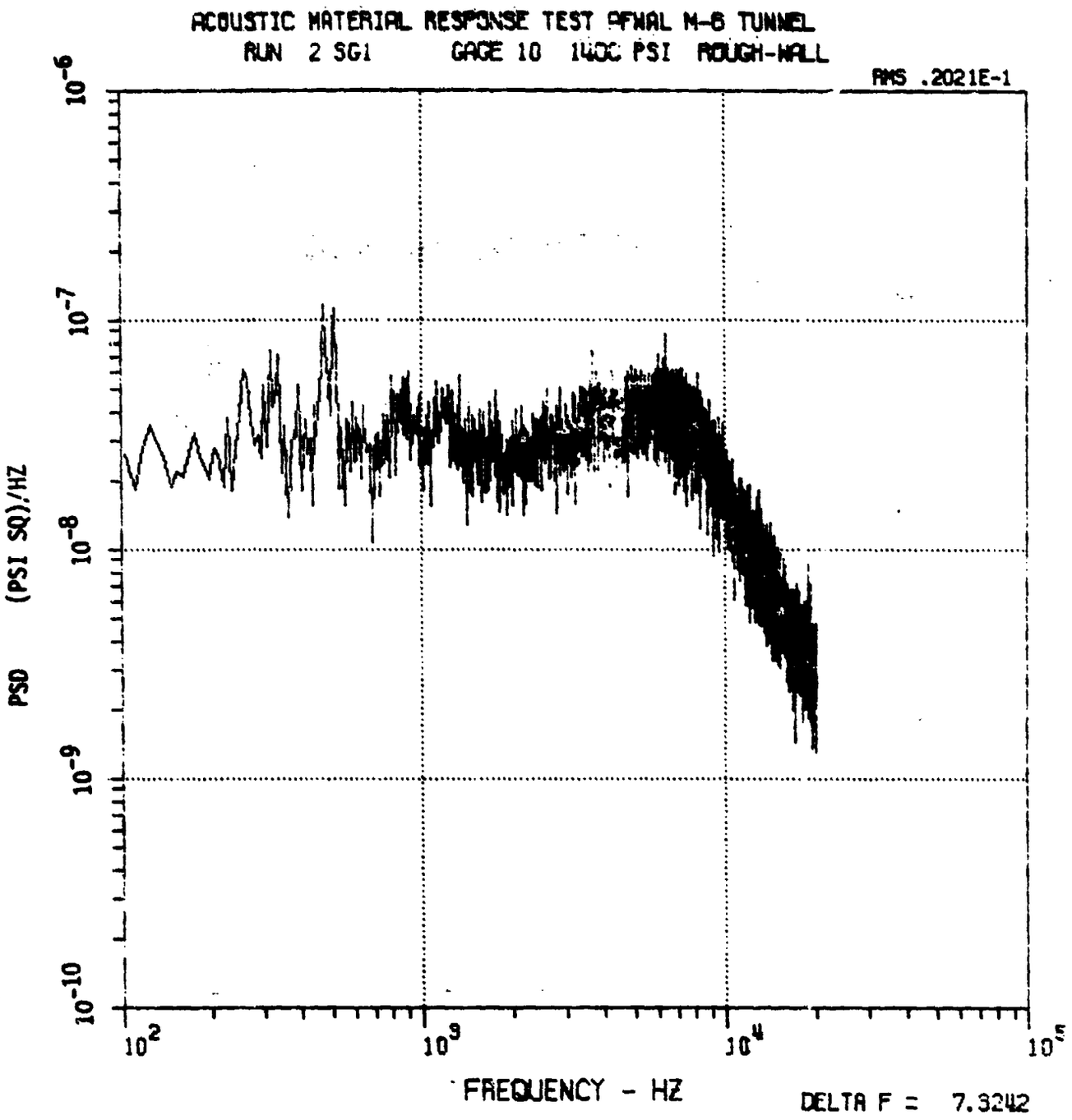

FIGURE B-29

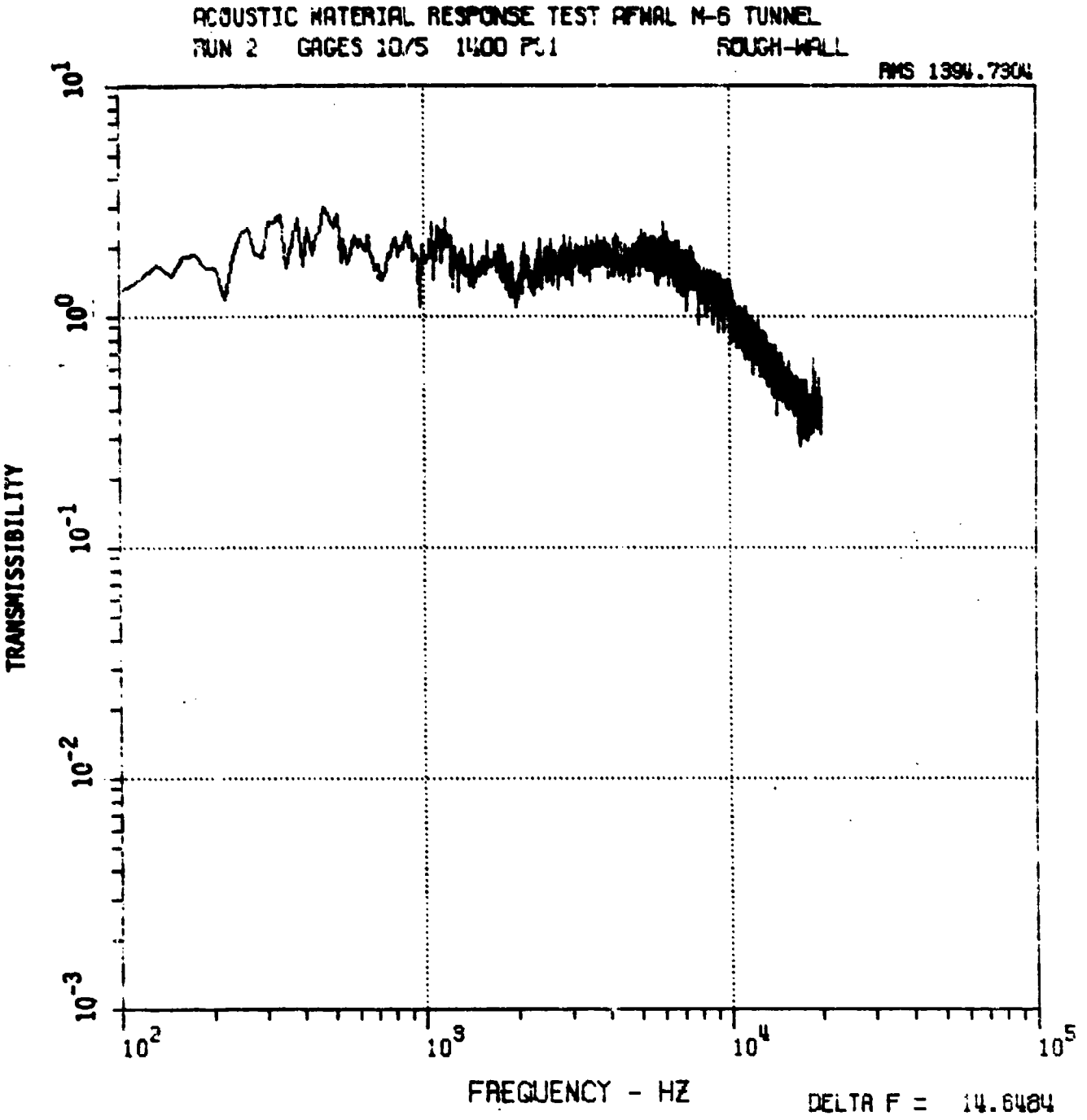
ACOUSTIC MATERIAL RESPONSE TEST AFWAL M-6 TUNNEL
RUN 2 GAGES 10/5 1400 PSI ROUGH-WALL
RMS 1394.7304
TRANSMISSIBILITY
10^{1}
10^{0}
10^{-1}
10^{-2}
10^{-3}
10^{2}
10^{3}
10^{4}
10^{5}
FREQUENCY - HZ
DELTA F = 14.6484

FIGURE B-30

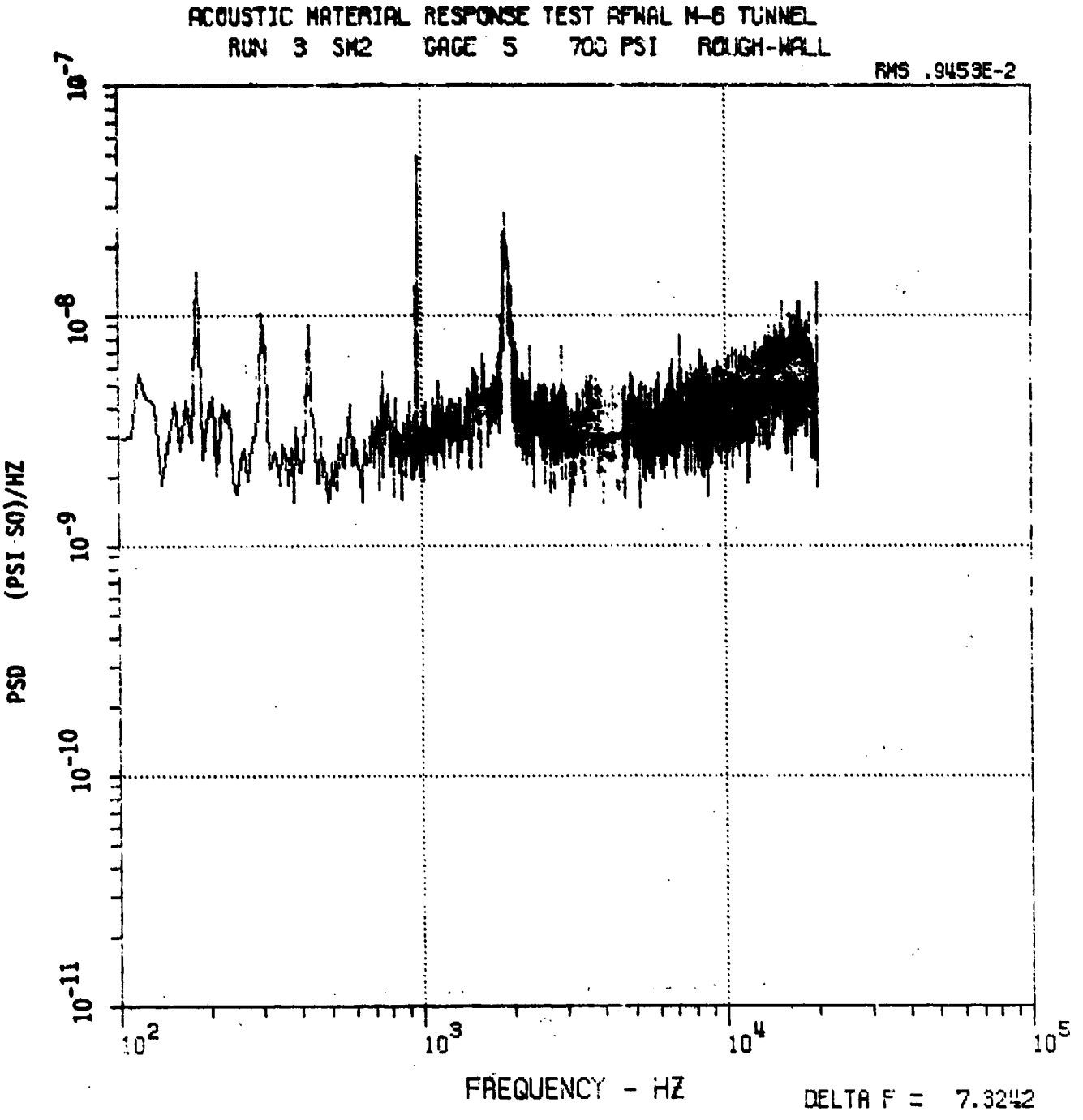
ACOUSTIC MATERIAL RESPONSE TEST AFWAL M-6 TUNNEL
RUN 3 SM2 GAGE 5 700 PSI ROUGH-WALL
RMS .9453E-2
PSD (PSI SQ)/HZ
10^{-7}
10^{-8}
10^{-9}
10^{-10}
10^{-11}
10^{2}
10^{3}
10^{4}
10^{5}
FREQUENCY - HZ
DELTA F = 7.3242

FIGURE B-31

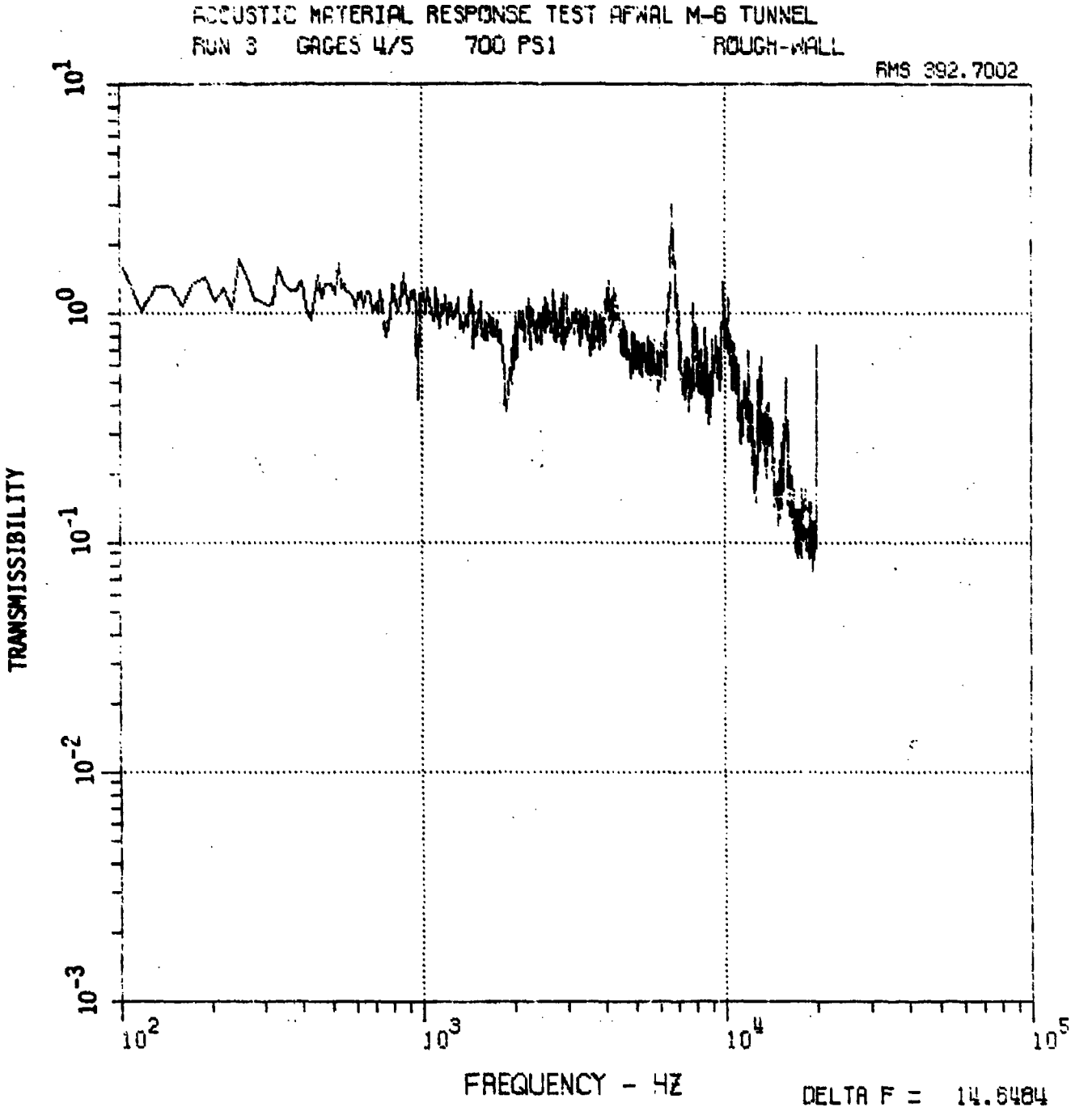
ACOUSTIC MATERIAL RESPONSE TEST AFWAL M-6 TUNNEL
RUN 3 GAGES 4/5 700 PSI ROUGH-WALL
RMS 392.7002
TRANSMISSIBILITY
10^{1}
10^{0}
10^{-1}
10^{-2}
10^{-3}
10^{2}
10^{3}
10^{4}
10^{5}
FREQUENCY - HZ
DELTA F = 14.6484

FIGURE B-32

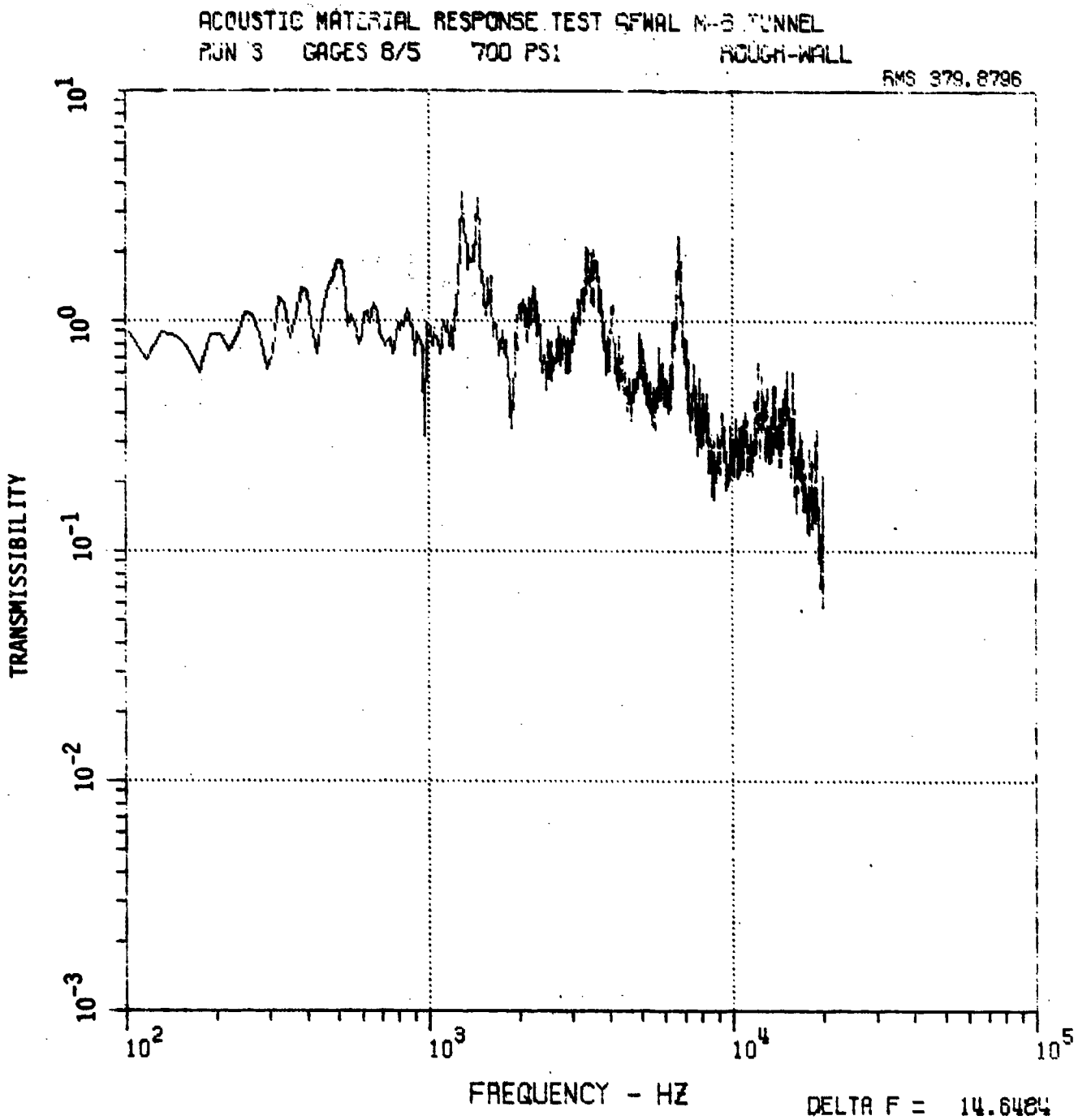
ACOUSTIC MATERIAL RESPONSE TEST GFWAL M-6 TUNNEL
RUN 3 GAGES 6/5 700 PSI ROUGH-WALL
RMS 379.8796
TRANSMISSIBILITY
10^{1}
10^{0}
10^{-1}
10^{-2}
10^{-3}
10^{2}
10^{3}
10^{4}
10^{5}
FREQUENCY - HZ
DELTA F = 14.6484

FIGURE B-33

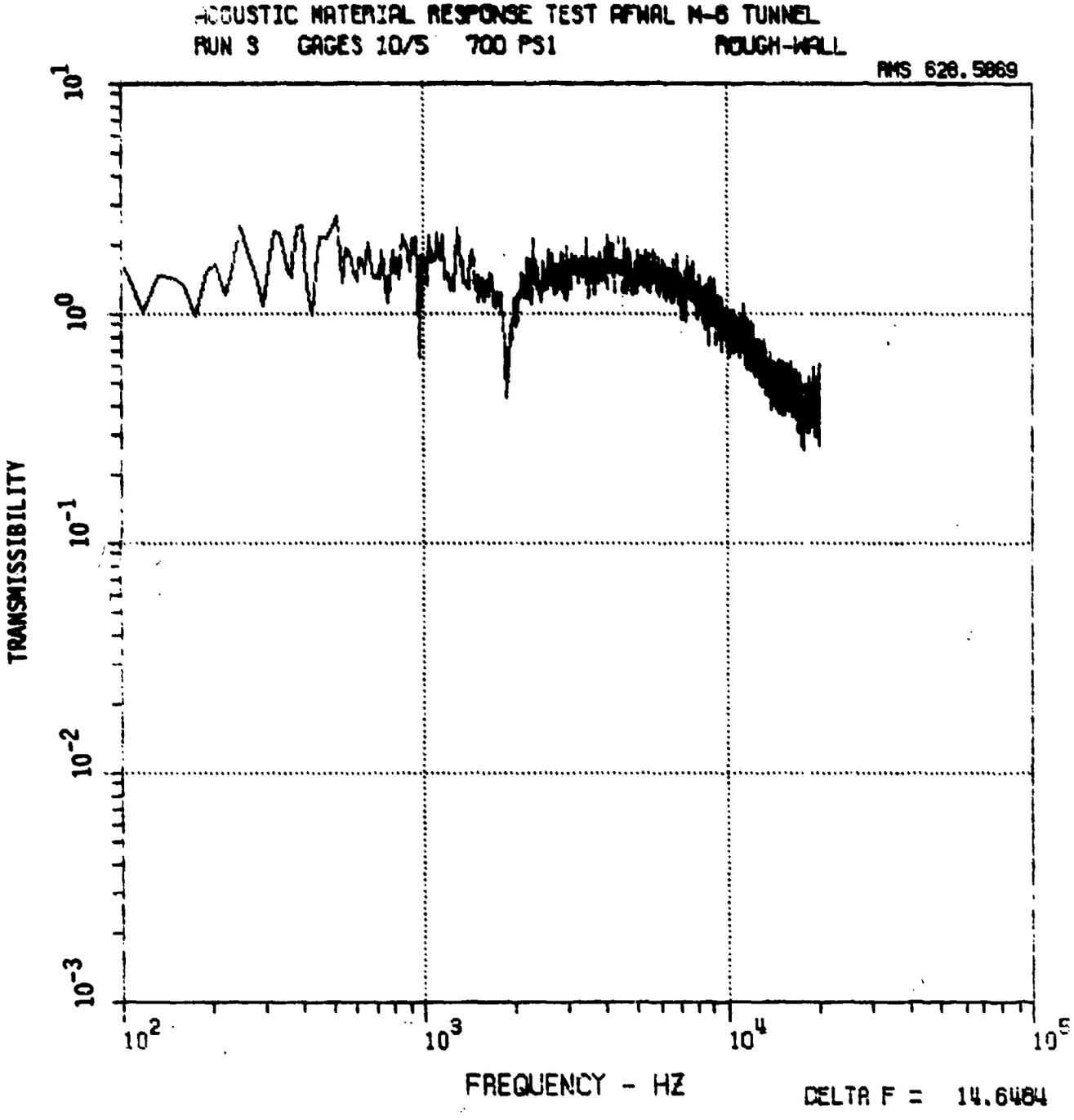
ACOUSTIC MATERIAL RESPONSE TEST AFWAL M-6 TUNNEL
RUN 3 GAGES 10/5 700 PSI ROUGH-WALL
RMS 628.5869
TRANSMISSIBILITY
10^{1}
10^{0}
10^{-1}
10^{-2}
10^{-3}
10^{2}
10^{3}
10^{4}
10^{5}
FREQUENCY - HZ
DELTA F = 14.6484

FIGURE B-34

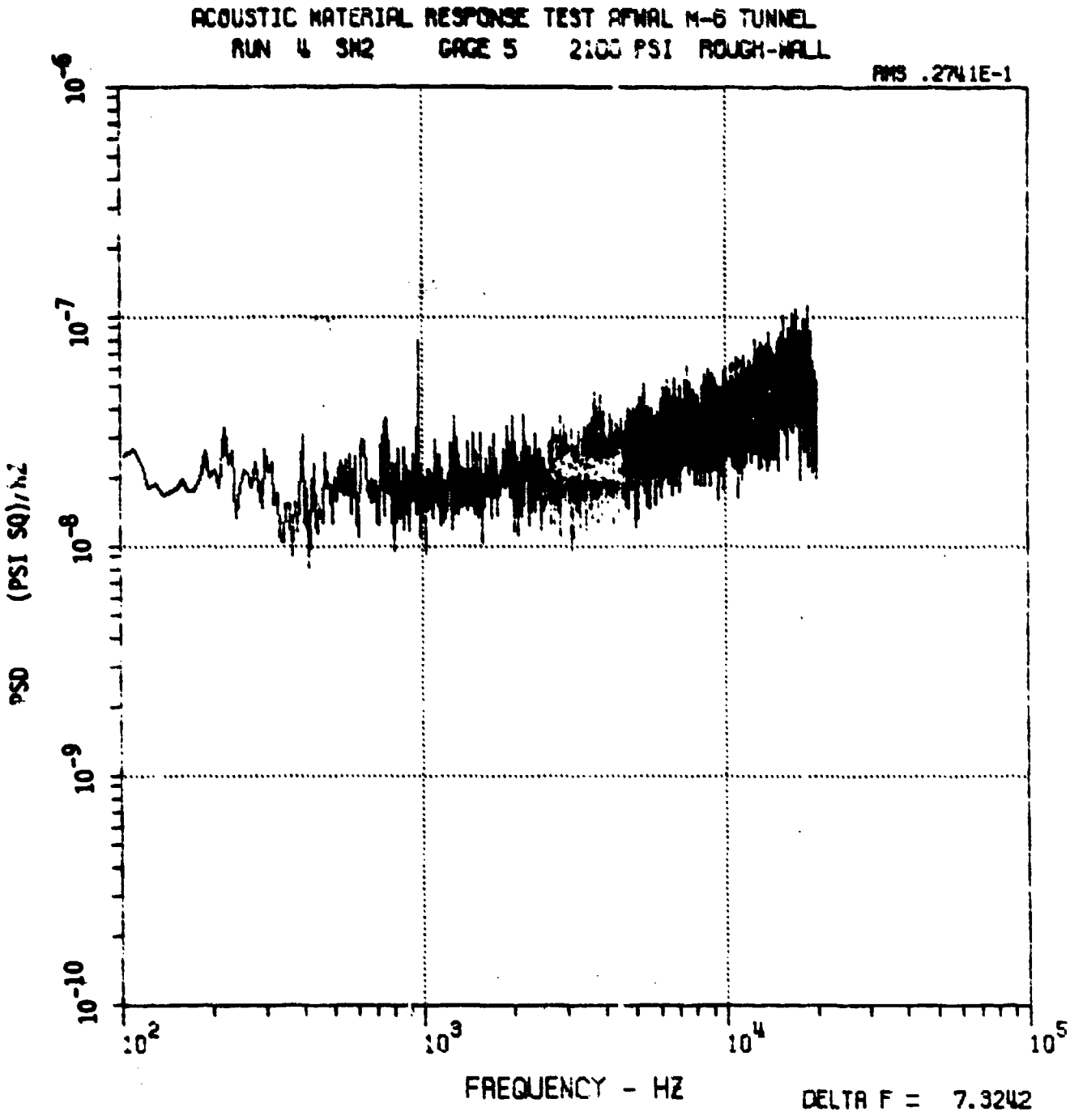
ACOUSTIC MATERIAL RESPONSE TEST AFWAL M-6 TUNNEL
RUN 4 SM2 GAGE 5 2100 PSI ROUGH-WALL
RMS .2741E-1
PSD (PSI SQ)/HZ
10^{-6}
10^{-7}
10^{-8}
10^{-9}
10^{-10}
10^{2}
10^{3}
10^{4}
10^{5}
FREQUENCY - HZ
DELTA F = 7.3242

FIGURE B-35

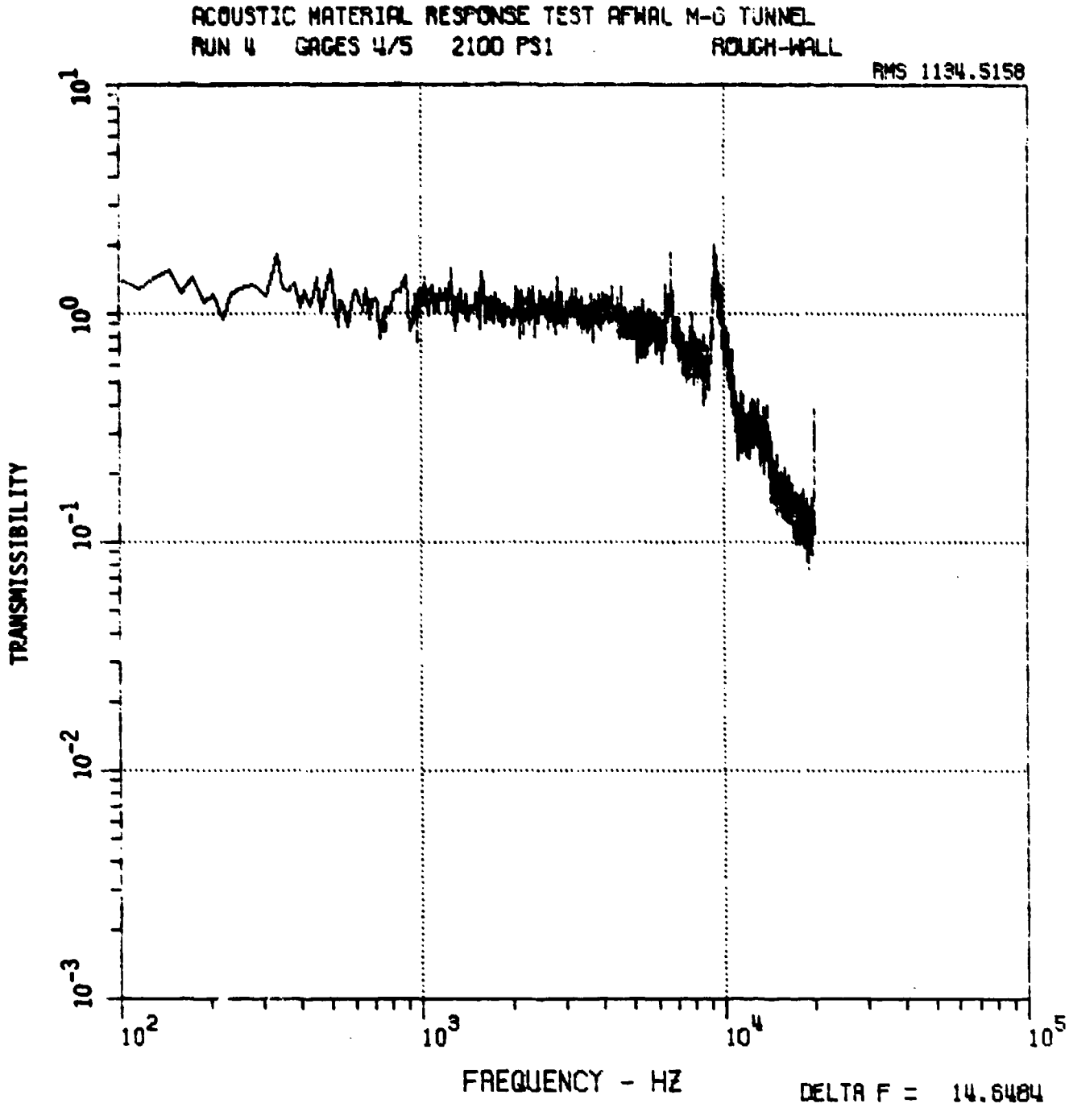
ACOUSTIC MATERIAL RESPONSE TEST AFWAL M-6 TUNNEL
RUN 4 GAGES 4/5 2100 PSI ROUGH-WALL
RMS 1134.5158
TRANSMISSIBILITY
10^{1}
10^{0}
10^{-1}
10^{-2}
10^{-3}
10^{2}
10^{3}
10^{4}
10^{5}
FREQUENCY - HZ
DELTA F = 14.6484

FIGURE B-36

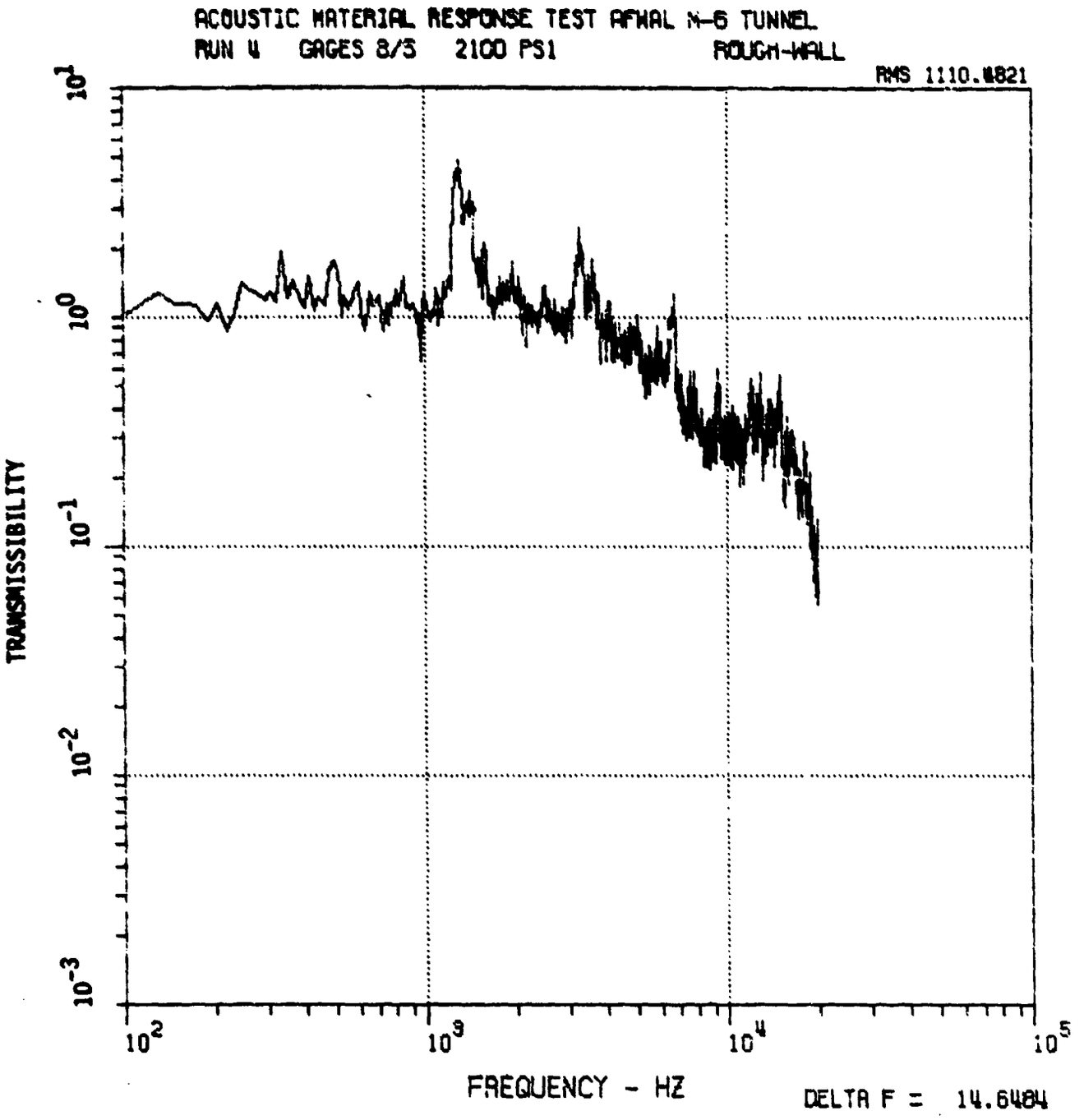
ACOUSTIC MATERIAL RESPONSE TEST AFWAL M-6 TUNNEL
RUN 4 GAGES 8/3 2100 PSI ROUGH-WALL
RMS 1110.4821
TRANSMISSIBILITY
10^{1}
10^{0}
10^{-1}
10^{-2}
10^{-3}
10^{2}
10^{3}
10^{4}
10^{5}
FREQUENCY - HZ
DELTA F = 14.6484

FIGURE B-37

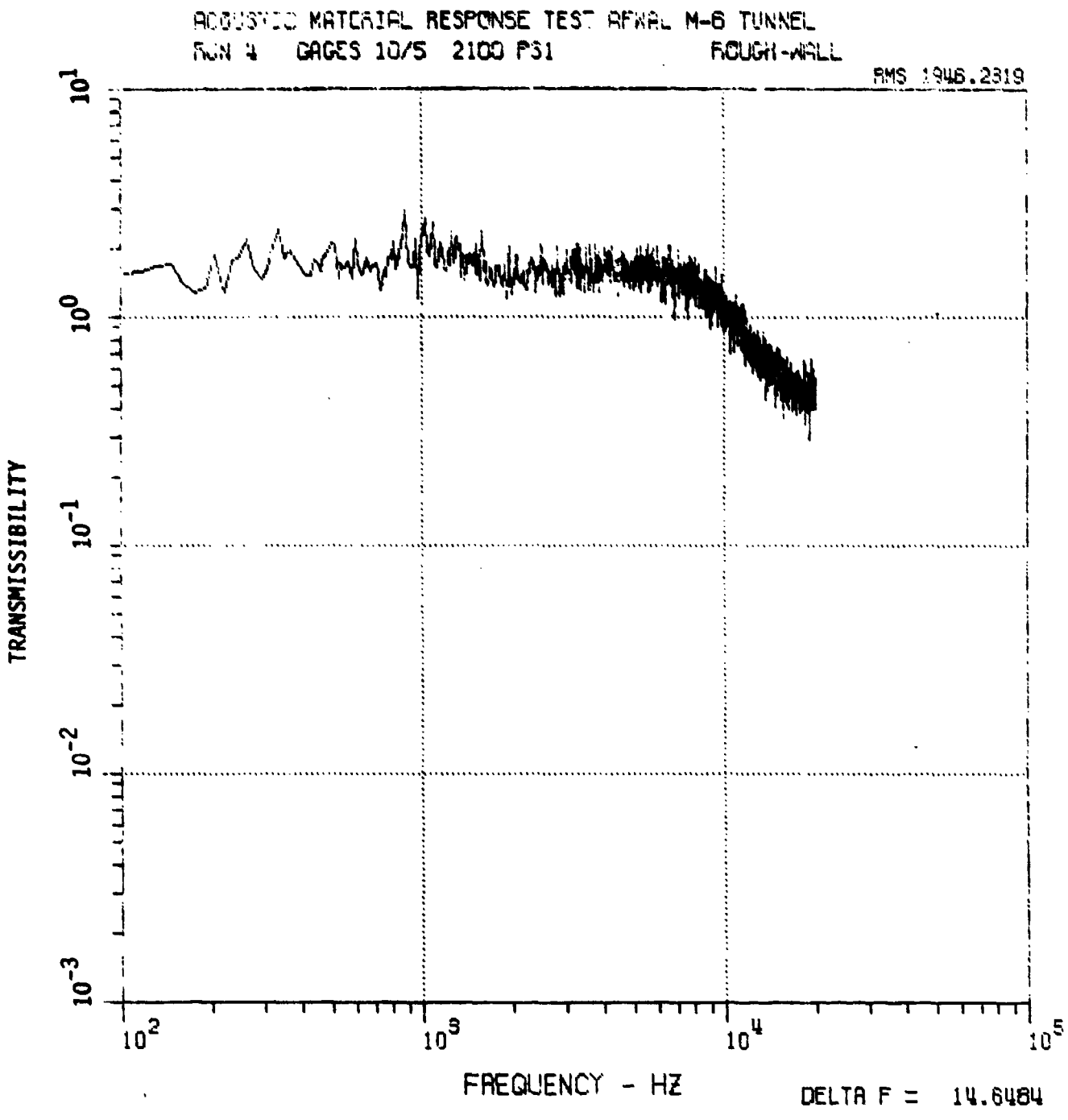
ACOUSTIC MATERIAL RESPONSE TEST AFWAL M-6 TUNNEL
RUN 4 GAGES 10/5 2100 PSI ROUGH-WALL
RMS 1946.2319
TRANSMISSIBILITY
10^{1}
10^{0}
10^{-1}
10^{-2}
10^{-3}
10^{2}
10^{3}
10^{4}
10^{5}
FREQUENCY - HZ
DELTA F = 14.6484

FIGURE B-38

12
6

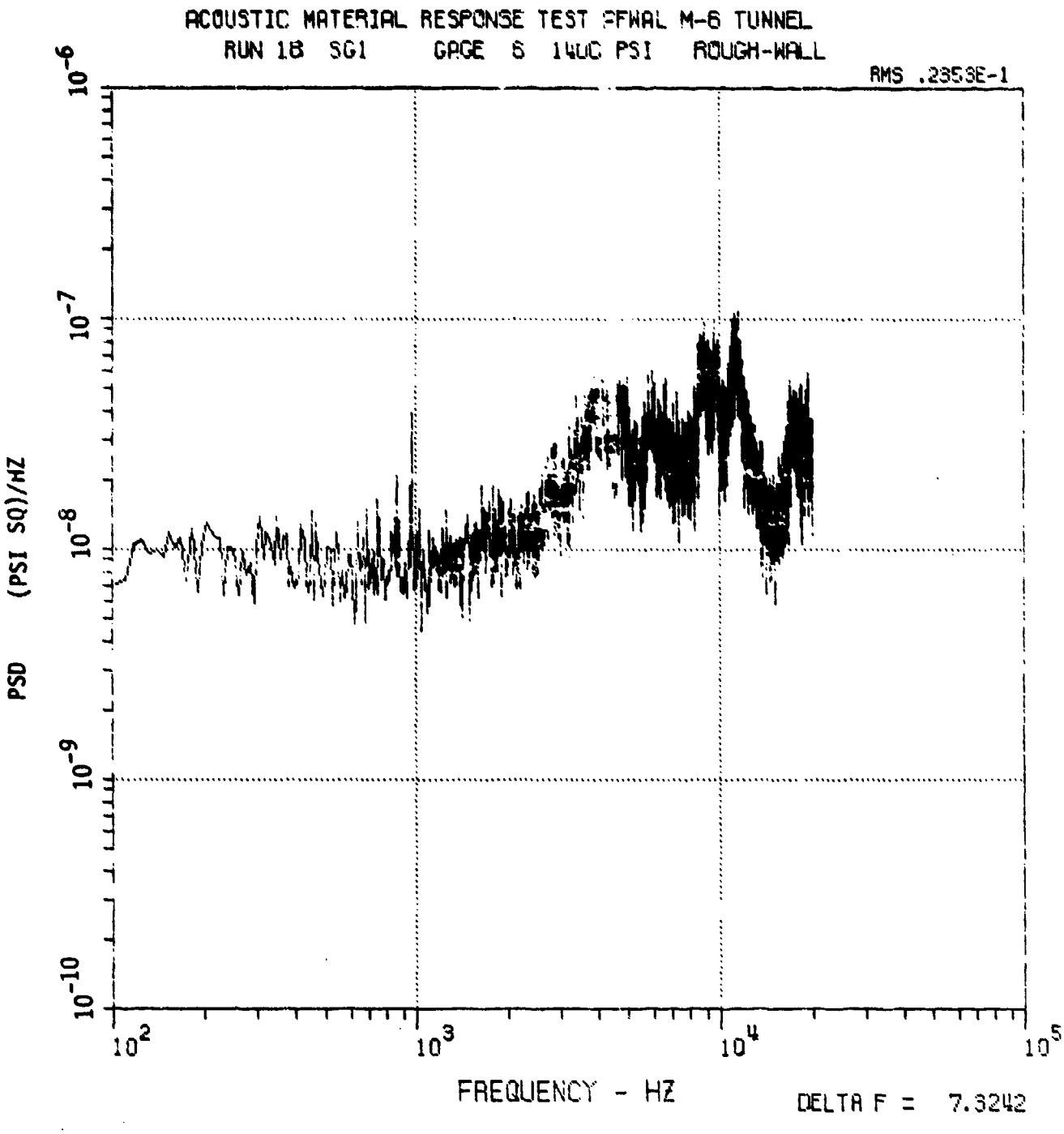

FIGURE B-39

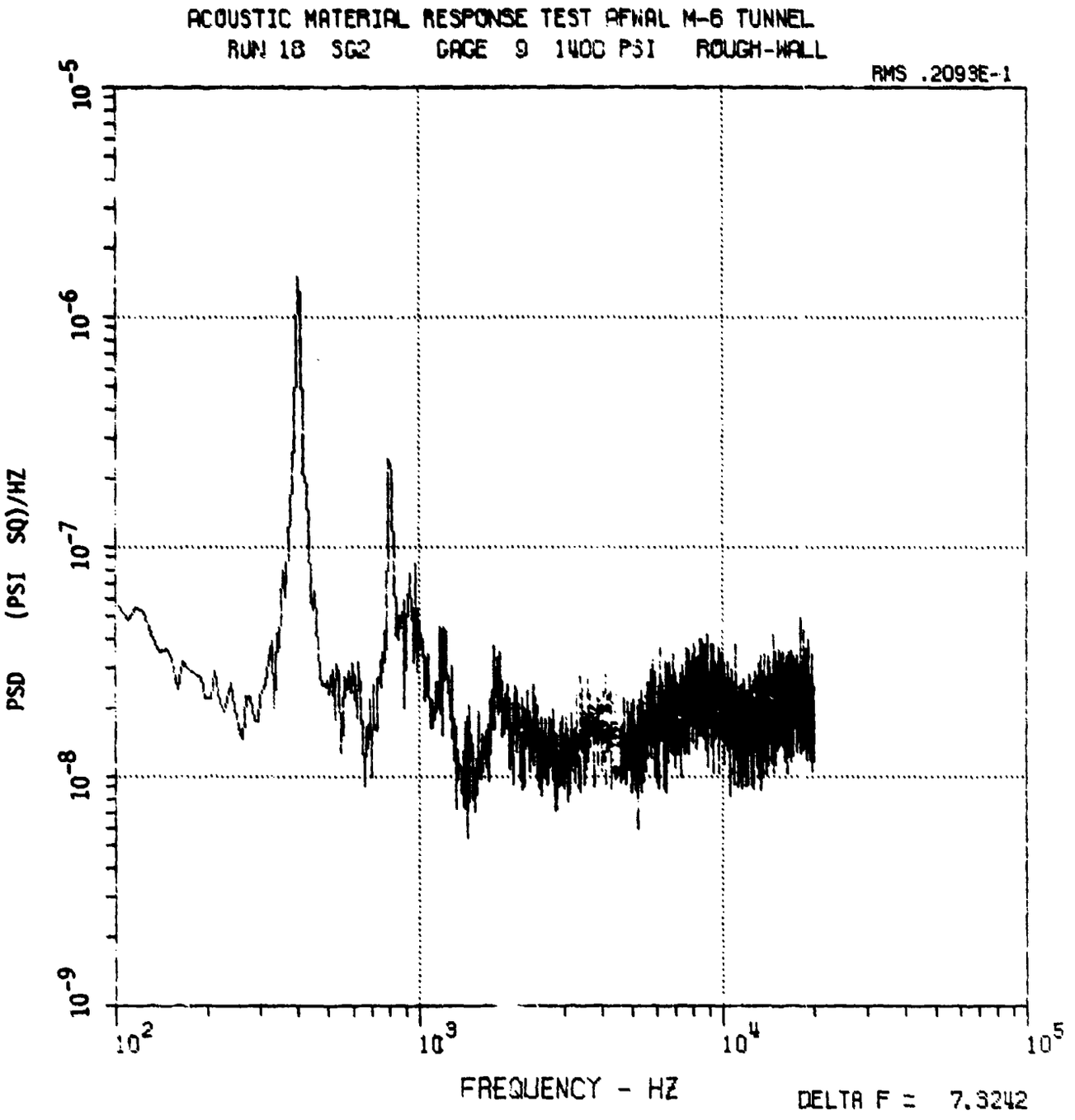
ACOUSTIC MATERIAL RESPONSE TEST AFWAL M-6 TUNNEL
RUN 18 SG2 GAGE 9 1400 PSI ROUGH-WALL
RMS .2093E-1
PSD (PSI SQ)/HZ
10^{-5}
10^{-6}
10^{-7}
10^{-8}
10^{-9}
10^{2}
10^{3}
10^{4}
10^{5}
FREQUENCY - HZ
DELTA F = 7.3242

FIGURE B-40

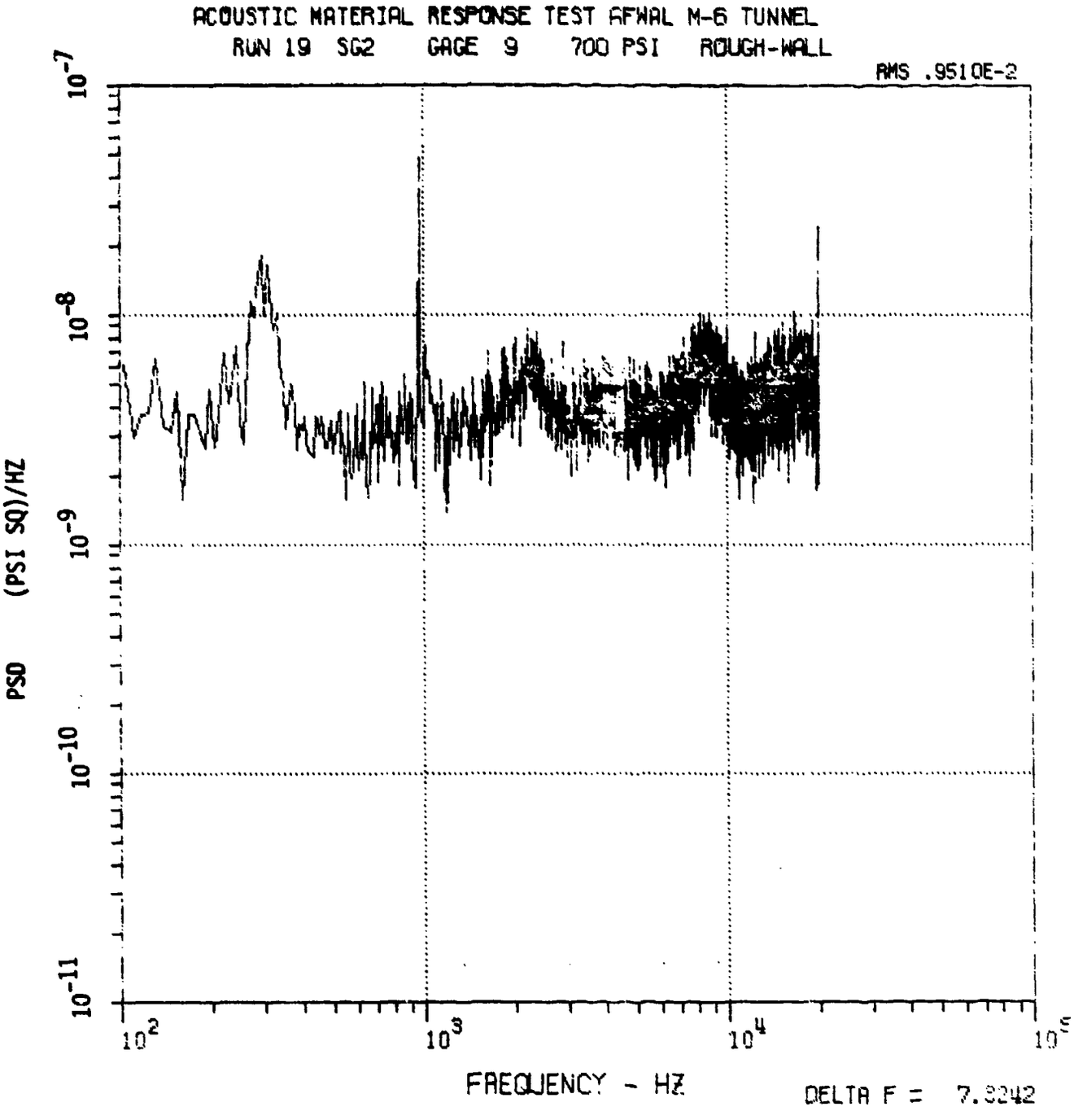
ACOUSTIC MATERIAL RESPONSE TEST AFWAL M-6 TUNNEL
RUN 19 SG2 GAGE 9 700 PSI ROUGH-WALL
RMS .9510E-2
PSD (PSI SQ)/HZ
10^{-7}
10^{-8}
10^{-9}
10^{-10}
10^{-11}
10^{2}
10^{3}
10^{4}
10^{5}
FREQUENCY - HZ
DELTA F = 7.3242

FIGURE B-41

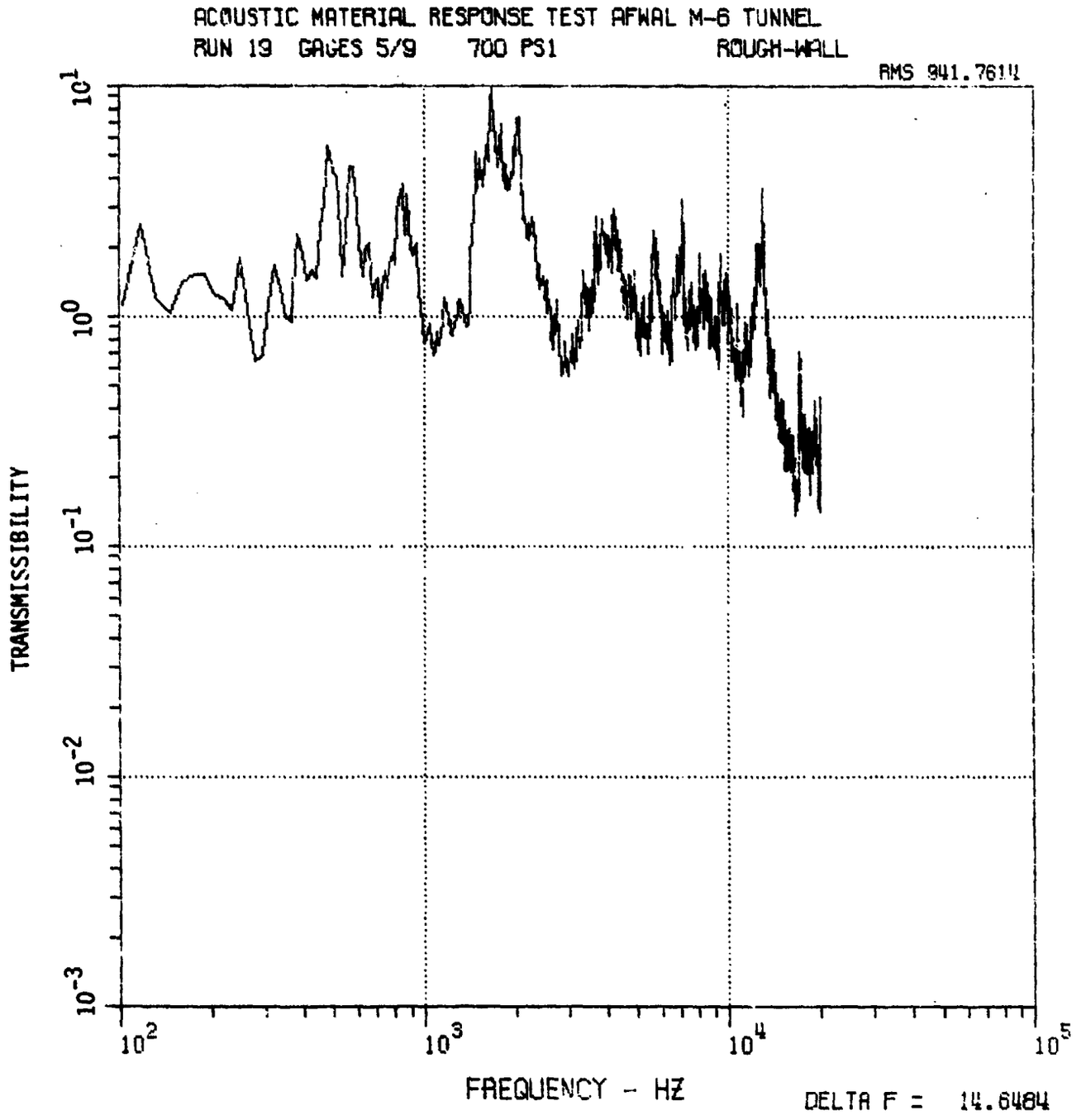
ACOUSTIC MATERIAL RESPONSE TEST AFWAL M-6 TUNNEL
RUN 19 GAGES 5/9 700 PSI ROUGH-WALL
RMS 941.7614
TRANSMISSIBILITY
10^{-1}
10^{0}
10^{-1}
10^{-2}
10^{-3}
10^{2}
10^{3}
10^{4}
10^{5}
FREQUENCY - HZ
DELTA F = 14.6484

FIGURE B-42

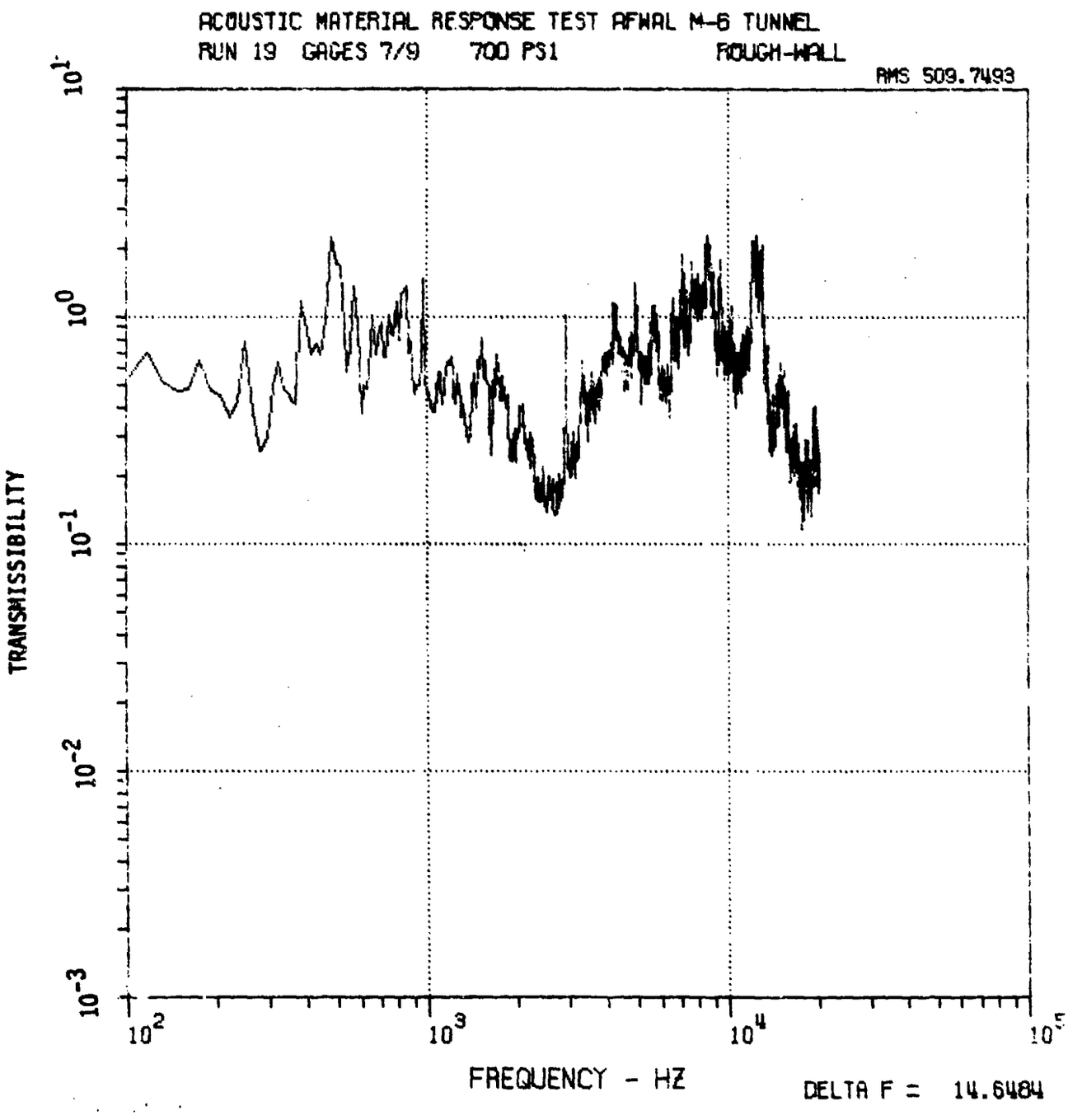
ACOUSTIC MATERIAL RESPONSE TEST AFWAL M-6 TUNNEL
RUN 19 GAGES 7/9 700 PSI ROUGH-WALL
RMS 509.7493
TRANSMISSIBILITY
10^{1}
10^{0}
10^{-1}
10^{-2}
10^{-3}
10^{2}
10^{3}
10^{4}
FREQUENCY - HZ
DELTA F = 14.6484

FIGURE B-43

20
9

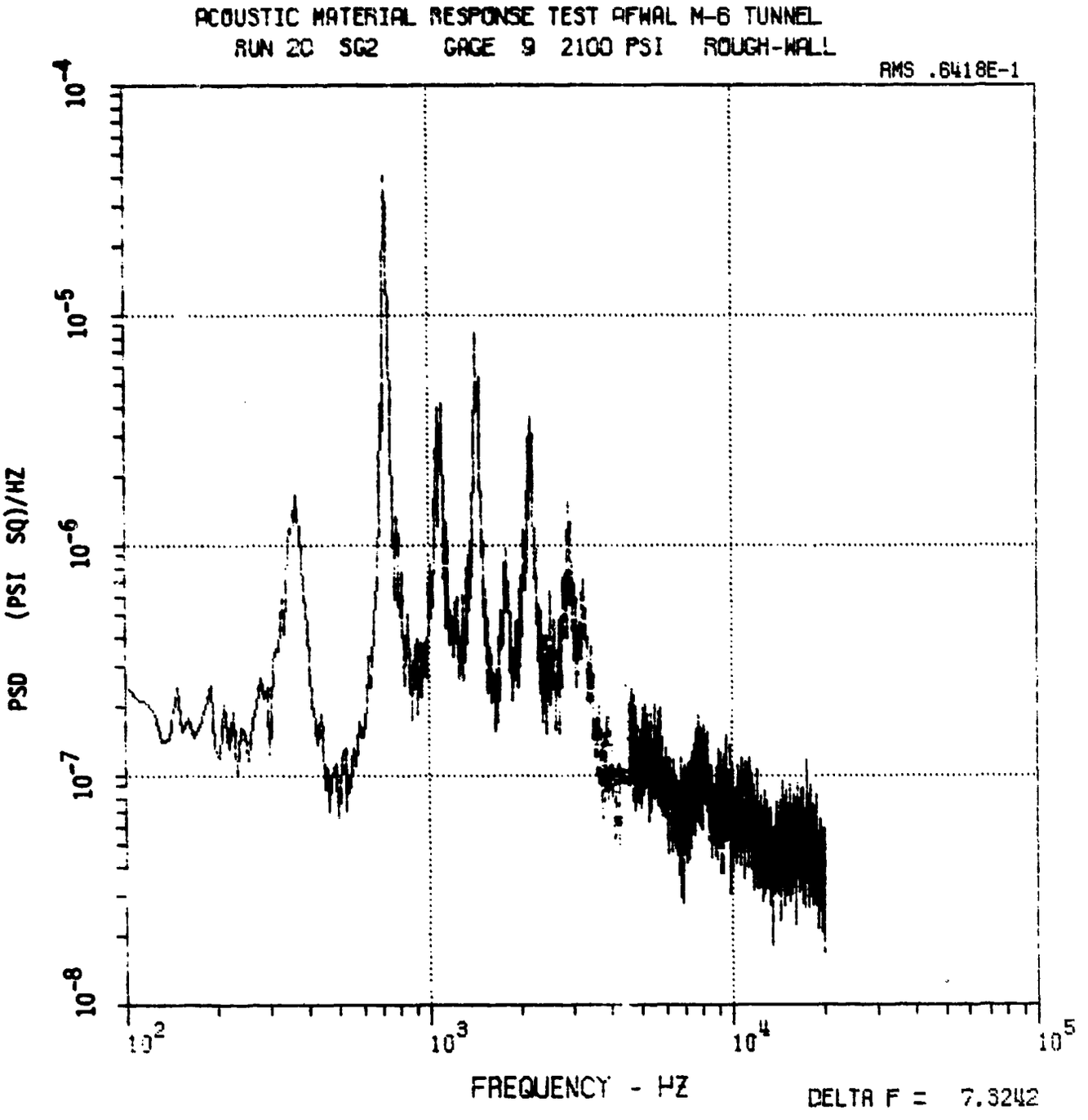

FIGURE B-44

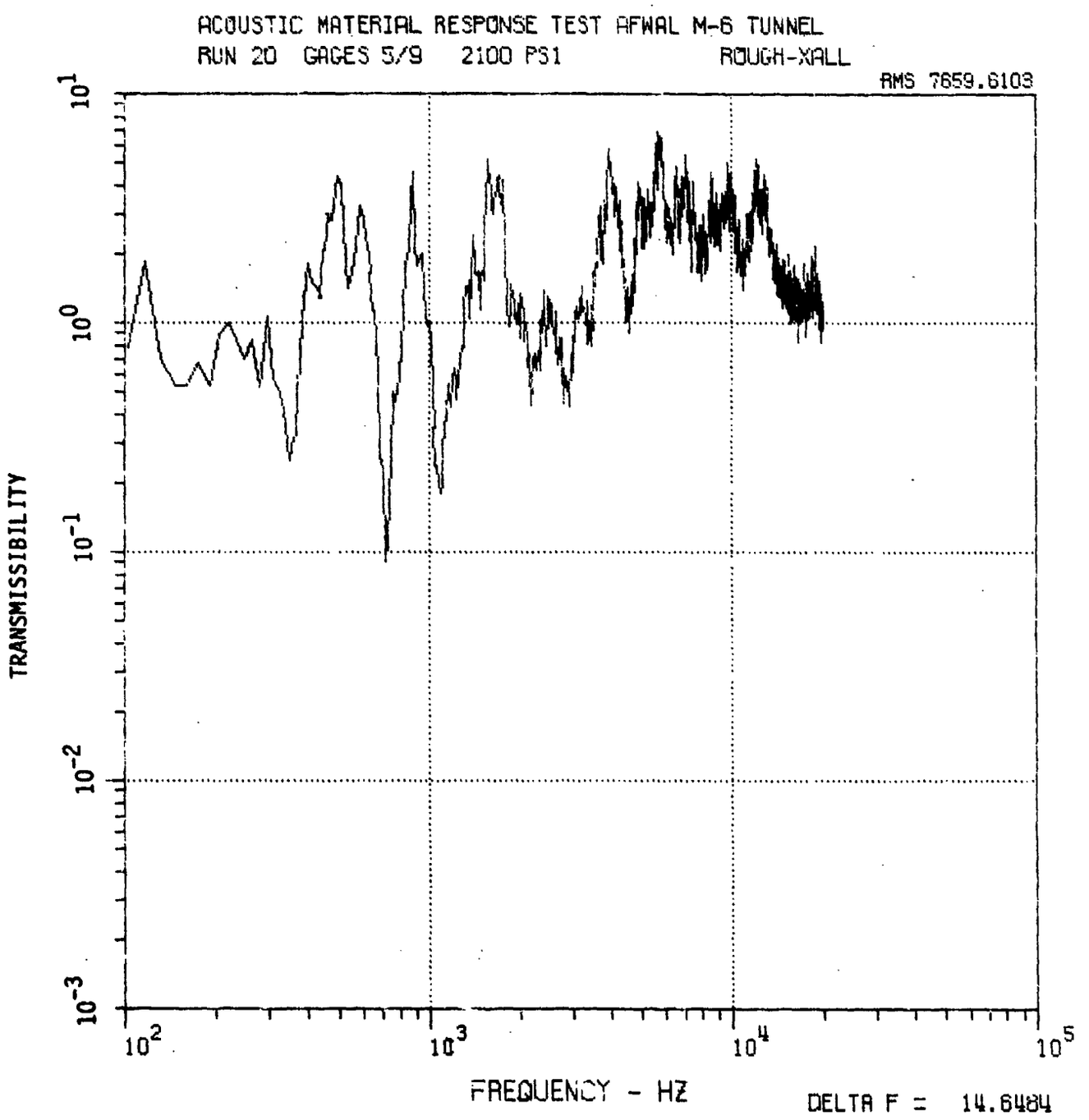
ACOUSTIC MATERIAL RESPONSE TEST AFWAL M-6 TUNNEL
RUN 20 GAGES 5/9 2100 PSI ROUGH-XALL
RMS 7659.6103
TRANSMISSIBILITY
10^{1}
10^{0}
10^{-1}
10^{-2}
10^{-3}
10^{2}
10^{3}
10^{4}
10^{5}
FREQUENCY - HZ
DELTA F = 14.6484

FIGURE B-45

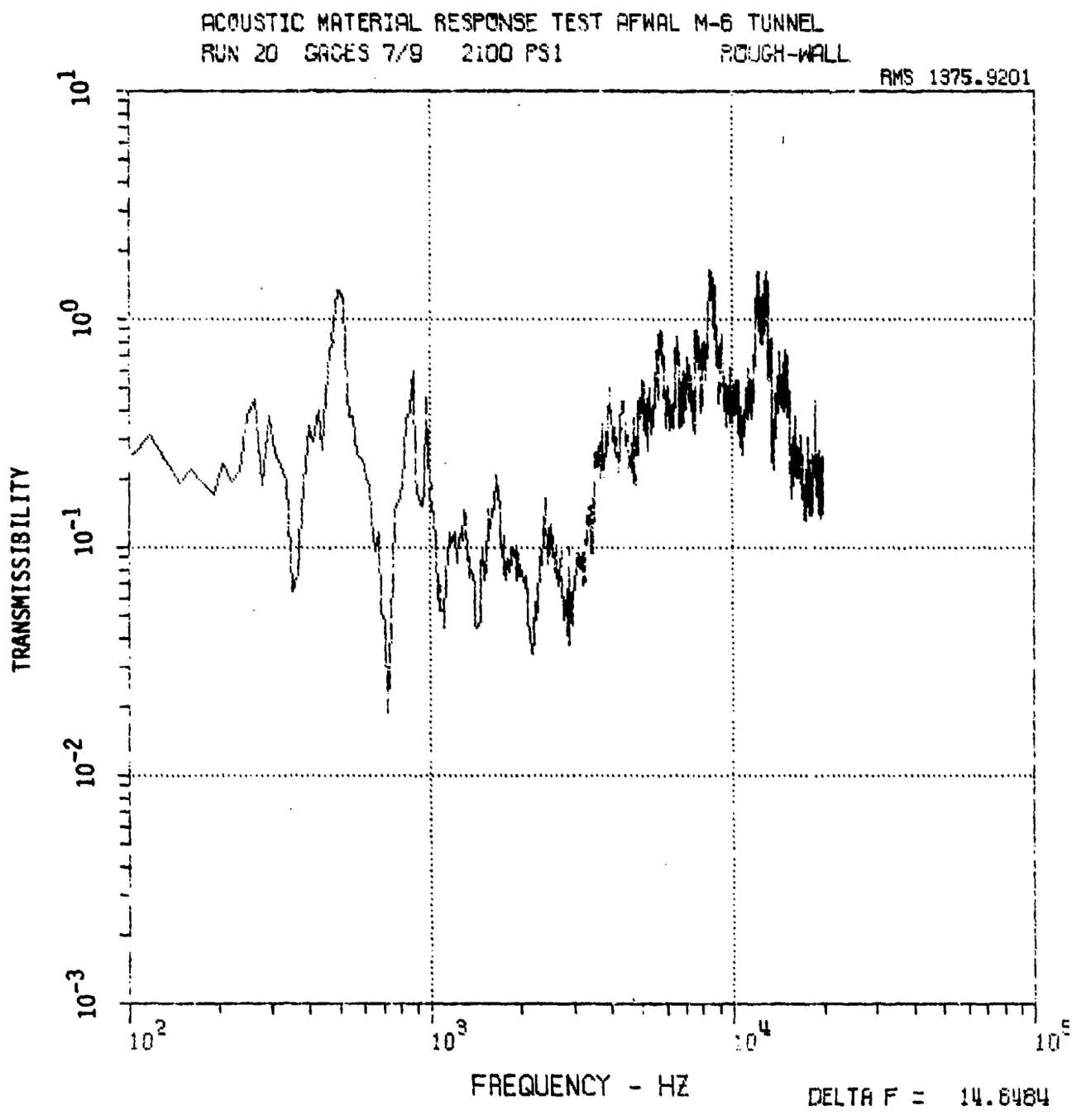
ACOUSTIC MATERIAL RESPONSE TEST AFWAL M-6 TUNNEL
RUN 20 GAGES 7/8 2100 PSI ROUGH-WALL
RMS 1375.9201
TRANSMISSIBILITY
10^{1}
10^{0}
10^{-1}
10^{-2}
10^{-3}
10^{2}
10^{3}
10^{4}
10^{5}
FREQUENCY - HZ
DELTA F = 14.6484

FIGURE B-46

25
7

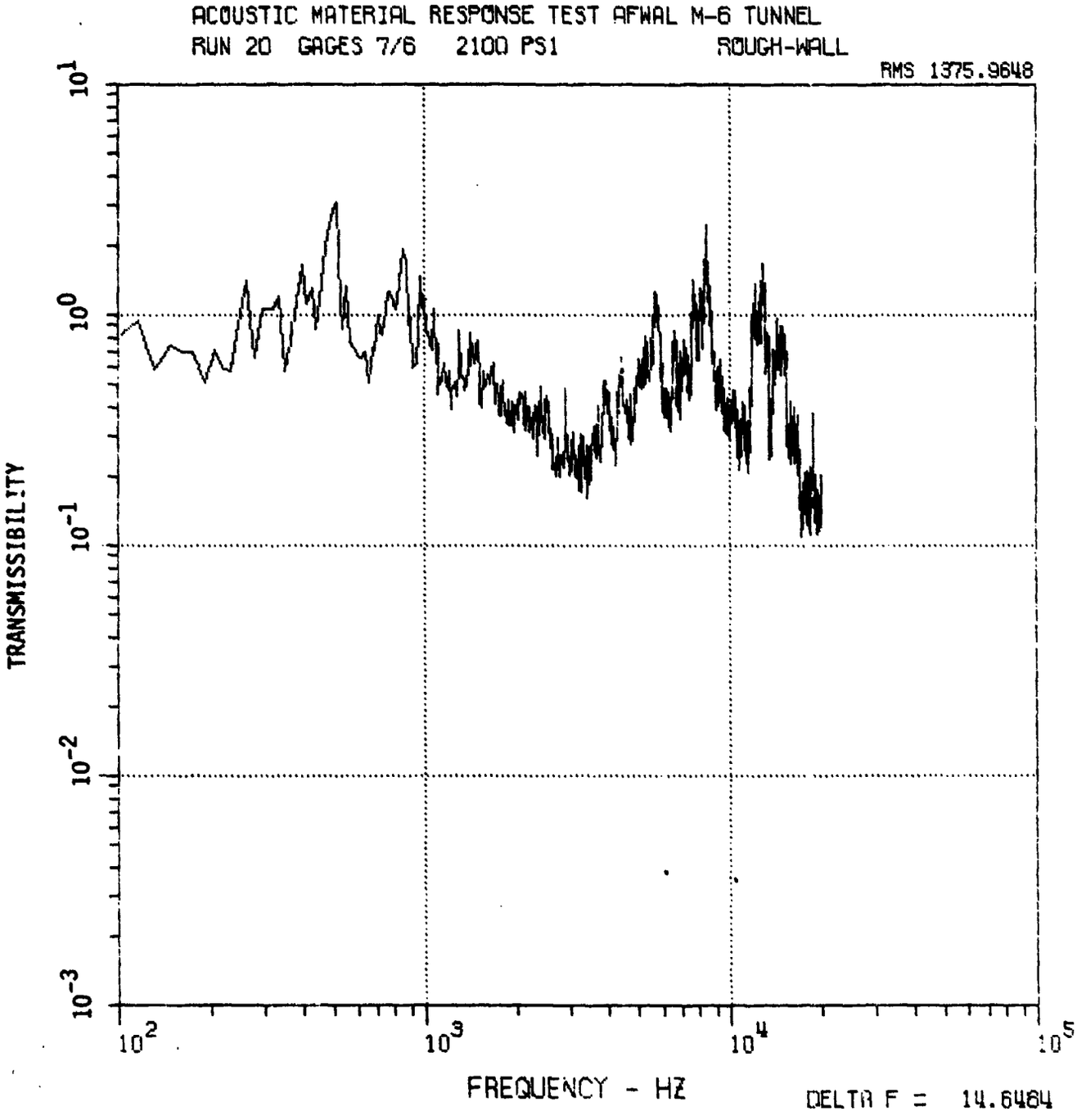

FIGURE B-47